NANOCOMPOSITE COATINGS
FOR
BIOMEDICAL APPLICATIONS

By

FENG SUN, B. Eng.

A Thesis

Submitted to the School of Graduate Studies

In Partial Fulfillment of the Requirements

For the Degree

Master of Applied Science

McMaster University

© Copyright by Feng Sun, March 2009

MASTER OF APPLIED SCIENCE (2009).............McMaster University

(Materials Science & Engineering)............................Hamilton, Ontario

TITLE: Nanocomposite coatings for biomedical applications

AUTHOR: Feng Sun, B. Eng. (Zhejiang University)

SUPERVISOR: Professor Igor Zhitomirsky

NUMBER OF PAGES: ix, 101

Abstract

New electrophoretic deposition methods for the fabrication of advanced organic-inorganic composite coatings on metallic substrates for biomedical applications have been developed. In the proposed methods, chitosan was used as a matrix for the fabrication of multilayer and functional graded chitosan- hydroxyapatite (HA) coatings. The HA particles showed preferred orientation of c-axis parallel to the layer surface, which is similar to the bone structure. Electrochemical studies showed that the obtained coatings provided corrosion protection of the metallic substrates, such as stainless steel and Nitinol.

The feasibility of co-deposition of chitosan and heparin has been demonstrated. Composite chitosan-heparin layers were used for the surface modification of chitosan-HA coatings. Obtained results paved the way for the electrophoretic fabrication of novel coatings for biomedical implants with improved blood compatibility.

The feasibility of co-deposition of hyaluronic acid and HA has also been demonstrated. The co-deposition of hyaluronic acid and HA resulted in the fabrication of novel nanocomposite films by electrodeposition. The chemical composition, microstructure, corrosion protection, and other functional properties of the nanocomposites have been investigated. Co-deposition of hyaluronic acid and multiwalled carbon nanotubes has been studied by TGA/DTA and SEM studies.

The feasibility of deposition of novel composites based on alginic acid has been demonstrated. New electrochemical strategies were used for the fabrication of alginic acid-HA, alginic acid-heparin and alginic acid -hyaluronic acid nanocomposites. The composition of these nanocomposite coatings can be varied by variation in bath composition for EPD.

The electrochemical mechanisms for the fabrication of all these advanced organic-inorganic composite coatings have been developed.

Acknowledgement

I would like to express my gratitude to all those who gave me the possibility to complete this thesis.

First of all, I would like to express my sincere appreciation to my supervisor, Professor Igor Zhitomirsky, whose help, stimulating suggestions and encouragement helped me in all the time of research for and writing of this thesis.

Also I would give many thanks to all the team members, Xin Pang, Jun Li, Gideon Moses Jacob, Travis Casagrande, Rong Ma, Chao Shi, Yaohui Wang, Marco Cheong, Jianmei Wei, for their kindness and friendship.

Last but not the least; I take this opportunity to express my profound gratitude to my beloved parents for their moral support and patience during my study in Canada.

Table of Contents

Table of Figures

1 Introduction

A biomaterial is any material, natural or man-made, that comprises whole or part of a living structure or biomedical device which performs, or replaces a natural function. The wide range of biomaterials includes heart valves, artificial blood vessels, orthopaedic, surgical and dental implants.

The development of biomaterials is not a new area of science, having existed for around half a century since the first biomaterials were developed. The area of biomaterials is becoming one of the most intellectually exciting areas of materials science and engineering. Significant interests have been generated in the development of orthopedic devices intended for implantation in the human body.

Orthopaedic implants are devices which can aid healing, correct deformities and restore the lost functions of the original parts. Different orthopaedic implants are currently under development, such as bone plates, screws, total hip joints, knee joins, elbow joints and shoulder joints. There are several strict restrictions related to the materials that can be used as biomaterials. First and foremost, a biomaterial must be biocompatible—it should not elicit an adverse response from the body. Additionally, it should match the physical and mechanical behavior of the implant with the tissue to be replaced. At the same time, it should be nontoxic and noncarcinogenic. Thus, only certain materials like metals and alloys, ceramics and polymers are able to meet these requirements.

As a class of materials, metals and alloys are the most widely used for load—

bearing implants because of their reasonable biocompatibility and sufficient fatigue strength to endure daily activities. However, they are still susceptible to chemical and electrochemical degradation in the body. Body fluid contains water, dissolved oxygen, and various ions such as chloride and hydroxide. These present a complex environment to the implants and the metals and alloys may corrode and/or wear.

Surface plays an important role in a biological system for most biological reactions occurring at the surfaces and interfaces. Surface modification of materials for medical applications presents the possibility of combining the ideal bulk properties (e.g. tensile strength or stiffness for implants) with the desired surface properties (e.g. biocompatibility). So an effective approach to reduce corrosion and achieve better biocompatibility of a metal or alloy implant is to modify its surface with a functional surface coating. The selection of appropriate coating materials and coating technologies is the major challenge for this area, which requires the manufacture of advanced biomedical devices or implants with comprehensive functionalities.

The purpose of this research is to develop the deposition technique for the fabrication of organic—inorganic advanced functional coatings on metallic substrates for applications in orthopedic implants.

2 Literature Review

2.1 Metals and alloys for orthopaedic and dental implant applications

Although many metals and alloys are used for medical device applications, the most commonly employed are stainless steels, commercially pure titanium and titanium alloys, and cobalt-base alloys. In this research stainless steels and Nitinol were used as substrates for the fabrication of advanced organic—inorganic coatings.

2.1.1 Stainless steel

Stainless steel has a long history as a metallic material for medical implants. The wide range of applications of the stainless steels includes bone implants, cardiovascular implants (stents), and dental implants.

At the beginning the quality of the stainless steel was poor, and many deficiencies such as fatigue failures and severe corrosion were reported [1]. The breakthrough of stainless steel as an implant material came with the development of the material with the designation AISI 316L. This type of steel is still used today, primarily in products for osteosynthesis like plates, nails and screws [1]. Endoprostheses made of this type of steel since the 1960s (e.g. Charnley hip stem) have been implanted and retained successfully for many years. Reports of corrosion phenomena and fatigue failures of this stainless steel in—vivo have been made in the literature [2, 3].

Type 316L is an austenitic chromium—nickel stainless steel containing molybdenum. The addition of molybdenum increases general corrosion resistance, improves resistance to pitting from chloride ion solutions, and provides increased strength at elevated temperatures. The corrosion resistance of this stainless steel is improved, particularly against sulfuric, hydrochloric, acetic, formic and tartaric acids; acid sulfates and alkaline chlorides. The extra low carbon content (max 0.03%) minimizes harmful carbide precipitation due to welding.

2.1.2 Nitinol

Nitinol is another important metallic material for biomedical application. It is a generic trade name for Nickel—Titanium alloy, which stands for Nickel (Ni), Titanium (Ti) and Naval Ordnance Laboratory (NOL) where it was first discovered in the early 1960s.

Nitinol is an advanced shape memory alloy containing approximately 50 at.% nickel and 50 at.% titanium [4]. In the last decade, it has attracted considerable interest for biomedical applications, due to the combination of mechanical properties (shape memory and superelasticity) and good biocompatibility. This alloy presents an elastic modulus which is closer to that of the bone, compared with other metal implant materials (Figure 2-1). In the figure, we can observe a similarity in the deformation behavior between Nitinol and the bone, which contributes to the biomechanical compatibility of this alloy. In fact the absence of recoverable strain of stainless steel may be one of the major reasons for the fracture of orthopaedic implants in the body. Therefore, Nitinol may be used with great advantage in orthodontics, in treatment of bone fracture and in bone suture anchors for attaching soft tissues [5].

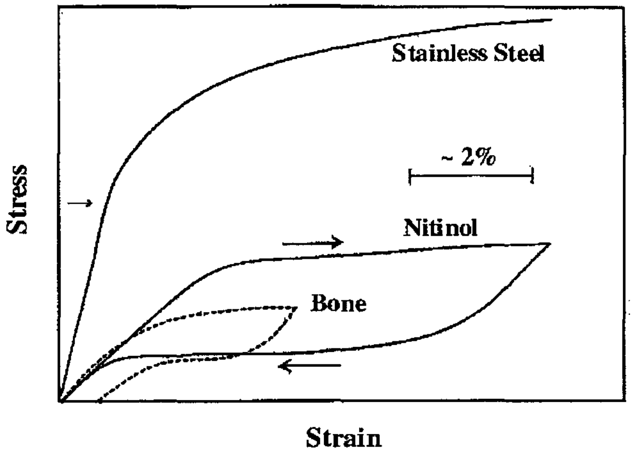

Figure 2-1 Schematic stress-strain diagram for bone, Nitinol and stainless steel

The wide spectrum of applications of Nitinol imposes special requirements on the biocompatibility of this alloy [5, 6]. Nitinol has high nickel content and Ni is known for its toxicity, carcinogenic and immune—sensitizing effects. Release of nickel ions is the greatest problem that can be faced after Nitinol implantation. So surface modifications are especially important for the fabrication of porous orthopaedic implants with high surface area, which will decrease the corrosion resistance of Nitinol [7].

2.2 Hydroxyapatite and other ceramics for orthopaedic and dental implant applications

Ceramics may call to mind such objects as teapots and tile floors. However, many of the current application of ceramics are in the field of biomedical applications. The term of "bioceramics" is used for the ceramics which can be utilized for the repair, reconstruction, and replacement of diseased or damaged part of the body [8].

Bioceramics can have structural functions as joint or tissue replacements, can be used as coatings to improve the biocompatibility of metal implants, and can function as resorbable lattices which provide temporary structures and a framework that is dissolved, replaced as the body rebuilds tissue. The thermal and chemical stability of ceramics, their high strength, wear resistance and durability all contribute to making ceramics good candidate materials for surgical implants. Some ceramics even feature drug-delivery capability.

One of the most important bioceramics is hydroxyapatite (HA), which is often used as the bioceramic coating for the metallic substrate. It is chemically similar to the mineral component of bones and hard tissues in mammals. The chemical formula is usually written as $Ca_{10}(PO_4)_6(OH)_2$ which denotes that the crystal unit cell comprises two molecules.

HA is one of few materials that are classified as bioactive, meaning that it will support bone in growth and integration when used in orthopaedic and dental applications. So, it has become the focus of a significant research effort [8-13].

The chemical nature of hydroxyapatite lends itself to substitution, meaning that it is common for non-stoichiometric hydroxyapatites to exist. The most common substitutions involve carbonate, fluoride and chloride substitutions for hydroxyl groups [14]. For example, fluorapatite is found in dental enamel and hydroxycarbonate apatite is present in bone.

Generally speaking dense hydroxyapatite does not have the mechanical strength to enable it to succeed in long term load bearing applications. So the first typical application of HA in biomedical field is the "bioceramic coating". HA is oftern used as a coating on materials such as stainless steel or Nitinol, where it can contribute its 'bioactive' properties, while the metallic component bears the load. A successful example is the bioactive coatings on total hip prosthesis. In this manner the body sees hydroxyapatite-type material which it is happy to accept. Without the coating the body would see a foreign body and work in such a way as to isolate it from surrounding tissues.

To date, plasma spraying is the most common accepted method of applying hydroxyapatite coatings to metallic implants. However, the high processing temperatures can result in the degradation of HA and the substrates [15-17]. Moreover, the microstructure and properties of sintered HA are different from those of natural nanostructured HA. It is important to note that natural bone is a nanocomposite material possessing unique properties determined by the size and orientation of HA nanoparticles, the organic—inorganic laminate structure, and the hierarchical organization of HA and an organic phase. So the new fabrication technique of HA coatings is required to be developed.

2.3 Polymers for orthopaedic and dental implant applications

Polymers are widely used in biomedical fields such as tissue engineering, implantation of medical devices and artifical organs, prostheses, opthalmology, dentistry, bone repair, and many other medical fields [18]. Polymer—based delivery systems enable controlled release of drugs into the body. Polymeric materials provide a safe way of gene delivery for gene therapy. The application of polymers for biosensors and testing devices also has been investigated. In the tissue engineering, biodegradable or bioresorbable polymers are particularly important because of the interactions between different functions groups of polymers and biological species including proteins and cells [19, 20].

Polysaccharides are a class of natural-origin polymers which are made up of many monosaccharides joined together by glycosidic bonds [21]. These biological polymers can be obtained by biosynthesis in plants, animals, and microorganisms from other carbon—containing compounds such as carbohydrates and lipids. A number of unique features make polysaccharides a class of particularly important materials for biomedical applications, which include the scaffold materials in tissue engineering, carriers for drug delivery system and other materials [22]. First of all, with few exceptions, natural polysaccharides generally are nontoxic and biodegradable. Next, the numerous hydroxyl groups in the molecule provide numerous sites for the attachment of side groups which can provide specific functionality and biological recognition features, give the tendency of polysaccharides to form cooperative intra- and interchain hydrogen bonds which can cause some insolubility or good film—forming properties. It also has low cost in comparison with others biopolymers such as collagen [23, 24].

A few of these polysaccharides are considered as promising candidates for biomedical applications, mainly alginate, hyaluronic acid, chitosan and heparin. In the research, these four polysaccharides, associated with hydroxyapatite, are used to modify the surface properties of metallic implants.

2.3.1 Chitin and Chitosan

Chitin is a natural biopolymer originating from the shells of shrimps and other sea crustaceans. It is the second most abundant organic resource on the earth just next to cellulose [25] and is estimated to be synthesized and degraded in the vast amount of billions of tons each year in the biosphere.

Chemically, chitin is composed of β(1→4) linked 2 -acetamido- 2-deoxy-β- D-glucose units (or N-acetyl-D-glucosamine) [26]. This long chain linear polymer is insoluble in most solvents, which is a major problem for the development of processing techniques and for its applications. This characteristic also makes it difficult to determine its molecular weight, which is very important for the determination of properties of the polymer. It also results in a lack of data on the physical properties of chitin in solution. The first well-developed study on chitin solubility was published by Austin [27, 28], who introduced the solubility parameters for chitin in numerous solvents. Later, a few papers were published which discussed the preparation of alkali chitin by dissolution of chitin at low temperature in NaOH solution [29, 30]. They found that in order to get water solubility, the degree of deacetylation of chitin has to be around 50%.

Chitosan is the product of alkaline deacetylation of chitin. However, the deacetylation process is rarely complete, so chitosan showed a partially deacetylated structure in Figure 2-2. It is the most important derivative of chitin, because it has lots of important properties for biomedical applications. First of all, the amino groups of chitosan have a pKa value around 6.5 which result in the formation of only pseudonatural cationic polymer [31-33]. The cationic chitosan can have electrostatic interactions with anionic glycosaminoglycans (GAG) and other negatively charged surfaces such as mucous membranes. So in other words, chitosan is bioadhesive. This indicates that the amino group of chitosan are reactive, which can employ lots of chemistries to functionalize chitosan or cross-link the chitosan backbone to confer elasticity [34].

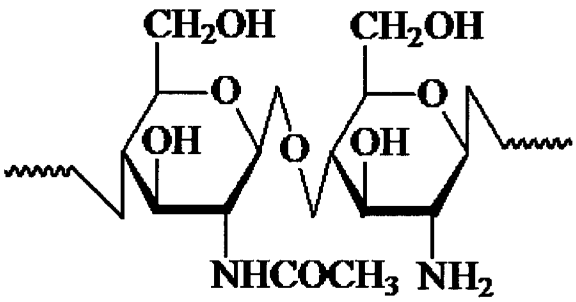

Figure 2-2 Structure of chitosan

Chitosan also has many other specific properties for biomedical applications such as good biocompatibility, antimicrobial properties, excellent film forming properties and so on. These generate great interest of many researchers and industries for applications of chitosan. The drug delivery application, which encompasses oral, nasal, parenteral and transdermal administration, implants, vaccine carriers and gene delivery, has been presented [35]. Chitosan gels and layer-by-layer polyelectrolyte capsules are often used for controlled release of drugs or proteins [36]. Wound dressing and tissue engineering applications also have been presented [37, 38]. Chitosan coatings containing hydroxyapatite, prepared by using electrophoretic deposition for the modification of surface properties of implant, have also been developed [39-41].

2.3.2 Alginate

Algae are the source of many important polysaccharides such as agar, alginate and carrageenan. These polysaccharides which have a relatively high molecular weight can be extracted from algae in different conditions. Alginates are mainly extracted from three types of marine brown algae. These include Ascophyllum nodosum, Macrocystis pyrifera and Laminaria hyperborea [42]. The annual production of alginates is around 40,000 tons and 30% is used in food and beverage industry. However, intensive interests have been focused on this natural biopolymer for biomedical application recently.

Alginate is an unbranched linear copolymer composed of two monomers: 1,4-linked β-D-mannuronic acid (M) and α–L-guluronic acid (G). These monomers can be organized in types of blocks: alternating M and G blocks (MG-blocks); block of GG; and block of MM [43, 44]. Figure 2-3 shows a structure of alginate showing both M and G blocks [45].

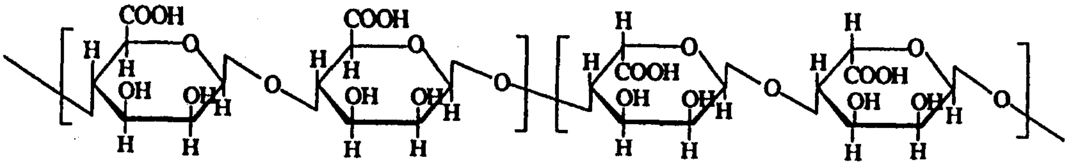

D-Mannuronic acid residues **L-Guluronic acid residues**

Figure 2-3 Structure of alginate [45]

It was demonstrated that the concentration of G and M units (G/M ratio) contributes to varied structural and biocompatibility characteristics [46]. The alternating MG blocks form the most flexible chains and M blocks have been found to be strongly immunostimulating. The G blocks are more rigid than the M blocks because of the axial-axial linkage. It was found that two G blocks of more than 6 residues each can form stable crosslinked junctions or gels with divalent cations (Ca^{2+}, Ba^{2+}, Sr^{2+}, etc.) [47, 48]. At low pH, alginates form acidic gels by hydrogen bonds. The homopolymeric blocks form the junctions, but the stability of the gel in mostly dependent on the content and length of G blocks [49].

This gel formation character combined with other advantages like non-toxic, biocompatible, biodegradable, less expensive and freely available paves an extensive way for the biomedical application of alginates. Alginates can be used for the encapsulation of a wide range of biologically active agents such as cells [50-53], proteins [54, 55], enzymes [56-58] and DNA oligonucleotides [59]. Alginates also can be fabricated as capsules, beads, fibers and films and then used as haemostatic materials and wound dressings [60]. In the tissue engineering area, alginates can be utilized to alter the surface properties of biomedical implants, combined with other biomaterials like chitosan, HA, proteins and drugs [61].

2.3.3 Hyaluronate

Hyaluronic acid (also named as hyaluronan or hyaluronate) was extracted from vitreous humor of cattle eyes for the first time by Meyer in 1934 [62]. It exists in all mammals and is identical in all species and tissues, and can be isolated from numerous sources such as bovine vitreous humor, rooster combs, or umbilical cords etc. However, this type of naturally extracted hyaluronic acid was very expensive and certainly associated with some proteins which can not be removed clearly. Now, a large scale production of hyaluronic acid which has high purity can be achieved by bacteria such as Streptococcus zooepidemicus and Streotococcus equi [63]. This reduces the price significantly and allows fast development of its application.

The chemical structure of hyaluronic acid is presented in Figure 2-4. It is a linear polysaccharide composed with alternating N-acetyl-D-glucosamine (GlcNAc) and D-glucuronic acid (GlcA) units. There are lots of unique properties of hyaluronic acid for biomedical applications. First of all, it has interesting viscoelastic and hydrating properties, resulting from the semiflexible properties of hyaluronic acid chains and the interactions between chains. Its water binding capacity gives structure to tissues, lubricate joints and muscles. It also has good biocompatibility and autocrosslinking capability by reaction between –OH and –COOH.

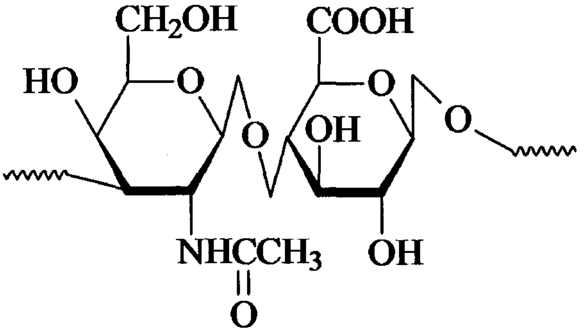

Figure 2-4 Structure of hyaluronic acid

So, significant interest has been generated in the applications of hyaluronic acid included ophthalmic viscosupplementation surgery [64-66], arthritis treatment [67], component of implant materials [68], scaffolds for wound healing and tissue engineering [69, 70], cancer metastasis control [71], biomedical hydrogels and biocompatible materials for artificial skin and bone filling [72], and novel drug carriers [73].

In detail, Gurny and his colleagues concluded that hyaluronic acid can directly interact with the cell membranes of the corneal tissue which resulted in the unique capability of prolonging the precorneal residence time of pilocarpine [74]. It conquered the problem of aqueous eye drops which have the disadvantage that more than 75% of the solution applied is lost due to drainage within the first 2 min after instillation.

Hyaluronic acid coatings are used for surface modification and tissue reconstruction for bone, cartilage and skin repair because of the prevention property of post-surgical tissue adhesion combined with its biocompatibility [75-78]. Particularly, hyaluronate coatings improved the biocompatibility of the luminal surfaces of small caliber artificial grafts [79]. In vitro studies showed that platelet adhesion on the coated surfaces was significantly reduced [79]. Coated drug carriers were used for breast cancer treatment [80]. It was shown that a controlled delivery of various bioactive compounds can be achieved using hyaluronic acid coated polylactide nanoparticles [81]. Surface modification of extrasynovial tendons with hyaluronic acid improved the gliding resistance of tendon grafts [82]. Hyaluronan has been utilized for the fabrication of drug eluting coatings for cardiovascular stents [83].

2.3.4 Heparin

Heparin was first discovered and isolated from canine liver cells by a second-year medical student named McLean in 1916 [84]. After that, understanding of the structure, properties and applications of heparin developed gradually.

Heparin is a linear polysaccharide composed with repeating disaccharide units of 1 → 4-linked pyranosyluronic acid and 2-amino-2-deoxyglucopyranose (glucosamine) residues, shown in the Figure 2-5. From the figure of structure of heparin, high content of negatively charged sulfo and carboxyl groups are observed, which results in the highest negative charge density of heparin compared to other known biological macromolecules [85].

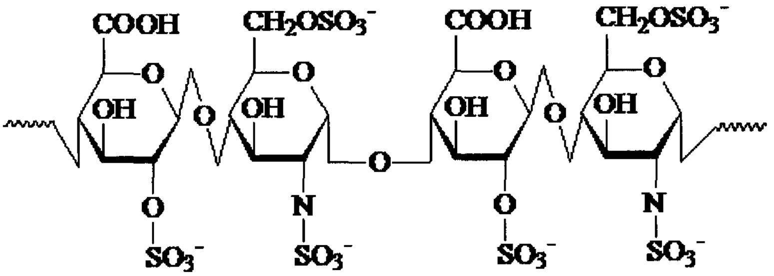

Figure 2-5 Structure of heparin

Heparin is the most frequently used agent for thrombin regulation, associated with its interaction with diverse proteins. The interaction between heparin and proteins resulted from the ion pairs which were formed between the clusters of positively charged basic amino acids on proteins and negatively charged sulfo and carboxyl groups on the heparin chain [85]. The interaction of heparin with antithrombin was the first reported case of a specific heparin—protein interaction [86]. Thrombin is a coagulation protein which can cause thrombosis when the thrombus generated and deposited on the surface of the materials used to construct or coat a variety of blood-contacting medical devices (e.g., catheters, vascular grafts, stents, extracorporeal circuits, intravascular chemical sensors, etc.). So, significant interests have been generated in the obtaining a surface that has fewer complications when in contact with blood. As an anticoagulant medicine, heparin can bind to the inhibitor antithrombin, significantly accelerating its reaction with many serine proteases, including thrombin [87]. This complex will prevent the formation of thrombus and improve blood compatibility [88]. So, heparin is sometimes called a blood thinner, although it does not actually thin the blood. Heparin will not dissolve blood clots that have already formed, but it may prevent the clots from becoming larger and causing more serious problems.

In recent years, increasing attention has been given to the use of heparin for the surface modification of biomedical implants and for the fabrication of new antithrombogenic biomaterials [85, 89]. Improved blood compatibility was achieved using chitosan–heparin complexes instead of pure chitosan [90-92]. The complexes were utilized for the surface modification of various biomaterials [93-95] and fabrication of advanced implant materials with controlled release of heparin [96-99].

2.4 Surface modification of biomaterials

2.4.1 Surface properties of biomaterials

Surface properties and composition of biomaterials can be designed for contact with body fluids. So, there are two key properties of biomaterials for the successful application. The bulk properties (e.g. tensile strength or stiffness) of a biomaterial are very important, especially when a biomaterial is used as an implant to carry out its functions, take up load, and withstand wear and tear in the rather harsh environment. However, the key factor which determines the success or failure of a biomaterial will be its surface property. It is found that surface plays an important role in a biological system for most biological reactions occurring at surfaces and interfaces. So surfaces are critical to the biocompatibility of biomaterials. Biocompatibility can be defined as an appropriate response that is within accepted tolerance limits of the host environment for a specific device and clinical application [100]. The surface characterization of biomaterials determines interaction with the body fluids and elicits a specific biological response [101].

The development of biomaterials for tissue engineering requires us to create the perfect surface which can provoke the specific cellular response and direct new tissue regeneration. The desired surface properties (e.g. biocompatibility or selectivity to a particular biomolecule) combined with the ideal bulk properties (e.g. tensile strength or stiffness for implants) will be possible for advanced biomedical implants.

For the improvement of the biocompatibility, corrosion protection, antimicrobial property and controlled degradation of implants, significant interest has been generated in the fabrication of films and coatings for the surface modification of biomedical implants [102-105]. There are many surface modification methods which can be utilized to tailor surfaces for specific applications, such as plasma treatments, sol-gel method, self assembly method, electrodeposition method and other methods. Usually more than one approach can satisfy the biomaterials requirements, and the ultimate selection must take into account the process reliability, reproducibility, and product yield [102].

2.4.2 Methods of surface modification

2.4.2.1 Plasma deposition

Plasma can be defined as a partially or wholly ionized gas with a roughly equal number of positively and negatively charged particles. The fourth state of matter, which is named so because plasma is neither gas nor liquid, is typically obtained when gases are excited into energetic states by radio frequency, microwave, and alternating or direct current. The energetic species (ions, electrons, radicals, and photons) in gas plasma will bombard the surface which contacted with the gas plasma and transfer their energy to the solid. These energy transfers provide a highly unusual and reactive chemical environment to change the surface properties of normally inert materials like ceramics without changing the bulk properties of the materials.

Therefore, plasma-surface modification will be an economical and effective materials processing technique for the surface modification of biomaterials because of the following advantages [105]: easy preparation; unique film chemistry; coated on various substrates with good adhesion; conformal and pin-hole free films; excellent permeation barriers with low level of leachables; sterile upon preparation.

The studies of Hanawa et.al. [106] showed promising results of plasma surface modification of titanium which improved the bone-conductivity through the formation of a calcium phosphate film by using calcium ion implantation into titanium. It is clear that calcium ion implantation accelerates calcium phosphate precipitation in titanium and a larger amount of new bone is formed on calcium ion implanted titanium compared to unimplanted titanium 2 days after implantation into rat tibia [107].

2.4.2.2 Sol-Gel method

Sol-gel is a wet-chemical technique for material fabrication. Generally speaking, the sol-gel process involves the transition of a system from a liquid “sol” into a solid “gel” phase. Inorganic metal salts or metal organic compounds are always used as the starting materials for the preparation of the sol. Then a chemical solution will be used to react with the starting materials to produce colloidal particles of metal oxide. The reaction is composed with simultaneous hydrolysis and condensation once the hydrolysis reaction has been initiated, resulting in the formation of an inorganic network of oxo (M-O-M), similar to the structure of polymeric materials. Further treatments such as dip, spin and spray will result in a rigid, porous network of gel and produce thin films on substrates.

The advantages of sol-gel thin film processing including low temperature processing, ease of fabrication, precise microstructure and chemical control induced intense research for biomedical applications. Typical applications of sol–gel biomaterials include selective coatings for biosensors, surface modification of metallic implants, matrices for encapsulation of enzymes, proteins and other compounds, immunoadsorbent and solid-phase extraction materials, controlled release of drugs and solid-phase biosynthesis [108].

Cheng et.al. [109] utilized sol-gel dip-coating with TiO_2 on the NiTi substrate, and then employed hydrothermal treatment to crystallize and densify the amorphous film and to remove the organic residue. The results of electrochemical tests such as electrochemical impedance spectroscopy (EIS) and polarization studies indicated a significant increase in the corrosion resistance.

2.4.2.3 Self assembly method

Self assembly (SA) can be defined as the processes in which a disordered system of pre-existing components forms an organized structure or pattern as a consequence of specific, local interactions among the components themselves, without external direction. There are two characteristics of SA. First of all, SA is thermodynamically stable, which means that in order for self assembly to take place without the intervention of external forces, the process must lead to a lower Gibbs free energy, and thus self-assembled structures are thermodynamically more stable than the single, unassembled components.

A direct consequence is the general tendency of self-assembled structures to be relatively free of defects. Secondly, SA is mediated by weak noncovalent interactions such as hydrogen bonds, electrostatic interactions and Van der Waals interactions.

SA is a very important technique for biomedical applications. Because of the unique properties of SA, we can design materials whose morphology is responsive to specific environmental cues. Therefore, the structure and consequent biological functions of such materials are responsive to the environment and can be controlled. Decher et.al. developed the electrostatic self assembly technique for the formation of multilayer thin films which allowed detailed structural control at the molecular level with ease of manufacturing [110]. This technique provides an effective approach to incorporate various biomaterials on substrate surfaces, and gives great opportunity to develop unique biocompatible materials with well controlled interfaces between the living system and the implanted material. Wang et.al. synthesised and characterized multi-layer thin films on gold-coated glass with various biocompatible materials such as alumina, zirconia, titania, PDDA, and PVP by using the SA process [111].

2.4.3 Electrodeposition

Electrodeposition is generally defined as the deposition of a substance on an electrode by the action of electricity (especially by electrolysis). It has a very long history since it was discovered by Luigi V. Brugnatelli, an Italian professor, who was able to electrodeposit gold on the surface of a metallic object in 1805. After that, electrodeposition is widely used commercially for covering the surface of various kinds of metallic objects with thin coatings of metals for corrosion protection and decorative purposes.

Recently, significant interest has been generated in the application of electrochemical processing techniques for the fabrication of thin films, coatings and fibers for biomedical applications [112-114]. This is mainly because electrodeposition offers lots of advantages compared with other surface modification techniques, such as high purity of deposited materials, to the possibility of uniform deposition on substrates of complex shape, rigid control of the composition and microstructure of deposits, low cost of equipment and materials, and easy scale up to industry level.

There are two commonly used processes of electrodeposition: electrophoretic deposition (EPD) and electrolytic deposition (ELD). EPD is a process in which charged particles, suspended in a liquid medium, migrate and deposit on an electrode under the influence of an electric field. ELD is a process in which particles are produced in electrochemical reactions from solutions of metal salts and precipitate at the electrode surface to form a deposit. Figure 2-6 shows such a difference of mechanisms [115].

Successful application of electrodeposition requires understanding of deposition mechanisms. It is important to note that the deposit formation in both EPD and ELD processes is achieved via particle coagulation. So a thorough understanding of the mechanisms of particle coagulation is crucial for successful electrodeposition.

The classical Derjaguin-Landau-Verwey-Overbeek (DLVO) theory of colloidal stability can be used for the understanding of EPD and ELD deposition mechanisms through particle interaction considerations.

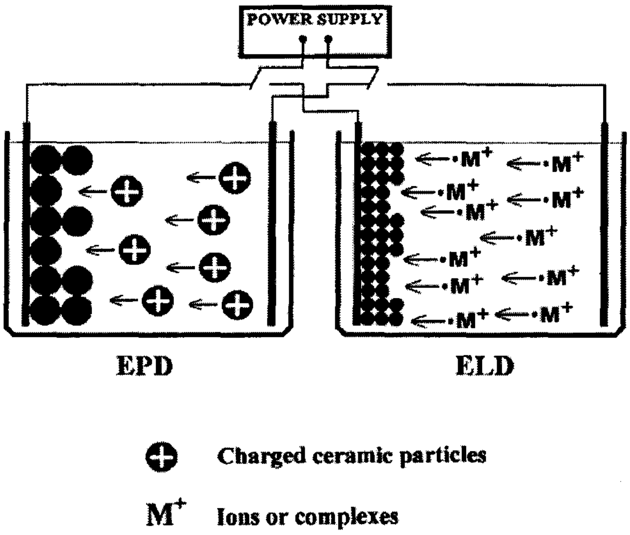

Figure 2-6 Schematic of cathodic electrophoretic deposition (EPD) and electrolytic deposition (ELD), showing electrophoretic motion of positively charged particles and ions (M^+) [115].

2.4.3.1 The DLVO theory

The DLVO theory quantitatively described the relationship between stability of suspensions and energies of interactions between colloidal particles and other surfaces in a liquid [116, 117]. According to this theory, the stability of a colloidal system is determined by the total pair interaction between colloidal particles, which is composed of coulombic double-layer repulsion and Van der Waals' attraction.

The total energy V_T of interaction of two isolated, identically charged particles may be defined as:

$$V_T = V_A + V_R \qquad \textbf{(2.1)}$$

The attractive energy V_A is the London-van der Waals' interaction between two spherical particles which can be expressed by:

$$V_A = -\frac{A}{6}\left(\frac{2}{s^2-4} + \frac{2}{s^2} + \ln\frac{s^2-4}{s^2}\right) \qquad \textbf{(2.2)}$$

where A is the Hamaker constant and s = 2 + H/a, with H the shortest distance between the two spheres and a is the particle radius. If H << a, Equation (2.2) can be simplified to:

$$V_A = -A\frac{a}{12H} \qquad \textbf{(2.3)}$$

The repulsive energy V_R is the coulombic double-layer repulsion which can be expressed by:

$$V_R = 2\pi\varepsilon\varepsilon_0 a\psi^2 \ln[1+e^{-\kappa H}] \qquad \textbf{(2.4)}$$

where ε is the dielectric constant of the solvent, ε_0 is the dielectric permittivity of free space, ψ is the surface potential, 1/κ is the Debye length:

$$\kappa = \left(\frac{e^2\sum n_i z_i^2}{\varepsilon\varepsilon_0 kT}\right)^{1/2} \qquad \textbf{(2.5)}$$

where e_0 is the electron charge, k is the Boltzmann constant, T is the absolute temperature, n_i is the concentration of ions with valence z_i. Repulsion between colloidal particles is directly related to the diffuse layer charge on the particles.

The DLVO theory describes the potential energy curve for pair interaction, as shown in Figure 2-7(a). When the diffuse-layer repulsion is sufficiently high compared to the van der Waals' attraction, the total energy of particle interaction exhibits a maximum, which makes an energy barrier to particle coagulation.

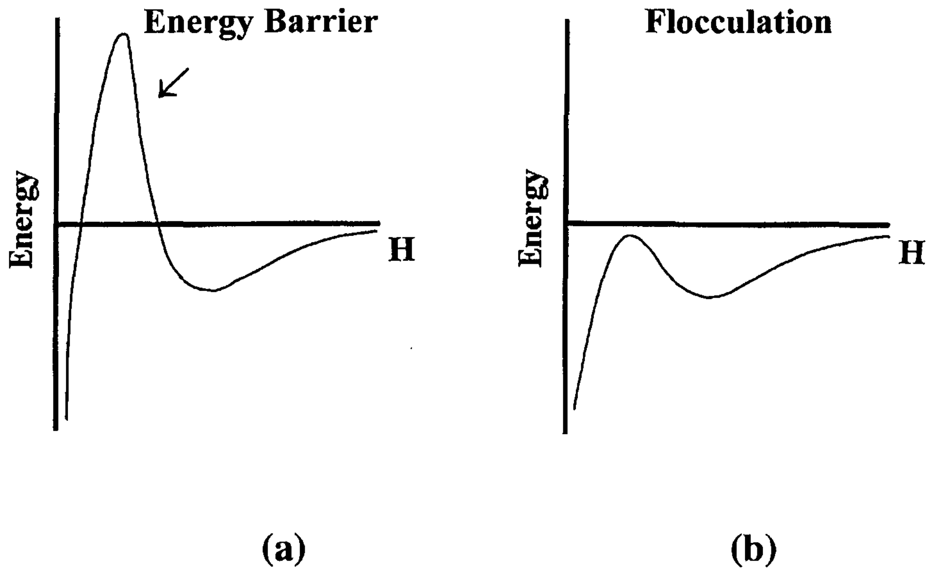

Figure 2-7 Total interaction energy between spherical particles as a function of interparticle separation according to the DLVO theory.

The thickness of the double layer (characterized by the Debye length, $1/\kappa$) is very sensitive to the electrolyte concentration [116, 117]. The DLVO theory explains the existence of a critical electrolyte concentration (flocculation value) for coagulation, decreasing with the valence of the electrolyte ions of a charge opposite to that of the colloidal particles (rule of Schulze and Hardey [116, 117]). It was demonstrated that the potential energy peak decreases as the electrolyte concentration increases. As the energy barrier disappears, coagulation becomes possible (Figure 2-7(b)).

Flocculation by ions compressing the double layer also follows the Hofmeister series [116, 117]. Therefore, a negatively charged sol is flocculated by large cations at a smaller concentration than by small cations of the same valency. In conclusion, flocculation values are affected by sol concentration, temperature, particle size of the colloid, and chemical nature of the sol.

2.4.3.2 Solvents

A solvent acts as a vehicle that carries the particles in suspensions (EPD) or ions in solutions (ELD). The solvent used in electrodeposition must dissolve inorganic salts and organic additives. Water and organic liquids are two principal types of solvent for electrodeposition [12, 118-121].

For ELD, a sufficient amount of water is needed for base generation. However, adsorbed water in green deposits leads to shrinkage and cracking during drying. In regarding to this, non-aqueous solvents can prevent the deposit from hydrating. For example, mixed methyl alcohol-water and ethyl alcohol-water solutions were found to be preferable in order to reduce cracking and porosity in the electrolytic deposits [120, 122]. The addition of alcohols to aqueous solutions reduces the total dielectric constant of the solvent, and thus reduces the solubility of the deposits.

Solvents for EPD should be inert with respect to the powder. The use of water-based suspensions will cause gas formation from the hydrolysis of water, which prevents the deposition of a uniform adherent layer and yields pinholes. Therefore organic liquids are superior to water as a suspension medium for EPD.

2.4.3.3 Binders

As mentioned above, the usage of water solvent may result in shrinkage and cracking during drying. So the binder is such a material which can be added to suspensions or solutions in order to increase the adherence and strength of the deposited material and prevent cracking. The optimal amount of binder depends on the particle size and particle surface area [115].

In the EPD process, there are generally two types of binders. The most common type of binder in electrophoretic deposition is the non-ionic-type polymer such as polyvinyl alcohol, polyvinyl butyral, ethyl cellulose, polyacrylamide and so on [123]. The polymer macromolecules adsorb onto the surfaces of ceramic particles. Positively charged ceramic particles provide electrophoretic transport of the polymeric molecules to form deposits on cathodic substrates. Recently, significant interest has been generated in another type of binder—the charged polyelectrolytes. This is because the application of neutral polymers presents difficulties for electrodepositon. The polyelectrolytes with inherent binding properties could be used for particle charging and electrophoretic deposition [123]. The charged polyelectrolytes include cationic polyelectrolytes, such as poly(dimethyldiallylammonium chloride) (PDDA), polyethylenimine (PEI), chitosan (CHIT), poly(vinylamine) (PVA) or poly(allylamine hydro-chloride) (PAH) and anionic polyelectrolytes such as alginate (ALG), and hyaluronate (HYA).

The role of binders in EPD processing is multifunctional. Polymer binders are used to obtain adherent deposits and prevent cracks. Moreover, the adsorbed polymer can provide steric stabilization of a suspension of particles and reduce viscosity of the suspension. The included polymer also may provide some functional groups which may be very important for the properties of the surfaces. For example, CHIT, ALG and HYA can also be used to improve the biocompatibility of the implants in biomedical applications [124, 125].

2.4.3.4 Suspension stability and particle charging

A suspension for EPD is a complex system, in which each component has a substantial effect on deposition efficiency, so it is important to obtain well dispersed and stable suspensions. Generally speaking, suspensions can be dispersed by electrostatic, steric or electrosteric stabilization mechanisms. Ceramic particles must be electrically charged to permit forming by EPD [123].

In aqueous media, the charge at the particle-solvent interface could originate from adsorption or desorption of ions, or dissociation of surface groups. Surfaces of oxide particles dispersed in water tend to coordinate water molecules to form hydroxylated surfaces. The surfaces may become positively or negatively charged, depending on pH [123]:

$$\mathbf{M\text{-}OH + H^+ \Leftrightarrow M\text{-}OH_2^+} \qquad \mathbf{(2.6)}$$

$$\mathbf{M\text{-}OH + OH^- \Leftrightarrow M\text{-}O^- + H_2O} \qquad \mathbf{(2.7)}$$

According to the DLVO theory, colloidal stability is related to the ζ potential of the colloidal particles. As shown in Figure 2-8 [123], ζ potential is positive for low pH values and negative at high pH.

In non-aqueous media, particle charging is achieved by electron transfer between the particle and solvent [123]. Damodaran and Moudgil [126] proposed a mechanism of particle charging in which the adsorbed alcohol ionizes into a protonated alcohol and an alkoxide ion, following by the dissociation of the protonated alcohol. The alkoxide ion then desorbs into the solution, leaving the proton on the particle surface.

A pure alcohol can ionize in the following way:

$$\mathrm{RCH_2OH + RCH_2O\text{-}H \rightarrow RCH_2O^- + RCH_2OH_2^+} \quad (2.8)$$

and an aqueous alcohol ionizes as follows:

$$\mathrm{RCH_2O\text{-}H + H_2O \rightarrow RCH_2O^- + H_3O^+} \quad (2.9)$$

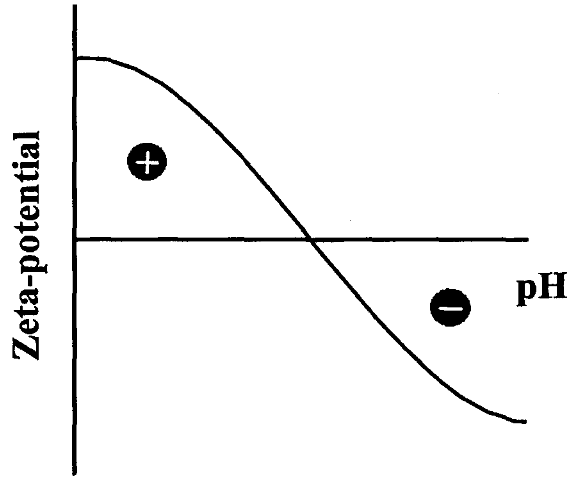

Figure 2-8 Zeta potential of ceramic particles versus pH of suspension [123].

A wide variety of additives can be used to control particle charge and produce well-dispersed suspensions. For example, the addition of acids has a dispersing effect and results in the development of surface charge [126]. Polyelectrolytes are widely used additives which can impart electrostatic and steric stabilization to a colloidal dispersion [123]. The charge on a colloidal particle could also be caused by dispersants such as phosphate ester, menhaden fish oil, and ethoxylate [127].

So, it can be concluded that the important factors when selecting a binder-dispersant-solvent system are: chemical compatibility of components; solubility of binder and additives; particle charge; viscosity and electric resistivity of the suspension [123].

2.4.3.5 Electrophoretic deposition

2.4.3.5.1 Mechanism of electrophoretic deposition

Electrophoretic deposition (EPD) [112, 113, 128, 129] is an attractive colloidal processing technique, which has generated substantial attention for the fabrication of thin films and coatings of organic, inorganic and composite materials for biomedical applications. EPD is achieved via the motion of charged particles towards an electrode under the influence of an electric field and deposition of the particles at the electrode surface. It is important to note that electrode reactions are not involved in the EPD [115]. The mechanisms of EPD have been discussed in numerous publications. One hypothesis is that charged particles undergo reactions at the electrode, which reduce their surface charge or neutralize them. A difference in pH near electrodes compared with the rest of the suspension is believed to play a major role in this reduction of charge.

There are two types of EPD processes: anodic and cathodic processes. In aqueous solutions, the electrolysis of water is the major electrochemical process which can be shown by the following two electrode reactions:

Anode: $2H_2O \rightarrow O_2 + 4H^+ + 4e^-$ **(2.10)**

Cathode: $4H_2O + 4e^- \rightarrow 4OH^- + 2H_2$ **(2.11)**

In anodic EPD, the negatively charged particles react with the positively charged hydrogen ions (protons) which are produced by the reaction (2.10) at the anode. Then the neutralized particles form deposits at the anode. In cathodic EPD the positively charged colloidal particles are neutralized by electrogenerated base produced in reaction (2.11) and form cathodic deposits. According to Hamaker and Verwey [130, 131], the deposition yield in the electrophoretic process can be described by the Hamaker equation:

$$Y = \mu EtSC_s \qquad \textbf{(2.12)}$$

where Y is the mass of a deposit obtained during deposition time t on the electrode area S, and μ and C are mobility and concentration of polymer macromolecules or inorganic particles, respectively.

This equation gives us a useful starting point for the refinement of the description of deposit formation rates in the EPD process. However, it only describes the EPD process from suspensions containing single component particles. Further work is still needed for the development of theories of electrophoretic co-deposition process.

Significant interest has been generated in the application of EPD for surface modification of materials for biomedical applications [122, 132, 133] because of the advantages of this method compared with other surface modification methods. It can produce high purity coatings; can apply to substrates of complex shape; enables rigid control the composition and microstructure of deposit; and is based on the use of low cost equipment and materials. Another important advantage of EPD is that it can be used to fabricate bone substitute materials which have composite microstructures similar to that of real bone.

2.4.3.5.2 Bone structure

It was found that bone has a hierarchical structure which enables diverse mechanical, biological and chemical functions [134, 135]. Figure 2-9 shows these different levels and structures: (1) the macrostructure: cancellous and cortical bone; (2)

the microstructure (from 10 to 500 mm): Haversian systems, osteons, single trabeculae; (3) the sub-microstructure (1–10 mm): lamellae; (4) the nanostructure (from a few hundred nanometers to 1 mm): fibrillar collagen and embedded mineral; and (5) the sub-nanostructure (below a few hundred nanometers): molecular structure of constituent elements, such as mineral, collagen, and non-collagenous organic proteins [134].

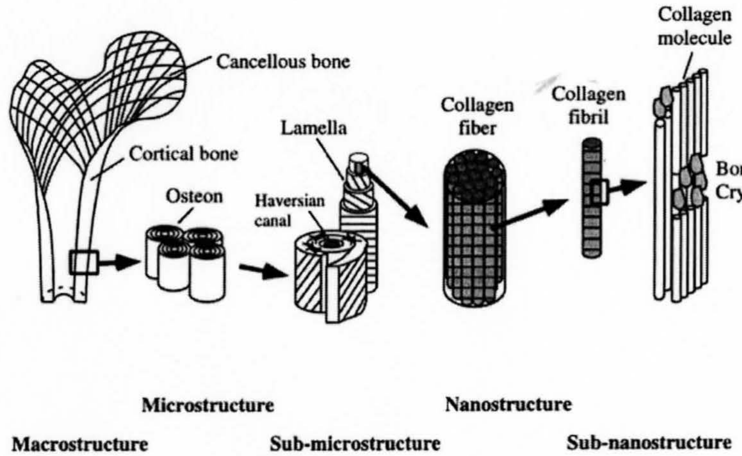

Figure 2-9 Hierarchical structural organization of bone [134]

The sub-nanostructure of bone is composed of mineral crystals, collagen and non-collagen polymers and they form a multilayer structure which can be observed in Figure 2-9. It was found that the mineral crystals of hydroxyapatite grow with a specific crystalline orientation—the c axes of the crystals are roughly parallel to the long axes of the collagen fibrils. The preferred orientation plays an important role in the mechanical and other properties of bone. Recently, it was discovered [136] that polysaccharides form the interface between the organic and mineral components, and govern the crystallization and orientation of mineral crystals.

2.4.3.5.3 EPD of organic-inorganic composite coatings

As was mentioned, bone has a complex collagen-fiber-reinforced microstructure and nanostructure, which result in a relatively high fracture toughness. However, pure HA is a brittle polycrystalline ceramic with low fracture toughness because of its properties and microstructure. Therefore, despite the advantageous bioactivity of HA, its poor mechanical properties have limited its clinical use. One solution to this problem is to use HA to produce bioactive coatings on metal implants. Such coatings promote the attachment of bone tissue and provide a mechanically stable interface between implant and bone [137].

Plasma spraying is the current commercial technique to apply HA coatings. However, the high processing temperatures result in thermal decomposition of HA. Moreover, it will induce phase transformations and oxidation of metallic substrates at elevated temperature.

Considering the composition and structure of natural bone, an alternative is to fabricate novel bioactive HA-polymer nanocomposite coatings instead of the pure HA coating by EPD. Then all the problems related to the sintering of HA can be eliminated by the fabrication of ceramic-polymer composites. Moreover, the addition of different polymers with different functional groups will include other functional properties to the implants including chemical stability, bioactivity, biocompatibility, and antimicrobial properties. Plasma-spraying and chemical/physical vapour deposition showed difficulties to achieve this goal. Therefore EPD will be a promising method for the fabrication of bone substitute materials containing polysaccharides, which have similar composite microstructure as natural bone.

3 Objective

- Development of EPD methods for the fabrication of advanced organic-inorganic composite coatings for metallic substrates:
    - Composite coatings containing heparin, chitosan, and HA
    - Composite coatings containing hyaluronic acid and HA
    - Composite coatings containing alginate, HA, heparin and hyaluronate
- Development of new deposition mechanisms for the fabrication of advanced organic-inorganic composite coatings.
- Development of new coating structures for the composite coatings in the form of monolayers, laminates, and functionally graded materials.
- Investigations of the chemical composition, microstructure, corrosion protection, and other functional properties of the nanocomposite coatings.

4 Experimental Procedures

4.1 Starting Materials

$Ca(NO_3)_2 \cdot 4H_2O$, $(NH_4)_2HPO_4$, NH_4OH, chitosan (degree of deacetylation of about 85%), acetic acid (Aldrich), sodium alginate (M_w = 12 to 80 kDa), heparin sodium salt (Alfa Aesar) and sodium hyaluronate (Alfa Aesar) were used for the fabrication of HA powders and EPD of composite coatings.

Stoichiometric HA nanoparticles were prepared by a wet chemical technique described in literature [11]. Precipitation was performed at 70 °C by the slow addition of a 0.6 M ammonium phosphate solution into a 1.0 M calcium nitrate solution. The pH of the solutions was adjusted to 11 by NH_4OH. Stirring was performed during 8h at 70 °C and then 24 h at room temperature. The precipitate was washed with water and finally with ethanol. It has been previously reported [40] that the average length of the needle shaped HA crystals, prepared by this method, is about 200 nm and the average aspect ratio is 8. The long axis of the needles corresponded to the c-axis of the hexagonal HA structure.

4.2 Fabrication by EPD method

4.2.1 Experimental setups for electrodeposition

The electrodeposition cell included a substrate centered between two Pt counter electrodes. The distance between the substrate and counter electrodes was 15 mm. The volume of the cell was 300 ml. An electrophoresis power supply EPS 601 (Amersham

Biosciences) was employed to provide the DC electric field for electrodeposition, either in a constant current density (galvanostatic) or a constant voltage mode.

4.2.2 Preparation of solutions and suspensions for electrodeposition

Chitosan was dissolved in a 1% acetic acid solution, which was then used to prepare 0.5 g/L chitosan solutions containing heparin or HA. The solutions with 0.5 g/L chitosan and different concentrations of heparin (0-0.2 g/L) were prepared for deposition. The heparin should be added into the solutions slowly in order to avoid precipitation. The suspensions of HA particles in the chitosan solutions were ultrasonicated for 30 min to achieve a homogeneous dispersion. Electrodeposition was performed in pure water and mixed ethanol-water solvents.

0-1.0 g/L sodium hyaluronate solutions were prepared in mixed ethanol-water solvent. Then 0.5-4.0 g/L HA was added into the solutions. The suspensions of HA particles in the sodium hyaluronate solutions were ultrasonicated for 30 min to achieve a homogeneous dispersion.

4 g/L sodium alginate solutions in water were prepared , which were then used to prepare 0.5-1.0 g/L alginate solutions containing HA, heparin and hyaluronic acid. The suspensions of HA particles in the sodium alginate solutions were ultrasonicated for 30 min to achieve a homogeneous dispersion.

4.2.3 Electrodeposition procedure

Cathodic and anodic deposits were obtained on various conductive substrates under constant current or constant voltage conditions. These substrates include stainless steel 304 foils (50×50×0.1 mm), Nitinol wires (0.4 mm diameter), Nitinol foils (50×50×0.2 mm), Pt foils (50×50×0.1 mm) and graphite plates (10×50×0.1 mm).

The deposition time was varied in the range of 0-10 min to obtain deposits with different thicknesses. The coatings obtained were dried in air at room temperature. Multilayer coatings were prepared by alternate deposition from different solutions without waiting after the deposition of individual layers.

4.3 Characterization

4.3.1 Investigation of deposition yield

The electrodeposition yield was studied by weighting the deposited coating. A Mettler Toledo AX105 DeltaRange analytical balance, which has a readability of 0.01 mg, was used to measure the weight of the foil substrate before and after the deposition, followed by drying at room temperature for 24 hr. Then the weight of a deposited coating was obtained.

4.3.2 X-ray diffraction analysis

X–ray diffractometry (XRD) was used for the analysis of as-prepared HA powders and composite coatings. A diffractometer (Nicolet 12) with monochromatized Cu Kα radiation at a scanning speed of 1°/min was used to determine the crystallinity and phase content of powders and coatings and orientation of the HA nanocrystals in the coatings.

4.3.3 Thermogravimetric and differential thermal analysis

Thermogravimetric analysis (TGA) is an analytical technique used to determine a material's thermal stability and fraction of volatile components by monitoring the weight change that occurs as a specimen is heated. In addition to weight changes, the instruments also record the temperature difference between the specimen and one or more reference pans (differential thermal analysis, DTA), which can be used to monitor the energy released or absorbed via chemical reactions or phase transformations during the heating process.

In this work, the deposits removed from Pt substrates were studied by TGA and DTA, carried out in air at a heating rate of 5 °C/min using thermoanalyzer (Netzsch STA–409).

4.3.4 Scanning electron microscopy

The surface morphology and microstructures of the deposited coatings were studied by scanning electron microscopy (SEM) using a JEOL JSM-7000F scanning electron microscope.

4.3.5 Fourier transform infrared spectroscopy

Fourier Transform Infrared Spectroscopy (FTIR) is an analytical technique used to identify organic (and in some cases inorganic) materials. This technique measures the absorption of various infrared light wavelengths by the material of interest. These infrared absorption bands identify specific molecular components and structures.

In this work, the deposits removed from Pt substrates were studied by FTIR using

Bio-Rad FTS-40 instrument.

4.3.6 Electrochemical methods

The protective properties of the composite coatings were studied by electrochemical methods using a potentiostat (PARSTAT 2273, Princeton Applied Research) controlled by a computer using the PowerSuite electrochemical software package.

A conventional three-electrode cell was utilized, with a platinum plate being the counter electrode and a saturated calomel electrode (SCE) as the reference electrode. The sample to be tested was placed as a working electrode, with a surface area of 1 cm^2 exposed to the testing solution. Testing was carried out in Ringer's physiological solution (NaCl 8.6 g/l, $CaCl_2 \cdot 2H_2O$ 0.33 g/l, KCl 0.30 g/l), which acted as the simulated body fluid.

There are two testing methods which are often utilized: Tafel plot and electrochemical impedance spectroscopy.

The Tafel technique provides a fast way of determining the corrosion rate of a specimen. In a typical experiment, a controlled potential scan was programmed to take place within ±250 mV of the corrosion potential of the specimen. The scan rate of the potentiodynamic polarization was set at 1 mV/s in this work. The resulting current is logarithmically plotted versus the potential (log current versus potential). The corrosion rate can be calculated from the Tafel plot data.

Electrochemical impedance spectroscopy (EIS) has been successfully applied to the study of corrosion systems for thirty years and been proven to be a powerful and accurate method for measuring corrosion rates. To make an EIS measurement, a small amplitude signal, usually an AC potential between 5 to 10 mV, is applied to an electrochemical cell over a range of frequencies of 0.001 Hz to 100,000 Hz. The real (resistance) and imaginary (capacitance) components of the impedance of the electrochemical system are recorded by measuring the current through the cell. The data will be presented in the form of Nyquist plot (imaginary part versus real part of the impedance). In this work, the corrosion protection properties of the obtained coatings were studied using EIS in the Ringer's solution. The measurements were performed at open circuit potential with perturbation signal amplitude of 10 mV. The spectra were acquired in a frequency range of 10 mHz–100 kHz.

4.3.7 Antithrombin adsorption test

The potential anticoagulant activity of the coated surfaces was assessed by evaluating the ability of heparin to bind ^{125}I-antithrombin. Antithrombin (Affinity Biologicals, Ancaster, ON) was labelled with Na^{125}I using the IODO-GEN method and Iodination Reagent (Pierce Chemical, Rockford, IL). The labelled protein solution was dialyzed overnight against phosphate buffered saline (PBS, pH 7.4) with three changes of buffer to remove unreacted iodide. The protein solutions for adsorption studies consisted of 0.15 mg/mL antithrombin (typical physiological plasma concentration) in PBS (98% unlabelled and 2% labelled protein).

Substrates with coatings were cut into 5×5 mm pieces. Then surfaces were incubated in 0.25 mL of the solution for 3 h at room temperature, rinsed three times in PBS (5 min each), dried, placed in counting vials and the radioactivity was determined.

5 Experiment Results and Discussions

5.1 EPD of chitosan with hydroxyapatite or heparin

5.1.1 Codeposition of chitosan and hydroxyapatite

5.1.1.1 XRD investigations

Figure 5-1 compares the X-ray diffraction patterns of the film deposited from the 0.5 g/L chitosan solution, as-prepared hydroxyapatite and films deposited from the 0.5 g/L chitosan solutions, containing 0.5 and 1 g/L hydroxyapatite.

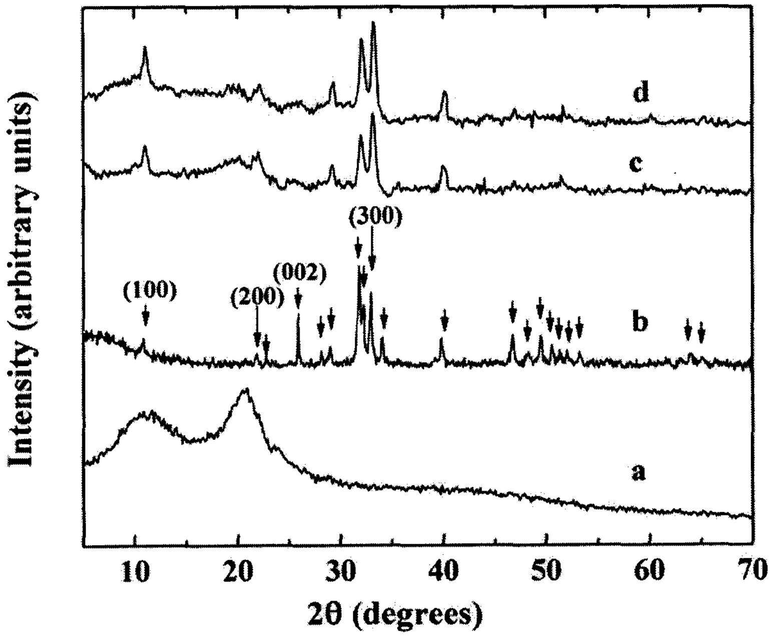

Figure 5-1 X-ray diffraction patterns of (a) the chitosan film, (b) as-prepared HA, and films prepared from the 0.5 g/L chitosan solutions containing (c) 0.5 g/L HA and (d) 1 g/L HA, deposition voltage of 20 V, arrows show peaks of HA corresponding to JCPDS file 09-0432.

The XRD pattern of the chitosan films revealed very broad peaks at $2\theta \sim 10^\circ$ and $\sim 21^\circ$. The XRD studies of as-prepared hydroxyapatite powders showed diffraction peaks corresponding to the JCPDS file 09-0432 of hydroxyapatite, with the (2 1 1) peak having the highest intensity. X-ray studies of the films prepared from the 0.5 g/L chitosan solutions, containing 0.5 and 1 g/L hydroxyapatite showed X-ray diffraction peaks of hydroxyapatite. A broad peak around $2\theta \sim 21^{\circ}$ can be attributed to chitosan. The X-ray diffraction patterns (Figure 5-1c and d) indicated the formation of composite films, containing hydroxyapatite.

The XRD patterns presented in Figure 5-1c and d showed increased intensity of the (1 0 0), (2 0 0) and (3 0 0) peaks. The intensity of the (3 0 0) peak was found to be higher than that of the (2 1 1) peak. And the (0 0 2) peak was suppressed. The analysis of the X-ray diffraction patterns of the composite films indicates the preferred orientation of the c-axis of the hydroxyapatite crystals parallel to the film surface.

It is important to note that the preferred orientation of hydroxyapatite crystals was observed in natural bones. Studies of natural bones revealed the interactions between organic and inorganic components in the lamellar organic-inorganic bone microstructure, which influence the orientation of hydroxyapatite nanoparticles and mechanical properties of bone. The orientation of hydroxyapatite nanoparticles can result from the interaction of hydroxyapatite with amino groups of chitosan. It was shown that chitosan and other polysaccharides can chelate Ca^{2+} ions.

Recently it was discovered that polysaccharides form interfaces between organic and inorganic components in bones and govern the crystallization of hydroxyapatite nanoparticles. This discovery has generated a new wave of interest in the fabrication of bone substitute laminate materials containing chitosan and other polysaccharides.

5.1.1.2 SEM studies of composite coatings

Pure hydroxyapatite deposits formed by EPD must be sintered in order to obtain dense and adherent films. However, sintering of such deposits presents difficulties attributed to the sintering shrinkage of the deposited materials, differences in the thermal expansion coefficients of films and metallic substrates, chemical reactions between the deposited materials and metallic substrates at elevated temperatures, and thermal and chemical degradation of metallic substrates at elevated temperatures. Moreover, the microstructure and properties of sintered hydroxyapatite are different from those of natural nanostructured hydroxyapatite.

The use of chitosan enables the room temperature processing of composite films and avoids the sintering problems. Dispersion stability and particle charging are important factors for film fabrication by EPD. Chitosan provided electrosteric stabilization of hydroxyapatite particles in suspensions and allowed cathodic electrodeposition of composite films. Moreover, the binding and film forming properties of chitosan were beneficial for the fabrication of the composite films.

Figure 5-2 shows SEM images at different magnifications of composite deposits on stainless steel substrates prepared from the 0.5 g/L chitosan solutions, containing (a and b) 0.5 g/L HA and (c and d) 1 g/L HA. The needle-shaped HA crystals are arranged in a chitosan matrix. The SEM pictures indicate that the coatings obtained are crack free. By comparison of images (a) and (c) or (b) and (d), we found that higher HA concentration in solutions resulted in higher HA content in the deposit.

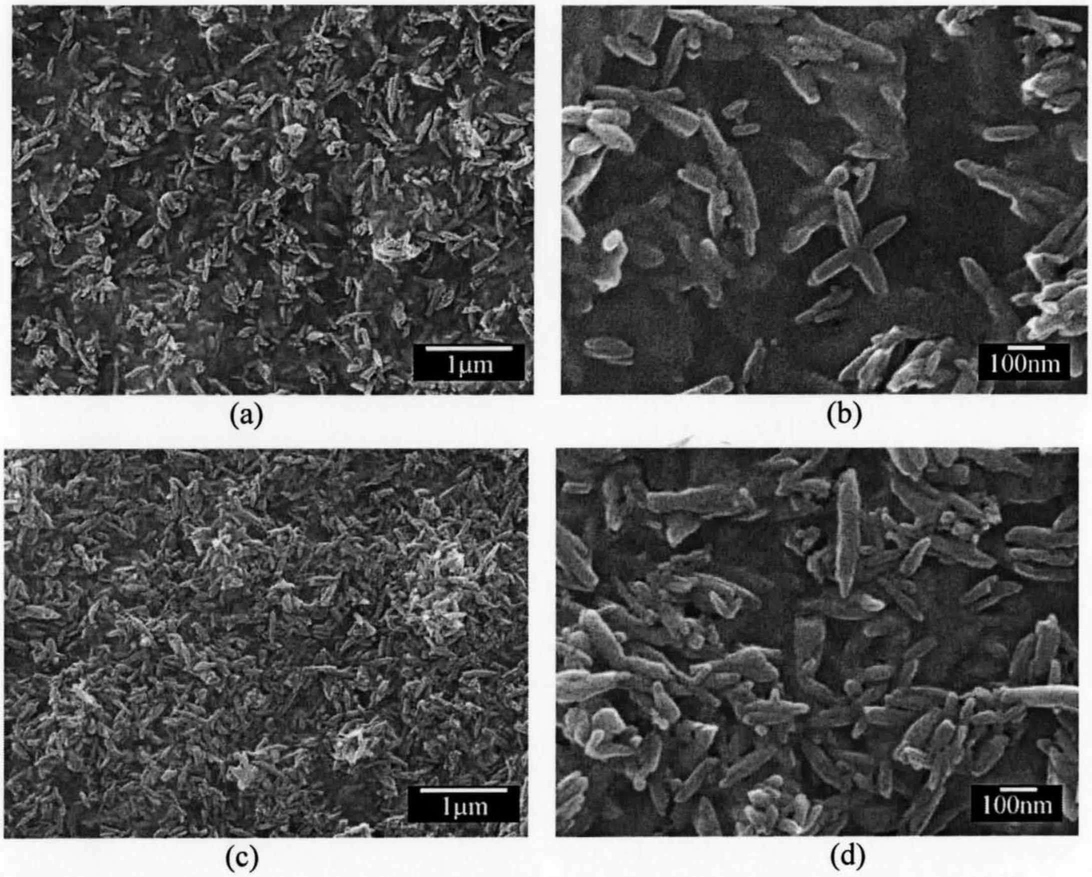

(a) (b) (c) (d)

Figure 5-2 SEM images at different magnifications of composite deposits on stainless steel substrates prepared from the 0.5 g/L chitosan solutions, containing (a and b) 0.5 g/L HA and (c and d) 1 g/L HA at deposition voltage of 20V.

Figure 5-3 shows SEM images of composite deposits prepared from the 0.5 g/L chitosan solutions containing 1 g/L HA on Nitinol wires. The monolayer film was about 20 μm. It was dense, crack free and relatively uniform.

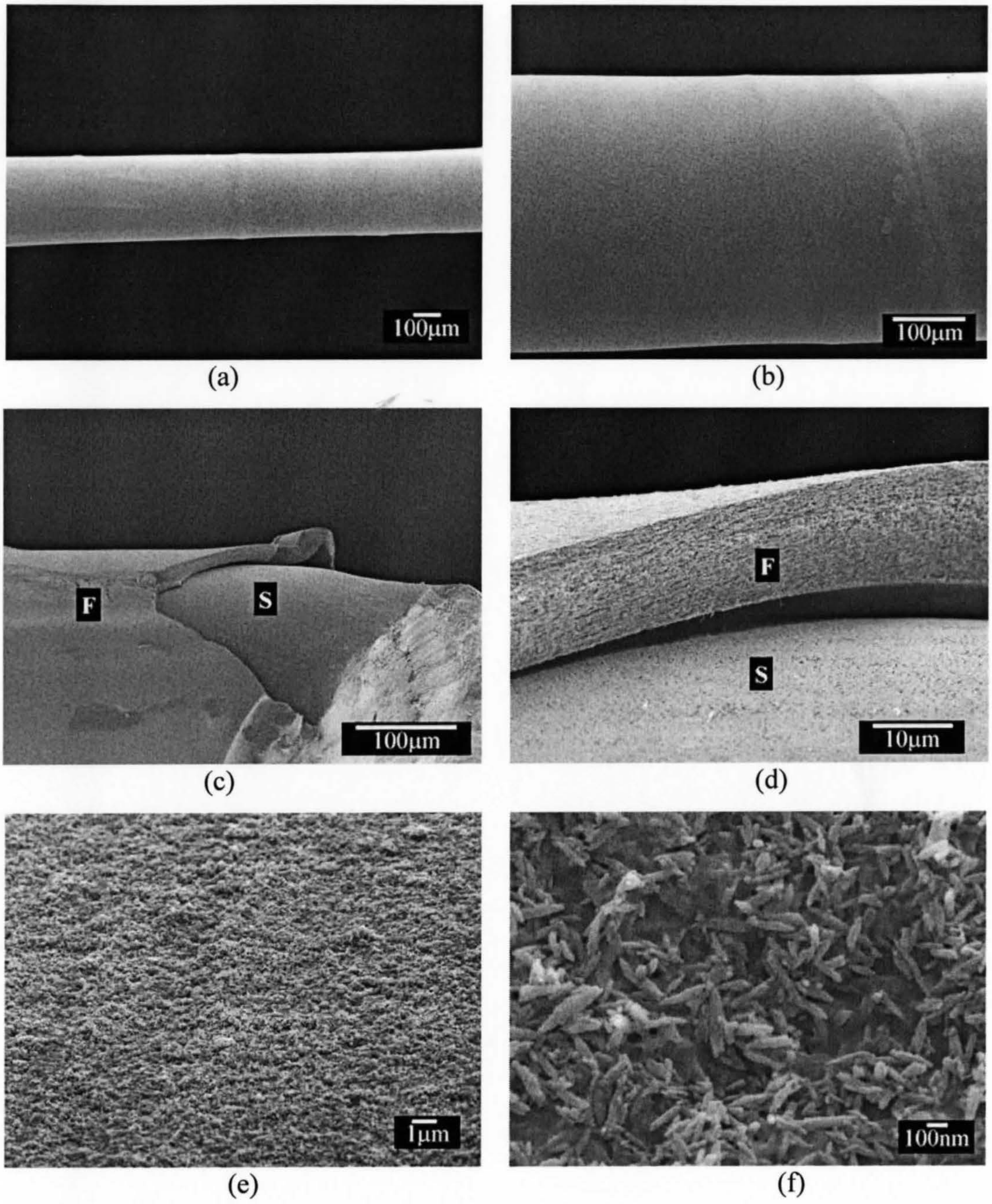

(a) (b)
(c) (d)
(e) (f)

Figure 5-3 SEM images at different magnifications of the composite films prepared from the 0.5 g/L chitosan solution containing 1 g/L HA at the deposition voltage of 20V on the Nitinol wire substrates (F-film, S-substrate).

5.1.1.3 FTIR studies of composite coatings

FTIR studies of the composite deposits showed spectra, similar to the spectra of HA–chitosan composites, prepared by other methods. The spectrum in Figure 5-4 shows a broad peak around 3450 cm^{-1} related to hydroxyl stretching and a peak at 1638 cm^{-1} attributed to C–O (amide I) stretching mode of chitosan. A peak at 1385cm^{-1} is related to –C–O stretching mode of $-CH_2-OH$ group of chitosan. The peaks at 1045, 602, 565 and 470 cm^{-1} can be attributed to phosphate groups of HA.

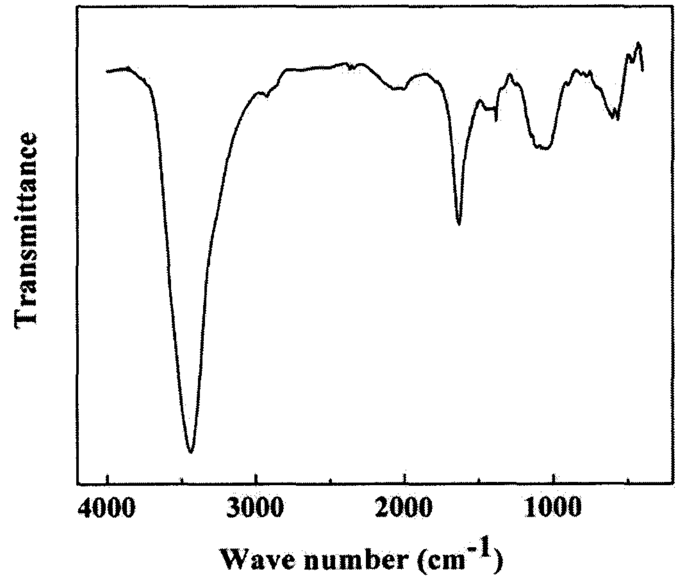

Figure 5-4 FTIR spectrum of a chitosan–HA composite deposit prepared from the 0.5 g/L chitosan solution, containing 1 g/L HA at deposition voltage of 20V.

The results of XRD, SEM and FTIR indicate the formation of composite material containing HA particles in a chitosan matrix.

5.1.1.4 Electrochemical testing of composite coatings

It was found that composite deposits provided corrosion protection of Nitinol in Ringer's solutions. The properties of coated and uncoated Nitinol were compared.

The EIS data was presented in the complex impedance diagram (Nyquist plot), where the imaginary component Z" of the impedance is plotted as a function of the real component Z' (Figure 5-5). It was observed that the impedance values for the coated sample were higher then those for the uncoated substrate. Higher impedance value was obtained for the higher HA concentration in the solution. This result indicates that the deposited film reduces the ion diffusion and corrosion rate of the substrate. This is in a good agreement with the result of the potentiodynamic investigations.

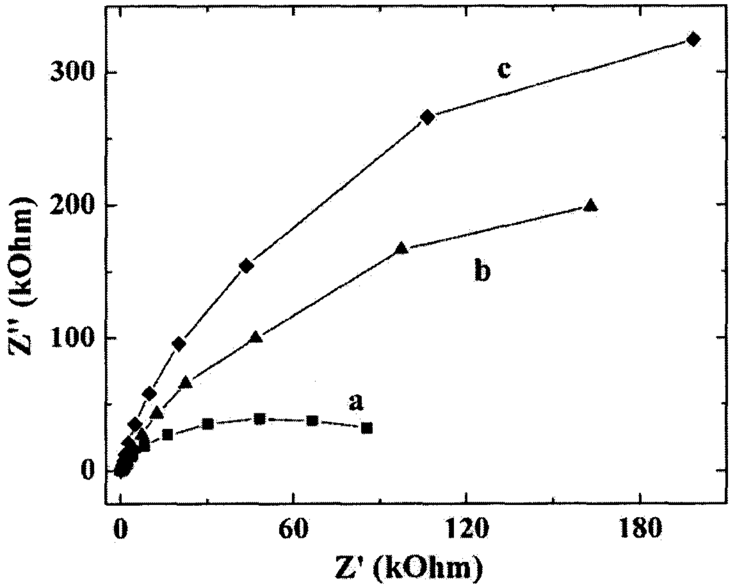

Figure 5-5 Nyquist plots for (a) the bare Nitinol substrates and the Nitinol coated with a composite CH-HA film prepared from the 0.5 g/L CH solution, containing (b) 0.5 g/L, (c) 1 g/L HA at the deposition voltage of 20 V.

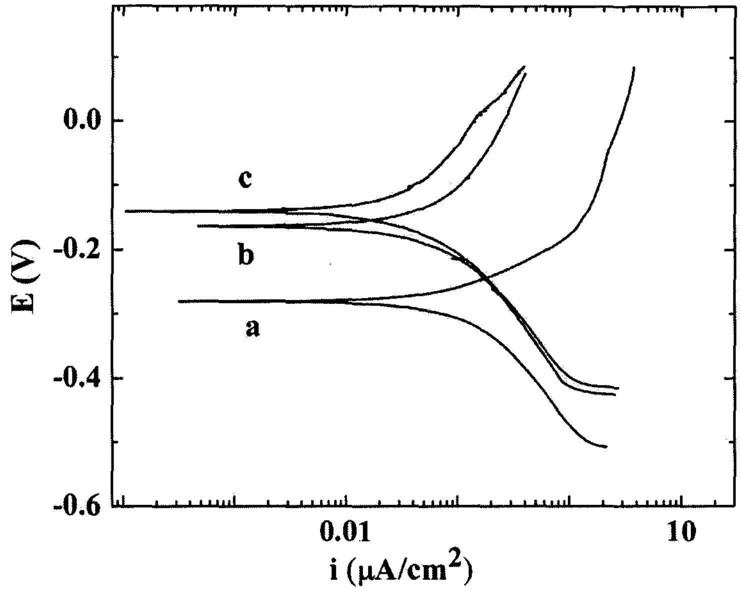

Figure 5-6 Tafel plots for (a) the bare Nitinol substrates and the Nitinol coated with a composite CH-HA film prepared from the 0.5 g/L CH solution, containing (b) 0.5 g/L, (c) 1 g/L HA at the deposition voltage of 20 V.

Figure 5-6 shows the Tafel curves for the uncoated and coated Nitinol. It can be seen that the corrosion current and therefore the rate of corrosion of the coated sample was reduced by the film. These results indicated that the composite films acted as protective layers and improved the corrosion resistance of the Nitinol substrates in Ringer's solutions.

5.1.2 Codeposition of chitosan with heparin

EPD has been further developed for the fabrication of composite coatings containing heparin. The important point to be discussed is the electrochemical mechanism of the codeposition of chitosan and heparin. It is known that chitosan is soluble in aqueous solutions below pH 6.5 and exhibits polycationic behavior. The protonation of amine groups of chitosan is achieved in acidic solutions:

$$\mathbf{CH\text{-}NH_2 + H_3O^+ \rightarrow CH\text{-}NH_3^+ + H_2O} \qquad \mathbf{(5.1)}$$

However, the increases in solution pH results in a decreasing charge, and at pH 6.5 chitosan's amino groups become deprotonated. High pH can be generated at the cathode surface using the cathodic reaction:

$$\mathbf{2H_2O + 2e^- \rightarrow H_2 + 2\ OH^-} \qquad \mathbf{(5.2)}$$

In the EPD process, electric field provides electrophoretic motion of charged chitosan macromolecules to the cathode, where chitosan forms an insoluble deposit:

$$\mathbf{CH\text{-}NH_3^+ + OH^- \rightarrow CH\text{-}NH_2 + H_2O} \qquad \mathbf{(5.3)}$$

5.1.2.1 Investigation of deposition yield

The deposition yield in the electrophoretic process is described by the Hamaker equation:

$$\mathbf{M=\mu tSCU/d} \qquad \mathbf{(5.4)}$$

where M is the mass of a deposit obtained during deposition time t on the electrode area S, μ and C are mobility and concentration of polymer macromolecules or inorganic particles, respectively.

$U=U_{ap}-U_{dep}$, where U_{ap} is applied voltage, U_{dep} is voltage drop in deposit, and d is distance between electrodes. U_{dep} is proportional to deposit resistivity, which increases with the increase in the deposit thickness.

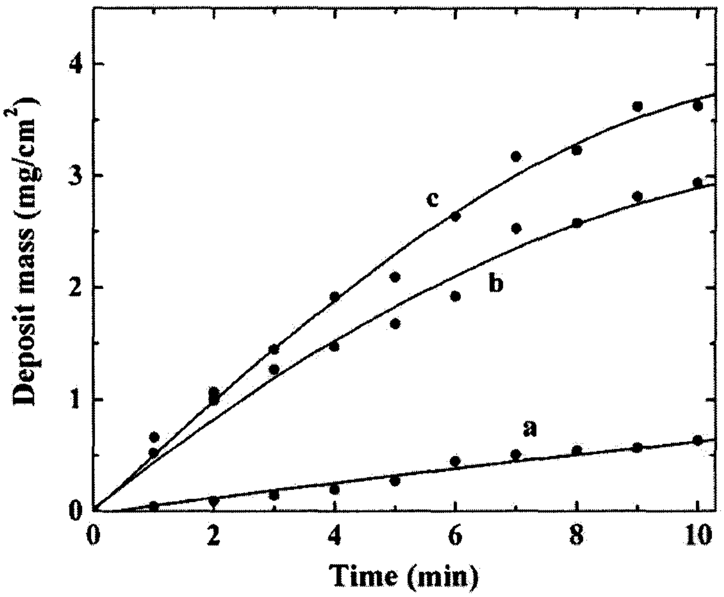

Figure 5-7 Deposit mass versus deposition time for the films prepared from the solutions: (a) 0.5 g/L chitosan, (b) 0.5 g/L chitosan and 0.1 g/L heparin, (c) 0.5 g/L chitosan and 0.2 g/L heparin, deposition voltage 15 V.

Figure 5-7a shows deposit mass versus deposition time for the chitosan films. The deposit mass increased with increasing deposition time, indicating the formation of chitosan films with different thickness, which is in qualitative agreement with the Hamaker equation. In contrast, no electrophoretic deposition (cathodic or anodic) was achieved from pure 0.05–2 g/L heparin solutions. It is important to note that heparin has a negative charge and anodic deposition can be expected. It is suggested that electrostatic repulsion of charged heparin macromolecules at the anode surface prevented deposit formation. However, it was found that the addition of heparin to chitosan solutions resulted in significant increase in the cathodic deposition rate (Figure 5-7). Higher deposition rate was obtained for the deposits prepared from the 0.5 g/L chitosan solutions, containing 0.2 g/L heparin, compared to that for the deposits prepared from the 0.5 g/L chitosan solutions, containing 0.1 g/L heparin.

From Figure 5-7, we found that deposition rate decreased with increasing deposition time. The decrease in the deposition rate can be attributed to the decrease in U during the deposition process, which is related to the formation of an insulating deposit and increase in U_{dep}. However, the decrease in U results in the decreasing current, lower rate of OH^- generation and chitosan charge neutralization in Reactions (5.2) and (5.3). As a result, deposition rate decreased with increasing deposition time.

Figure 5-8 shows deposition yield obtained from different solutions at a constant voltage of 20 V and deposition time of 3 min. The deposition yield increased approximately 5 times with increasing heparin concentration in the range of 0-0.1 g/L, at higher heparin concentrations only 20 % increase in the deposition yield was observed.

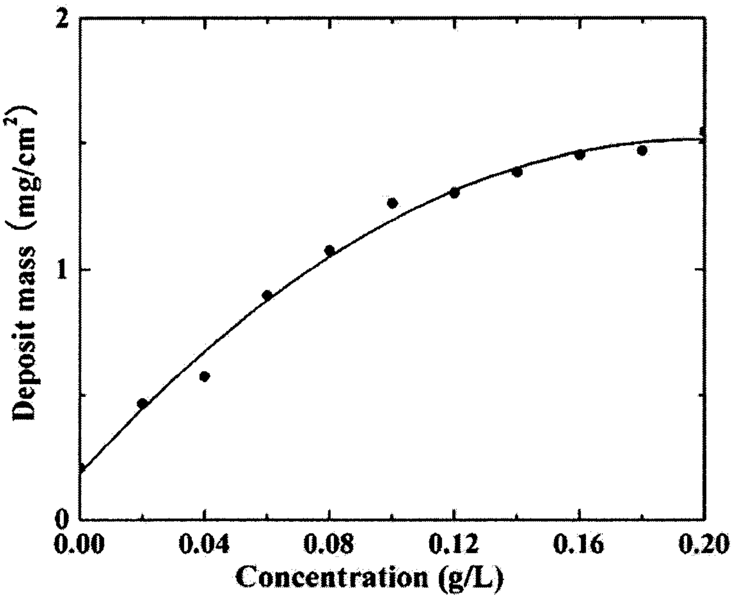

Figure 5-8 Deposit mass versus heparin concentration in the 0.5 g/L chitosan solutions at a deposition voltage of 20 V and deposition time of 3 min.

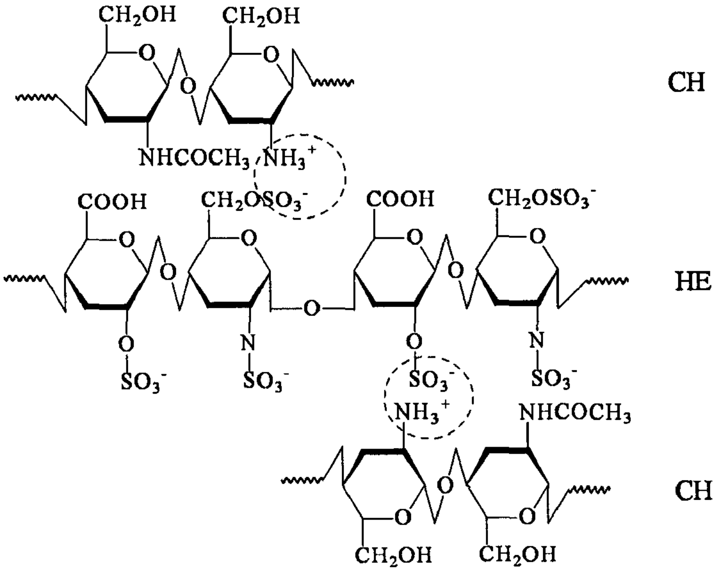

Figure 5-9 Chitosan (CH)-heparin (HE) complex

It is suggested that the addition of anionic heparin to cationic chitosan resulted in the formation of non-stoichiometric complexes (Figure 5-9), which were positively charged and deposited cathodically. Therefore, the results indicate the possibility of the deposition of chitosan films containing heparin. The increase in the deposition yield with increasing heparin concentration can be attributed to the increasing heparin content in the deposits.

However, co-deposition of heparin and chitosan cannot explain the significant increase in the deposition yield in the heparin concentration range of 0-0.1 g/L. It is important to note that electrophoretic mobility of polyelectrolyte is proportional to the charge density. The formation of chitosan-heparin non-stoichiometric complexes resulted in a reduced charge; therefore the decrease in the deposition rate with increasing heparin concentration can be expected. However, it is known that the hydrodynamic radius of polyelectrolyte complexes can be significantly smaller than that of the uncomplexed polyelectrolyte. The decrease in the hydrodynamic radius can result in increasing electrophoretic mobility. Therefore, the increase in the deposition rate with increasing heparin concentration can be partially attributed to the decreasing hydrodynamic radius of the polyelectrolyte complexes.

It is important to note that EPD is essentially a two step process, which includes electrophoresis and deposit formation. The electrophoretic motion of chitosan towards the electrode provides accumulation of chitosan macromolecules at the electrode surface but does not necessarily result in the deposit formation. The Hamaker equation is based on the assumption that all inorganic particles or polymer macromolecules accumulated at the electrode surface are deposited. However, the electrostatic repulsion of charged polymers at the electrode surface reduces the deposition efficiency. The deposition efficiency depends on the rate of OH^- generation (Reaction 5.2) and chitosan charge neutralization (Reaction 5.3). It is suggested that the formation of non-stoichiometric chitosan-heparin complexes resulted in partial charge compensation, which promoted deposit formation at the electrode surface and increased the deposition yield (Figure 5-7 and Figure 5-8).

5.1.2.2 SEM studies of chitosan-heparin composite deposits

Fig.5.10 (a,b,c,d) shows SEM images of chitosan-heparin composite films on Nitinol wires. These figures show the surface morphology of the composite coatings. The deposits are relatively uniform, dense and pinhole free. Fig. 5.10 (e,f) shows the cross section of composite coatings deposited on the graphite substrates. It can be seen that the coating thickness can be varied in the range of 0.5-5 μm for different deposition durations.

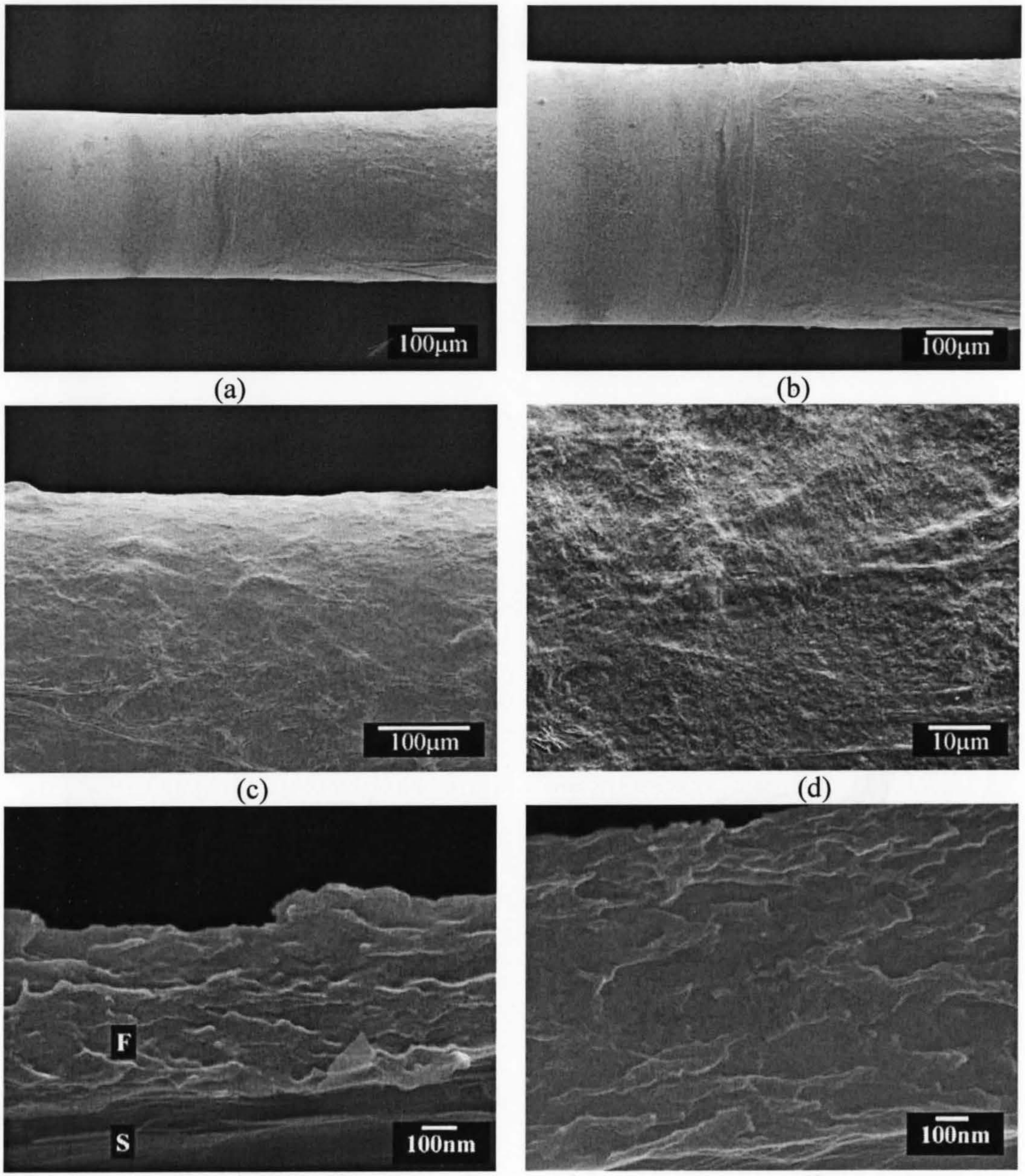

(a) (b)
(c) (d)
(d) (f)

Figure 5-10 SEM images of (a,b,c,d) the surface at different magnifications and (e,f) the cross section of the films prepared from the 0.5 g/L chitosan solution, containing 0.2 g/L heparin.

5.1.2.3 TGA&DTA studies of chitosan-heparin composite deposits

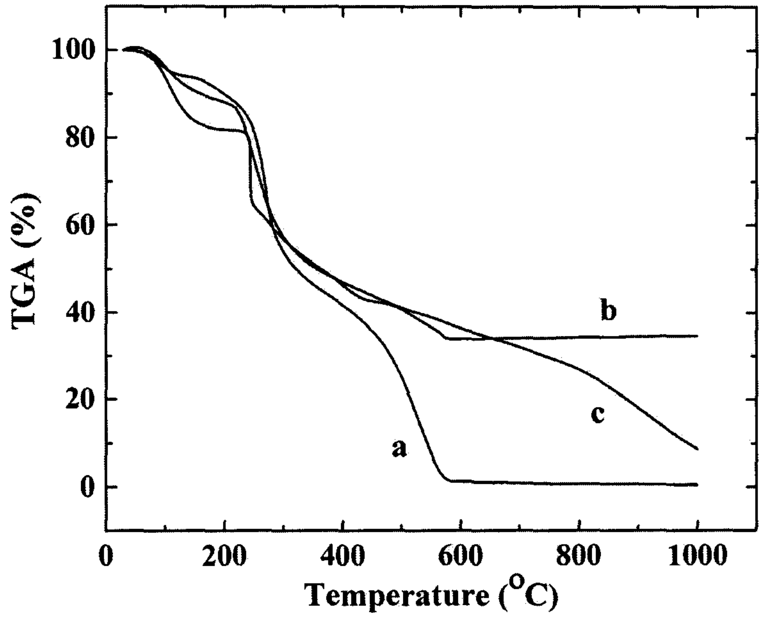

Figure 5-11 TGA data for (a) a deposit prepared from the 0.5 g/L chitosan solution, (b) as-received heparin and (c) a deposit prepared from the 0.5 g/L chitosan solution containing 0.2 g/L heparin, deposition voltage 10V.

Figure 5-11 and Figure 5-12 compare the TGA and DTA data for pure chitosan deposit, as-received heparin and chitosan–heparin coatings. The weight loss observed in the TGA data is attributed to dehydration and burning out of chitosan and heparin. The weight loss occurs in several steps. The TGA data (Figure 5-11) showed differences in thermal behavior of the chitosan–heparin deposit compared to pure chitosan coating and as-received heparin. The DTA data (Figure 5-12) showed very broad endotherm around ~ 100 °C, related to dehydration of the materials and exotherms at higher temperatures related to the burning out of the organic materials. The DTA data are in a good agreement with the results of TGA investigation and indicate the difference in thermal behavior of chitosan–heparin deposits, compared to pure chitosan and heparin.

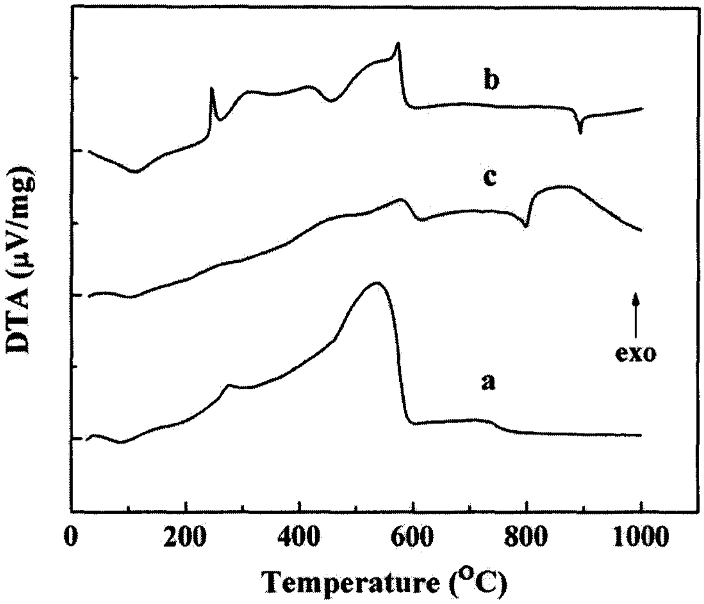

Figure 5-12 DTA data for (a) a deposit prepared from the 0.5 g/L chitosan solution, (b) as-received heparin and (c) a deposit prepared from the 0.5 g/L chitosan solution containing 0.2 g/L heparin, deposition voltage 10V.

5.1.2.4 FTIR studies of chitosan-heparin composite deposits

The FTIR spectrum of deposited chitosan (Figure 5-13) shows a broad peak around 3450 cm^{-1} related to hydroxyl stretching, a peak at 1638 cm^{-1} attributed to C–O (amide I) stretching mode, a peak at 1385 cm^{-1} related to –C–O stretching mode of –CH_2–OH group and a broad peak around 1090 cm^{-1} related to vibrational C–O stretching. The FTIR spectrum of heparin showed a broad peak centered at 3450 cm^{-1} assigned to hydroxyl stretching, a peak related to the stretching vibration of C–H bonds at 2942 cm^{-1}, as well as peaks attributed to asymmetric at 1634 cm^{-1} and symmetric at 1429 cm^{-1} axial deformations of carboxylate anions. The absorbance at 1232 cm^{-1} and

1040 cm^{-1} is due to $-SO_3^-$ asymmetric and symmetric stretching. The bands observed in the region 797–818 cm^{-1} are related to sulphate half esters absorptions. The spectrum of chitosan–heparin deposits is similar to the spectrum of pure chitosan. However, the formation of chitosan–heparin complexes resulted in additional shoulder corresponding to the heparin absorbance at 1232 cm^{-1} and a peak corresponding to heparin absorbance at 1040 cm^{-1}. Such absorptions are characteristic for $-SO_3^-$ groups of heparin. The sulphate half ester absorptions were also observed in the FTIR spectrum of chitosan–heparin deposits at 797–818 cm^{-1}.

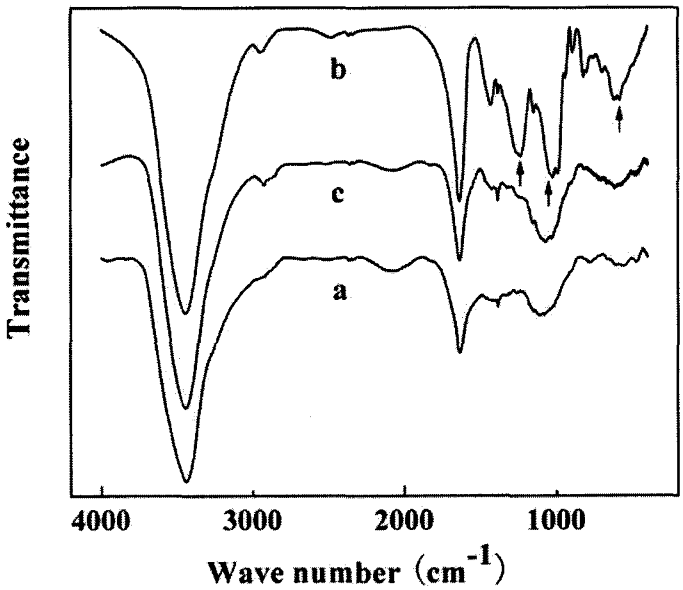

Figure 5-13 FTIR spectra for (a) a deposit prepared from the 0.5 g/L chitosan solution, (b) as-received heparin and (c) a deposit prepared from the 0.5 g/L chitosan solution containing 0.2 g/L heparin, deposition voltage 10V. The arrows show absorbance at 1232 and 1040 cm^{-1} due to $-SO_3^-$ asymmetric and symmetric stretching and the bands in the region 797–818 cm^{-1} related to sulphate half ester absorption.

Therefore, the results of FTIR (Figure 5-13) combined with the results of deposition yield measurements (Figure 5-7, Figure 5-8), SEM (Figure 5-10), TGA (Figure

5-11) and DTA (Figure 5-12) indicate the possibility of electrophoretic deposition of chitosan coatings containing heparin.

5.1.2.5 Antithrombin adsorption test

Figure 5-14 compares the results of antithrombin adsorption on the surface of films prepared from 0.5 g/L chitosan solution, 0.5 g/L chitosan solution containing 0.1 g/L heparin, 0.5 g/L chitosan solution containing 0.2 g/L heparin in pure water and mixed ethanol–water solutions. The surfaces of chitosan–heparin composite films showed significant increase in the antithrombin adsorption compared to the surfaces of pure chitosan films. The higher antithrombin adsorption on the surface of films prepared from chitosan solution containing 0.2 g/L heparin compared to the films prepared from chitosan solution containing 0.1 g/L heparin can be attributed to higher heparin content in the former films.

It also can be observed that films prepared in pure water solvent have much higher antithrombin adsorption than films prepared in mixed ethanol–water solutions. It can be attributed to the much rougher surface of the former films than that of the later ones, which resulted in a higher amount of heparin on the surface.

The results are in good agreement with investigations of chitosan–heparin complexes and films prepared by other methods, which indicate antithrombogenic properties and blood compatibility. It is important to note that heparin is widely used as an anticoagulant drug because of its ability to accelerate the rate at which antithrombin inhibits serine proteases in the blood coagulation cascade. Surface modification of materials is an important approach for the control of biological processes at solid-liquid interface. Therefore, EPD is a promising method for the fabrication of coatings with improved hemocompatibility.

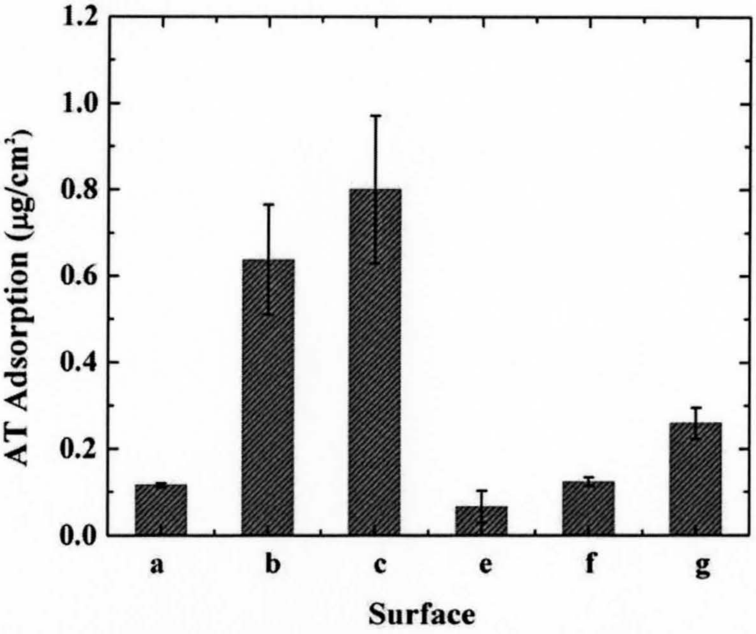

Figure 5-14 Antithrombin adsorption on the surface of films prepared from (a) 0.5 g/L chitosan solution, (b) 0.5 g/L chitosan solution containing 0.1 g/L heparin, (c) 0.5 g/L chitosan solution containing 0.2 g/L heparin in pure water solvent; (e) 0.5 g/L chitosan solution, (f) 0.5 g/L chitosan solution containing 0.1 g/L heparin, (g) 0.5 g/L chitosan solution containing 0.2 g/L heparin in mixed ethanol–water solvent, at a deposition voltage of 15 V. Values are mean ±CD (n=4).

5.1.3 EPD of multilayer and functionally graded coatings

EPD is ideally suited for the fabrication of laminates of different materials. Therefore, it would be important to apply this technique for the fabrication of multilayer organic–inorganic thick films, containing hydroxyapatite and chitosan. The number of individual layers can be varied. As an example, Figure 5-15(a) shows a multilayer structure, containing two individual layers of different thickness and composition. Another multilayer structure, containing 10 individual layers, is shown in Figure 5-15 (b).

Turning again to the literature data on the microstructure of natural bones, it should be noted that bulk multilayer structures, containing inorganic particles, separated by an organic phase, exhibit advanced mechanical properties.

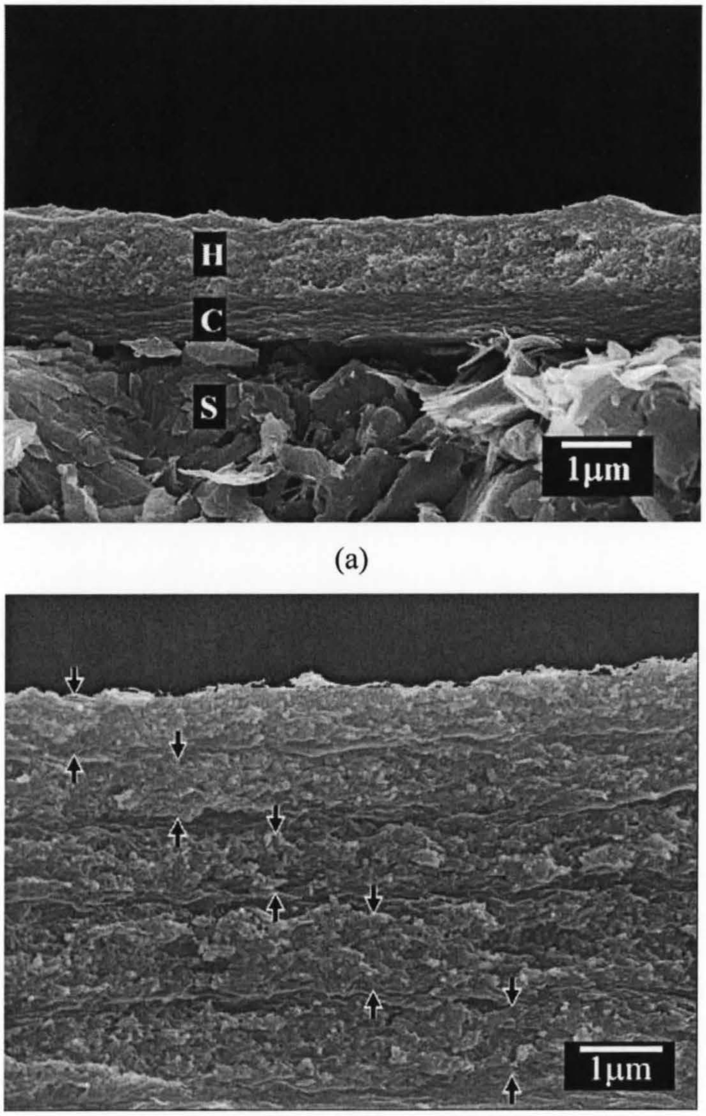

(a)

(b)

Figure 5-15 SEM image of the composite films, which consists of the composite chitosan-HA layers (H), prepared from the 0.5 g/L chitosan solution, containing 1 g/L HA and layers of pure chitosan (C), prepared from the 0.5 g/L chitosan solution on graphite substrates (S), arrows show chitosan-HA layers.

The importance of heparin for surface modification of biomaterials has motivated the EPD of multilayer and FGM chitosan–HA coatings containing heparin. As an example, Fig. 5.16 shows an SEM image of a composite film containing chitosan bottom layer, chitosan–HA intermediate layer and chitosan–heparin top layer.

Compared to other techniques for surface modification and treatment of biomaterials and devices using heparin, EPD offers the advantages of simple processing, high-deposition rate, the possibility of deposition of uniform coatings of controlled thickness and composition on substrates of complex shape as well as deposition of multilayer and FGM coatings.

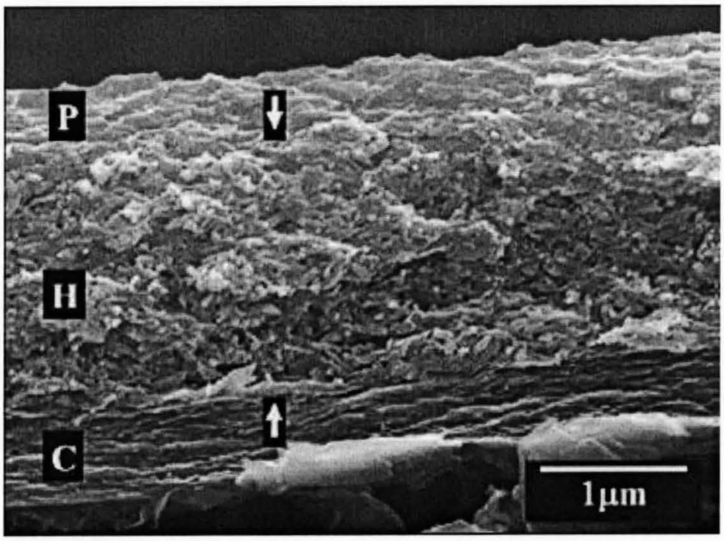

Figure 5-16 SEM image of a fracture of a deposit, containing a pure chitosan layer (C), prepared from the 0.5 g/L chitosan solution, a HA–chitosan composite layer (H), prepared from the 0.5 g/L chitosan solution containing 1 g/L HA (shown using arrows) and a chitosan–heparin layer (P) prepared from the 0.5 g/L chitosan solution containing 0.2 g/L heparin on graphite substrate.

5.2 EPD of hyaluronate with hydroxyapatite

5.2.1 Electrodeposition from pure hyaluronate solution

5.2.1.1 Investigation of deposition yield from pure hyaluronate solution

Figure 5-17 shows deposit mass versus deposition time for the 0.5 g /L sodium hyaluronate solution at a constant voltage of 30 V in mixed ethanol-water solvent. The deposition yield increased with increasing deposition time, indicating the formation of films of different mass.

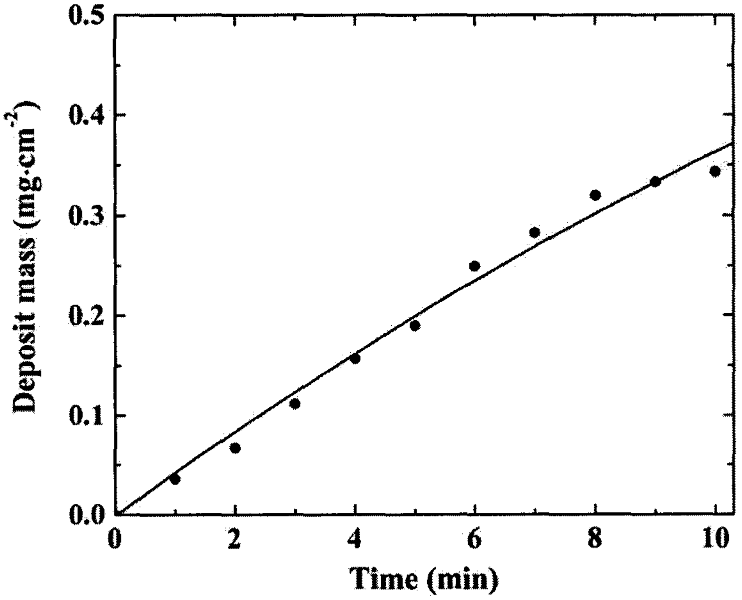

Figure 5-17 Deposit mass versus deposition time for films prepared from 0.5 g /L sodium hyaluronate solution at deposition voltage of 30 V.

An interesting phenomenon is that electrodeposition experiments performed using the aqueous 0.5-1 gL^{-1} sodium hyaluronate solutions have not revealed deposit formation. It was suggested that the dissociation of sodium hyaluronate (HY-Na) resulted in the formation of anionic HY^- species:

$HY\text{-}Na \rightarrow HY^- + Na^+$ (5.6)

Electric field provided electrophoretic motion of the anionic HY^- species towards the anode surface, where the pH decreased owing to the electrochemical decomposition of water:

$2H_2O \rightarrow O_2 + 4H^+ + 4e^-$ (5.7)

The formation of hyaluronic acid gel (HY-H) in the low pH region at the electrode surface was expected as a result of the charge compensation of $-COO^-$ groups:

$HY^- + H^+ \rightarrow HY\text{-}H$ (5.8)

However, electrodeposition of hyaluronic acid films from aqueous sodium hyaluronate solutions has not been achieved. It is important to note that hyaluronic acid exhibits an isoelectric point located at pH=2.5. A gel-like behavior was observed in bulk solutions at pH =2.5. However, the reduction in pH resulted in the dissolution of the gel at pH=1.6. Below the isoelectric point, the protonation of the –NH– groups resulted in a positive charge of the hyaluronic acid macromolecules.

It is suggested that the positive charge of hyaluronic acid at the anode surface prevented anodic deposition in aqueous solutions. However, electrodeposition from mixed ethanol-water solutions resulted in the formation of anodic deposits. The deposit formation can be attributed to cross-linking of hyaluronic acid in ethanol-water solutions in acidic conditions at the electrode surface. The cross-linking in acidic ethanol-water solutions occurs without change in chemical structure and is related to the formation of hydrogen-bonding network among the chains. According to the literature, the cross-linking of hyaluronic acid results in water insoluble gels.

The proposed deposition mechanism is different from the deposition mechanism of other weak anionic polyelectrolytes, such as alginate, which don't have an isoelectric point.

5.2.1.2 SEM studies of films prepared from pure hyaluronate solutions

SEM investigations showed that film thickness was varied in the range of 0.1-10 µm. Figure 5-18 shows a typical SEM image of a film deposited on a graphite substrate. The SEM image indicates that relatively uniform films can be obtained.

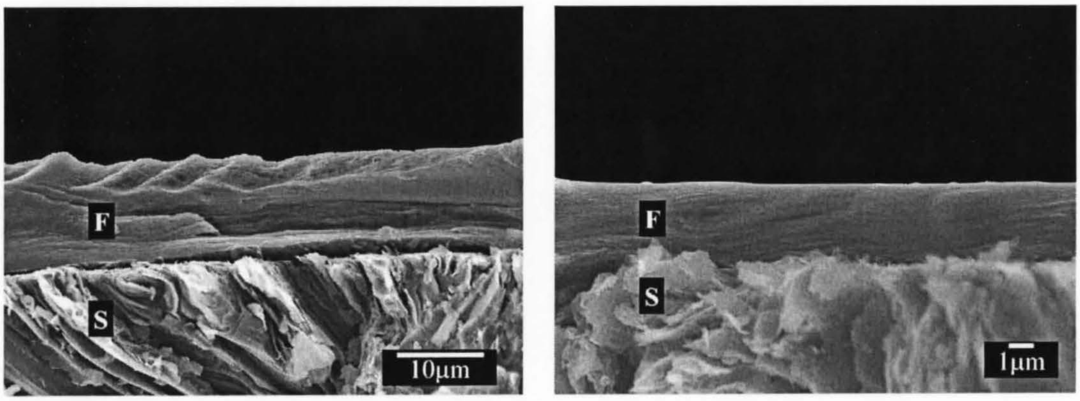

(a) (b)

Figure 5-18 SEM image of a cross section of film prepared from the 0.5 g/L sodium hyaluronate solution at a deposition voltage of 30V and deposition time of 3 min (F - film, S - substrate).

As–received sodium hyaluronate and the films prepared from the sodium hyaluronate solutions were studied by FTIR, TGA and DTA.

5.2.1.3 FTIR studies of pure hyaluronate solution

The FTIR spectra of as-received sodium hyaluronate and deposited hyaluronic acid films are shown in Figure 5-19. The FTIR spectra are in a good agreement with the literature data for sodium hyaluronate and hyaluronic acid. The characteristic peaks at 1037 cm^{-1}, 1078 cm^{-1} and 1155 cm^{-1} were attributed to the C–O– C, C–O and C–O–H stretching and peaks at 3440 cm^{-1} to OH$^-$ stretching. Observed bands at 1625 and 1402 cm^{-1} for as-received sodium hyaluronate (Figure 5-19a) were attributed to the presence of salified carboxylic groups and can be assigned to the asymmetric and symmetric stretching vibrations, respectively. The band at 1739 cm^{-1} in the spectra of the film (Figure 5-19b) is related to the stretching of the protonated carboxylic group of hyaluronic acid. The difference in the FTIR spectra of sodium hyaluronate and deposited films are related to ion exchange of carboxyl groups from –COO$^-$Na$^+$ to –COO$^-$H$^+$ in the acidic solutions at the electrode surface. Therefore, FTIR data obtained indicated the formation of hyaluronic acid films from the sodium hyaluronate solutions.

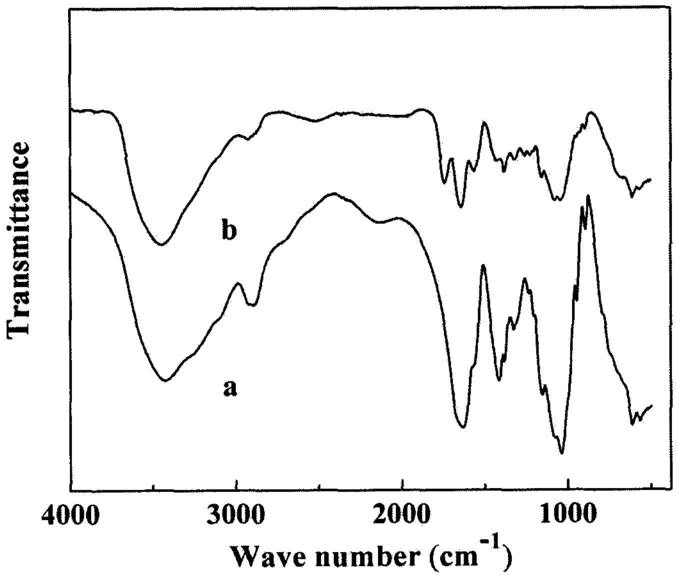

Figure 5-19 Spectra (FTIR) for (a) as-received sodium hyaluronate, and (b) film prepared from 0.5 g/L sodium hyaluronate solution at deposition voltage of 30 V.

5.2.1.4 TGA&DTA studies of films prepared from pure hyaluronate solutions

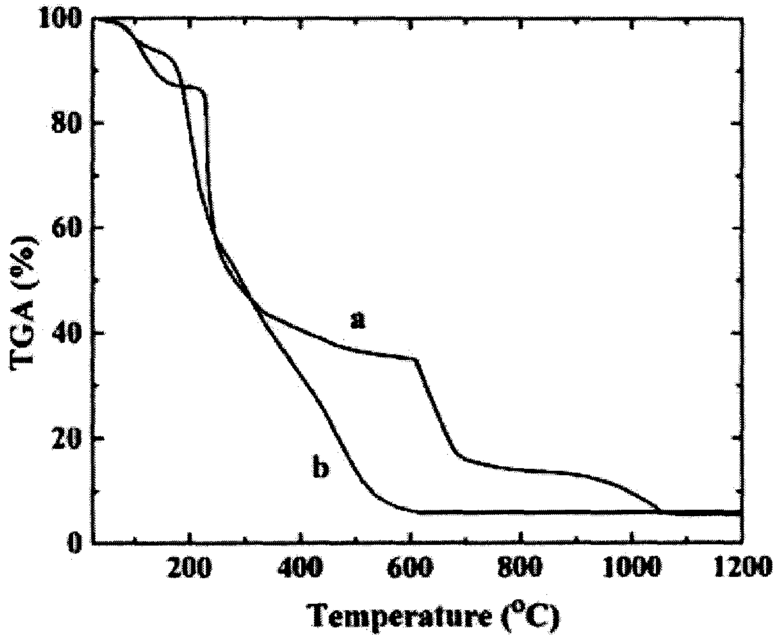

Figure 5-20 TGA data for (a) as-received sodium hyaluronate, and (b) film prepared from 0.5 g/L sodium hyaluronate solution at deposition voltage of 30 V

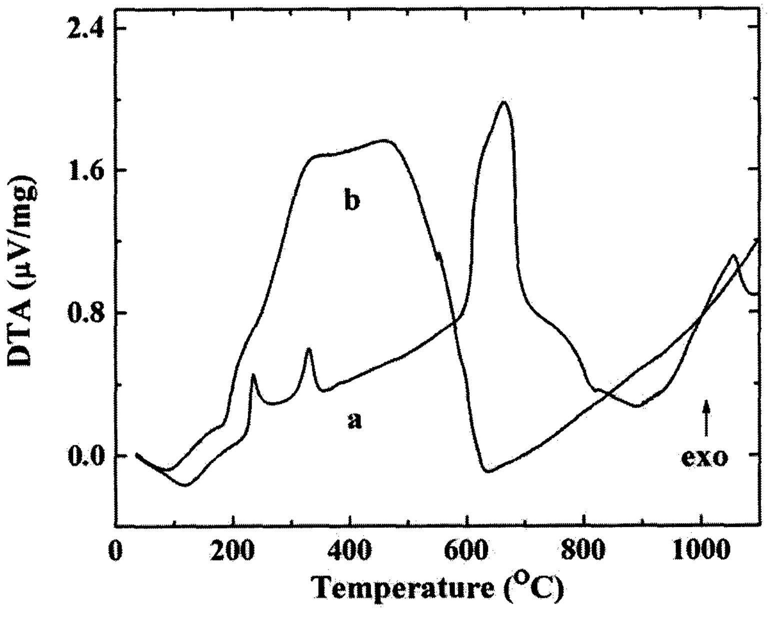

Figure 5-21 DTA data for (a) as-received sodium hyaluronate, and (b) film prepared from 0.5 g/L sodium hyaluronate solution at deposition voltage of 30 V

The TGA and DTA studies revealed the differences in the thermal behavior of as-received polymer and prepared films. The TGA curve for as-received sodium hyaluronate (Figure 5-20a) showed several steps in weight loss. The reduction in sample weight below ~ 150 °C can be attributed to dehydration.

It is suggested that the corresponding broad endotherm in the DTA curve (Figure 5-21a) around ~120 °C is attributed to the liberation of absorbed water. A sharp reduction in the sample weight was recorded in the range of 225-300 °C, and then the sample weight decreased gradually (Figure 5-20a). Similar steps in the weight loss were reported in the literature. Additional steps in weight loss were observed in the ranges of 620-680° and 950-1050 °C. It is suggested that the weight changes in the range of 225-620°C (Figure 5-20a) and corresponding small exotherms at 225 and 320 °C (Figure 5-21a) are related to the decomposition of sodium hyaluronate. The weight loss at temperatures of 620-680°C (Figure 5-20a) and corresponding exotherms in the same range are related to an additional step in the thermal degradation of sodium hyaluronate. In this temperature range, thermal degradation of the polymer can result in the formation of Na_2CO_3. The weight loss at temperatures exceeding 950°C (Figure 5-20a) and corresponding exotherms (Figure 5-21a) can be attributed to the decomposition of Na_2CO_3.

The TGA (Figure 5-20b) and DTA (Figure 5-21b) data for the deposited film showed thermal decomposition at much lower temperatures, compared to the as-received sodium hyaluronate. A reduction in sample weight was observed in the temperature range below ~550°C (Figure 5-20b). The sample weight at 600°C was 6.3 wt-%. It is noted that for the sodium hyaluronate the sample weight at the same temperature was 35.2 wt-%.

The total weight loss for the deposited film was attributed to deposit dehydration and burnout of the polymer. The broad endotherm at ~ 95°C (Figure 5-21b) can be attributed to the liberation of adsorbed water. The broad exotherms in the temperature range of 200-600°C were attributed to the thermal decomposition of the deposited polymer. The difference in the thermal behavior of as-received sodium hyaluronate and deposited films can be attributed to the ion exchange of carboxyl groups from $-COO^-Na^+$ in sodium hyaluronate to $-COO^-H^+$ in the deposited films. It is suggested that the formation of Na_2CO_3 resulted in higher temperature of thermal decomposition of sodium hyaluronate compared to the deposited hyaluronic acid films.

The results of FTIR, TGA and DTA investigations indicate that the deposition process resulted in the formation of hyaluronic acid films.

5.2.2 Codeposition of hyaluronate and HA

Hydroxyapatite suspensions in water or in a mixed ethanol–water solvent were unstable and showed rapid HA particle sedimentation when ultrasonic agitation was interrupted. The addition of HA particles to the sodium hyaluronate solutions enabled the formation of well dispersed HA suspensions, which were stable against sedimentation for 1–2 days. It is suggested that the adsorption of HY^- on the surface of the HA particles resulted in the electrosteric stabilization and provided electrical charge to the HA particles. The obtained suspensions, containing charged hyaluronate and HA, were used for electrodeposition. The deposits were obtained from the 0.5–1 g/L sodium hyaluronate solutions containing 0.5–4 g/L HA.

5.2.2.1 Investigation of deposition yield of composite coatings

Figure 5-22 shows deposit mass versus HA concentration in the 0.5 g/L sodium hyaluronate solutions at a constant deposition voltage of 30 V. The increase in HA concentration in the solutions resulted in an increasing deposit mass, indicating the formation of composite hyaluronic acid–HA films with different HA contents.

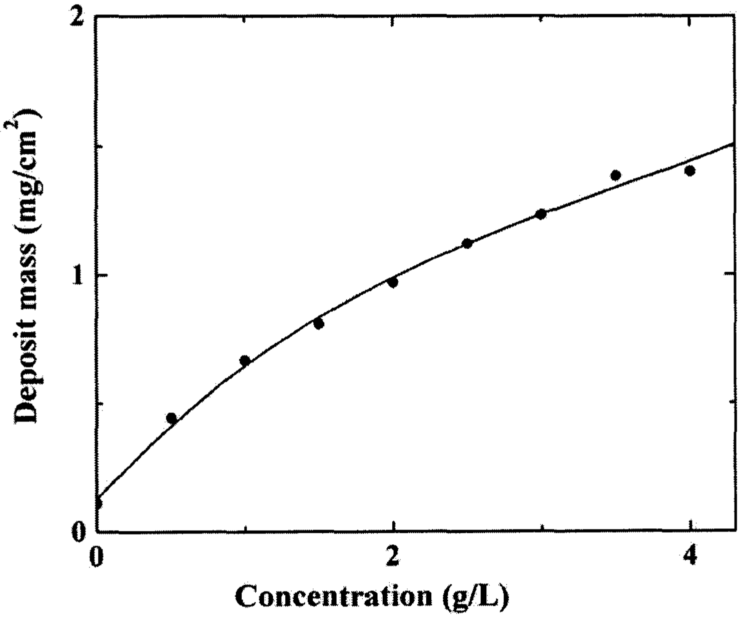

Figure 5-22 Deposit weight versus HA concentration in 0.5 g/L sodium hyaluronate solution at deposition voltage of 30 V and deposition time of 3 min

5.2.2.2 FTIR studies of composite coatings

Figure 5-23 compared the FTIR spectra of pure hyaluronic acid film and composite films of hyaluronate and HA. FTIR studies of the composite deposits (Figure 5-23b) showed peaks at 1041, 602 and 561 cm^{-1} which can be attributed to phosphate groups of HA. It is evidence of the codeposition of hyaluronate and HA.

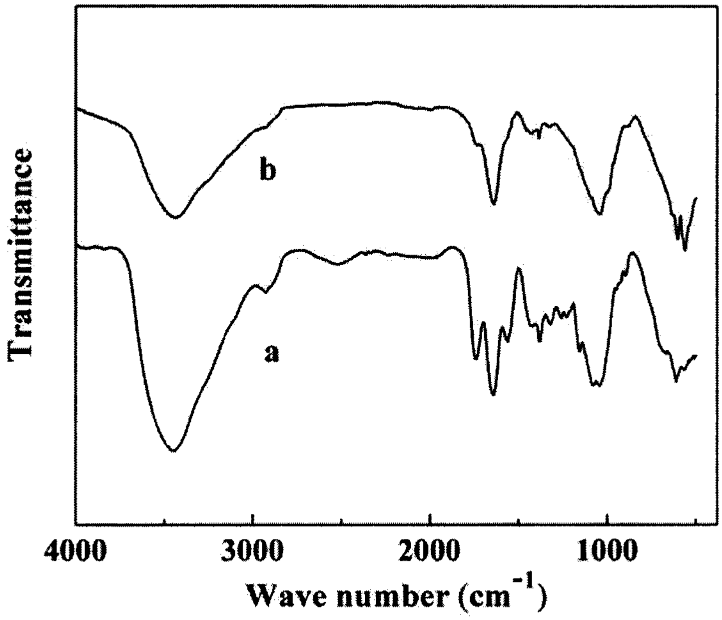

Figure 5-23 Spectra (FTIR) for films prepared from 0.5 g/L sodium hyaluronate solution: (a) without HA and containing (b) 4 g/L HA at deposition voltage of 30 V

5.2.2.3 TGA&DTA studies of composite coatings

Figure 5-24 and Figure 5-25 compare TGA and DTA data for the as-prepared HA powders and films deposited from the 0.5 g/L sodium hyaluronate solutions containing 1 and 4 g/L HA. The TGA studies of the as-prepared HA powders revealed weight loss attributed to dehydration (Figure 5-24a). This weight loss occurs mainly below 400°C. The total weight loss at 1200°C was found to be 8.1 wt %. The TGA data (Figure 5-24b and c) for the films showed additional weight loss, which can be attributed to the burnout of hyaluronic acid. The total weight loss for the films prepared from the 0.5 g/L sodium hyaluronate solutions containing 1 and 4 g/L HA was found to be 38.0 and 18.4 wt-% respectively. Therefore, the deposits contained 62.0 and 81.6 wt% of HA. The obtained

TGA data indicated that the HA content in the deposits can be varied. The higher HA concentration in the solutions resulted in the higher HA content in the deposits.

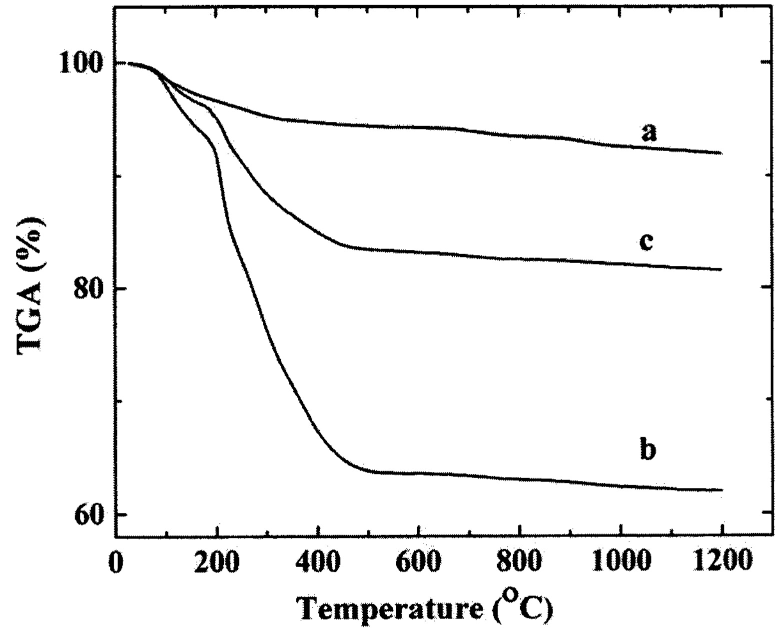

Figure 5-24 TGA data for (a) as-prepared HA, films prepared from 0.5 g/L sodium hyaluronate solution containing (b) 1 g/L HA and (c) 4 g/L HA at a deposition voltage of 30 V

The DTA data for the HA powders and the films are in good agreement with the results of TGA studies. The endotherms at 80–100°C (Figure 5-25a–c) are attributed to the liberation of the adsorbed water. The exotherms (Figure 5-25b and c) in the temperature range of 230–550°C are attributed to the burnout of an organic phase.

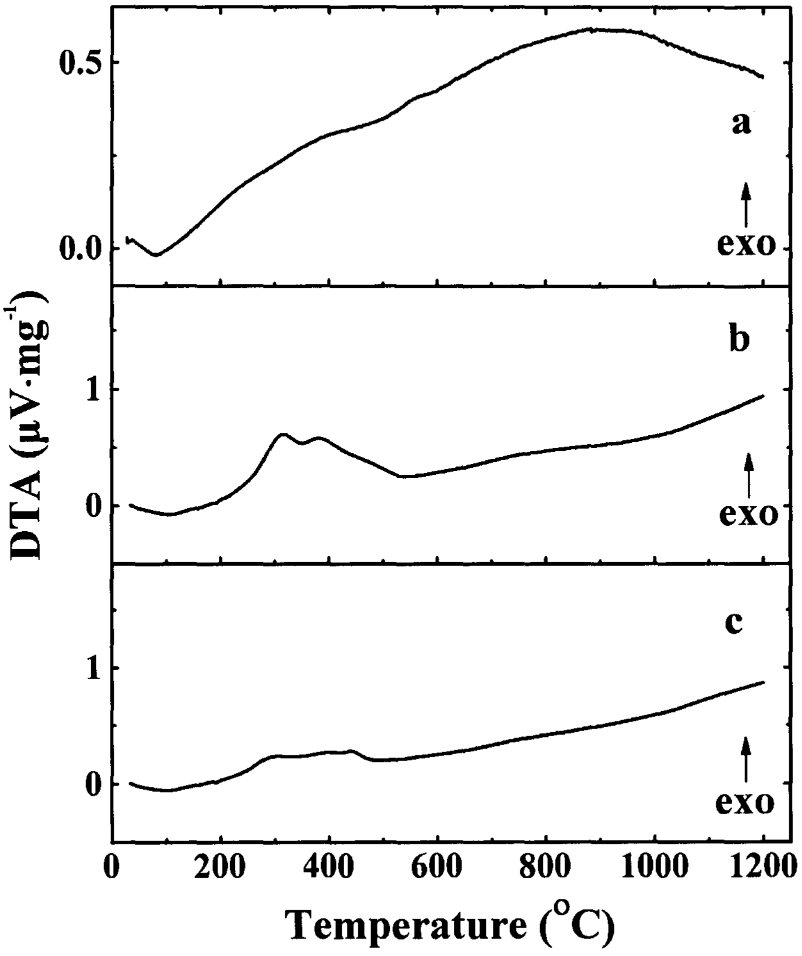

Figure 5-25 DTA data for (a) as-prepared HA, films prepared from 0.5 g/L sodium hyaluronate solution containing (b) 1 g/L HA and (c) 4 g/L HA at a deposition voltage of 30 V

5.2.2.4 XRD studies of composite coatings

XRD studies of as prepared HA (Figure 5-26) showed diffraction peaks corresponding to JCPDS file 09-0432. The deposited films showed similar HA peaks, indicating co-deposition of HA and hyaluronic acid.

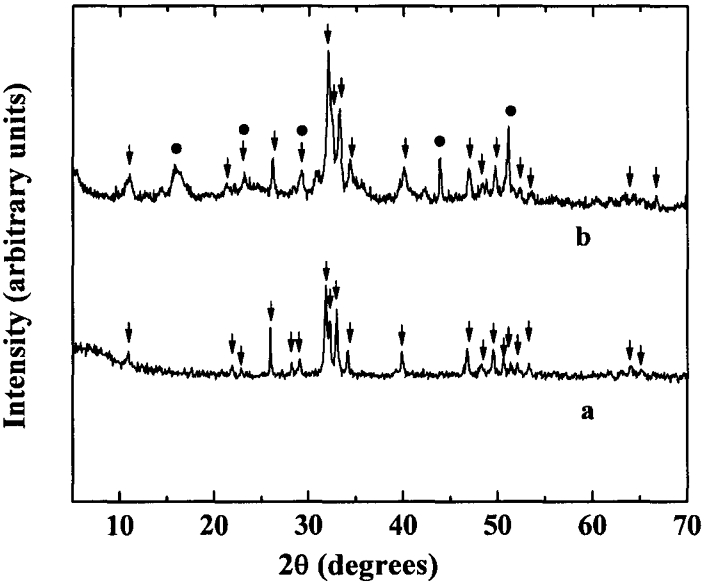

Figure 5-26 X-ray diffraction pattern of (a) as-prepared HA and (b) a coating prepared from the 0.5 g/L sodium hyaluronate solution containing 4 g/L HA at a deposition voltage of 30 V (arrows show peaks of HA, corresponding to JCPDS file 09-0432, • –substrate)

5.2.2.5 SEM studies of composite coatings

The SEM images of the film prepared from the sodium hyaluronate solutions containing HA, showed HA nanoparticles in a hyaluronic matrix (Figure 5-27). The films shown in Figure 5-27a and b are relatively dense with larger amounts of HA included in the deposit prepared from the sodium hyaluronate solution of lower concentration (Figure 5-27a). The increase in HA concentration in solutions resulted in the increasing amount of HA in the deposit (Figure 5-27c) in agreement with the TGA data (Figure 5-24) and with observed deposition yield increase with increasing HA concentration in the solutions (Figure 5-22). However, the films prepared from 0.5 g/L sodium hyaluronate solutions containing 4 g/L HA showed porosity (Figure 5-27c). The porosity resulted from the packing of HA particles. The pore size was in the range of 20-100 nm. The thickness of the composite films was varied in the range of 1-100 μm by variation in deposition time in the range of 0.5-10 min and deposition voltage in the range of 10-50 V. For example, Figure 5-27d shows a fracture of a film deposited on the graphite substrate. The thickness of the film is about 50 μm.

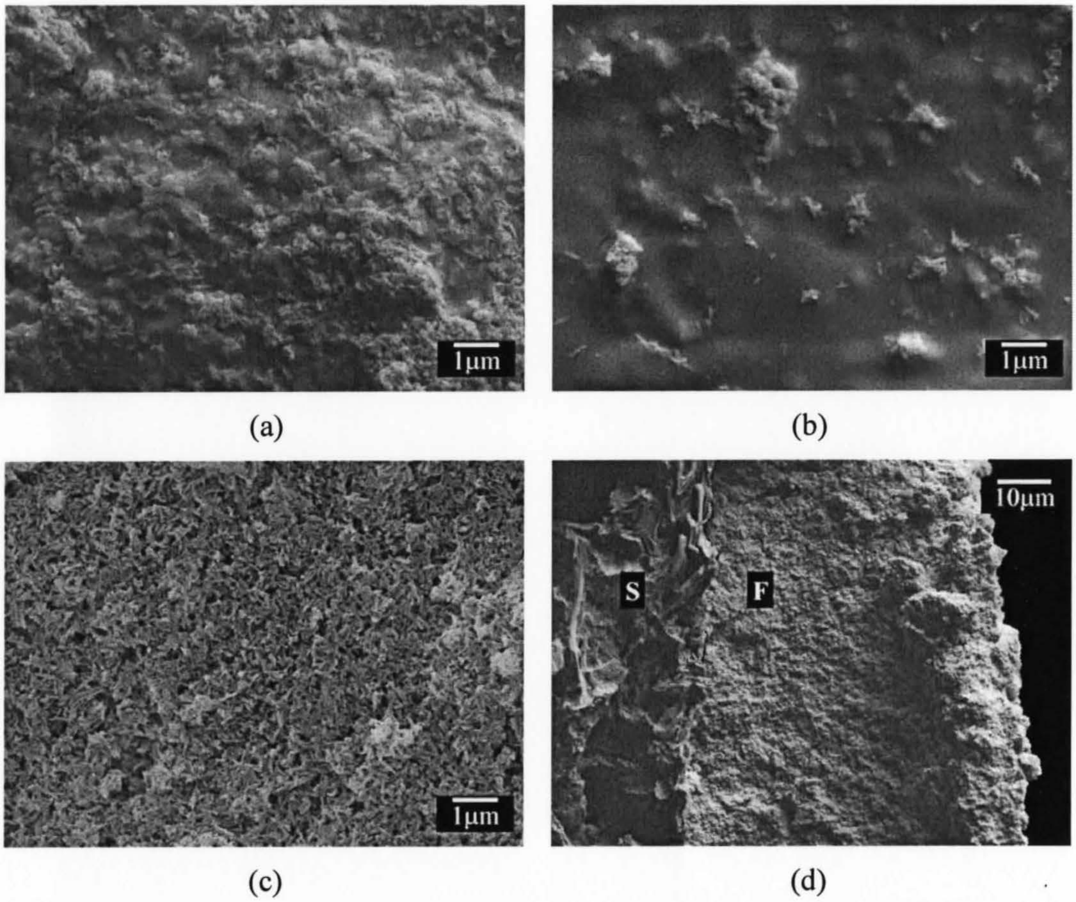

(a) (b)

(c) (d)

Figure 5-27 SEM images of (a-c) surfaces and (d) a cross section of the coatings prepared from sodium hyaluronate solutions containing HA particles at a deposition voltage of 30 V and deposition time of 3 min: (a) 0.5 g/L sodium hyaluronate and 0.5 g/L HA, (b) 1 g/L sodium hyaluronate and 0.5 g /L HA, (c,d) 0.5 g/L sodium hyaluronate and 4 g/L HA (F-film, S-substrate)

5.2.2.6 Electrochemical testing of composite coatings

The composite HA–hyaluronic acid films provided corrosion protection of stainless steel (Figure 5-28) and Nitinol (Figure 5-29) substrates in Ringer's physiological solutions. Figure 5-28 shows potentiodynamic polarization curves for the uncoated and coated stainless steel samples. It can be seen that the corrosion current and therefore the rate of corrosion of the coated samples were reduced by the film. This result indicates that the composite deposit can act as a protective layer and improves the corrosion resistance of the stainless steel in the simulated physiological environment. Figure 5-29 shows similar results for the coatings on NiTi substrates. The composite coatings improved the corrosion protection of Nitinol in the simulated body fluid solutions.

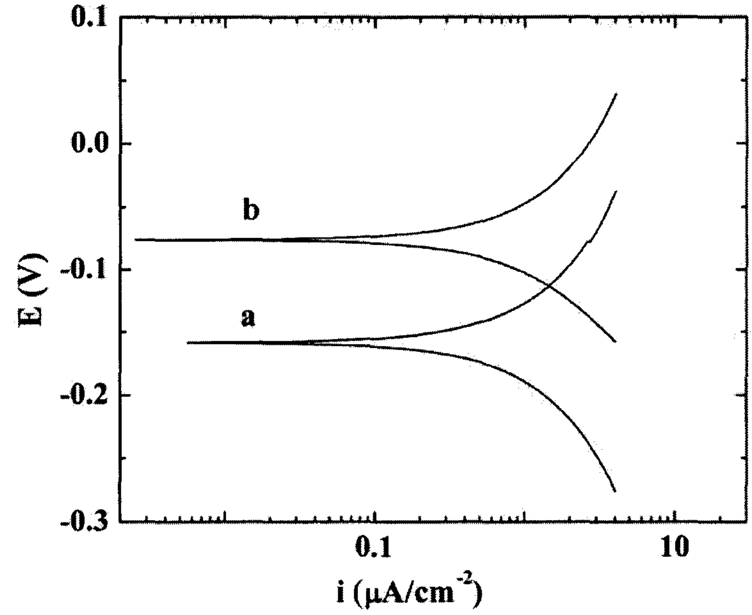

Figure 5-28 Tafel plots for the samples tested in the Ringer's solutions: (a) the bare stainless steel substrate, and (b) the stainless steel coated with composite coatings prepared from the 0.5 g/L sodium hyaluronate solution, containing 1 g/L HA at a deposition voltage of 30 V and deposition time of 3 min

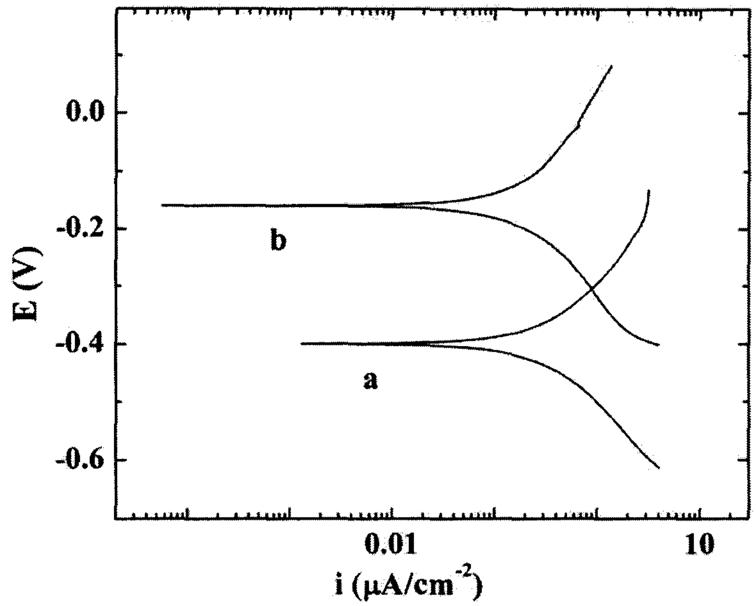

Figure 5-29 Tafel plots for the samples tested in the Ringer's solutions: (a) the bare Nitinol substrate, and (b) the Nitinol coated with composite coatings prepared from 0.5 g/L sodium hyaluronate solution, containing 1 g/L HA at a deposition voltage of 30 V and deposition time of 3 min.

5.2.3 Codeposition of hyaluronate and carbon nanotubes

Hyaluronate was used for the electrosteric stabilization of multiwalled carbon nanotubes (MWCNT) in suspensions and EPD of composite films. Hyaluronic acid-MWCNT films were obtained by anodic EPD and studied by TGA, DTA and SEM. Figure 5-30 and Figure 5-31 compared DTA and TGA data for as-received MWCNT, pure hyaluronic acid films and composite hyaluronic acid-MWCNT films. The data (Figure 5-30c and 5-31c) for as-received MWCNT showed that burning out of MWCNT was achieved in the range of 550–670 °C. The TGA and DTA results revealed a difference in thermal behavior of films prepared from pure hyaluronate solutions and the solutions containing MWCNT.

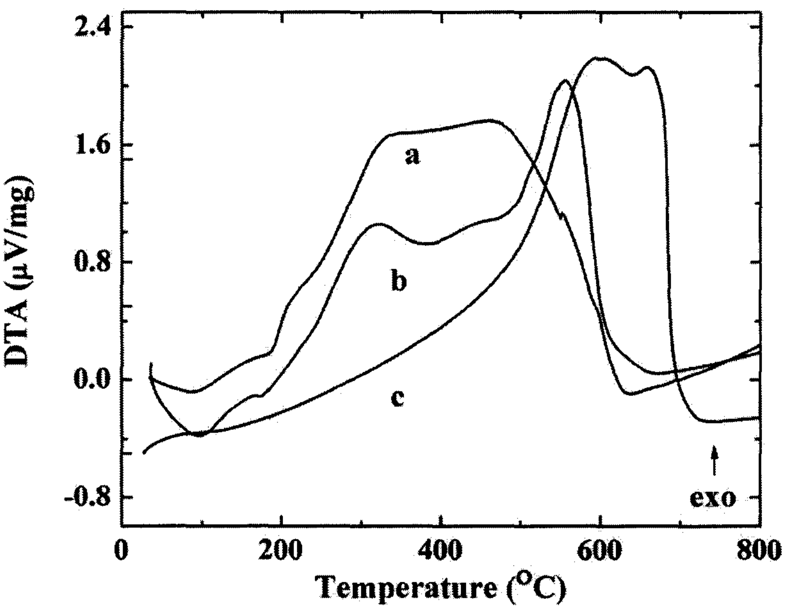

Figure 5-30 DTA data for films prepared from (a) 0.5 g/L hyaluronate solution, (b) 0.5g /L hyaluronate solution containing 0.1 g/L MWCNT and (c) as-received MWCNT

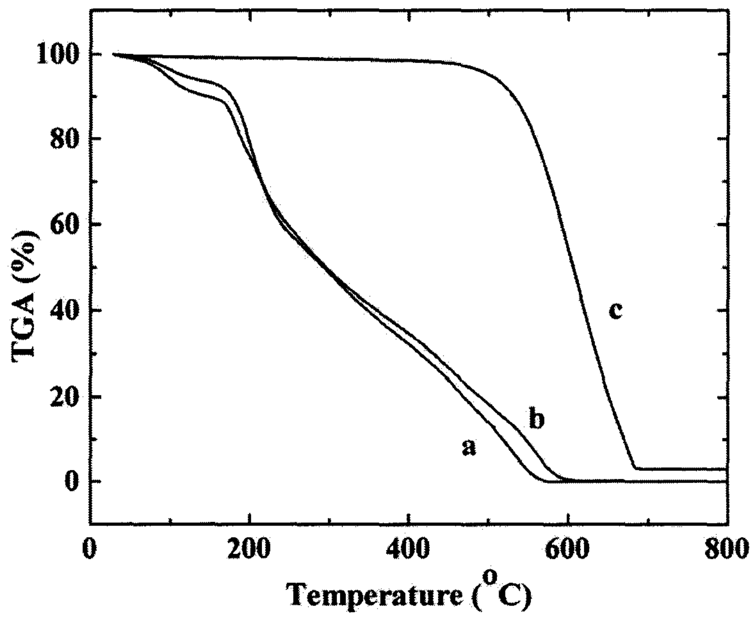

Figure 5-31 TGA data for films prepared from (a) 0.5 g/L hyaluronate solution, (b) 0.5g /L hyaluronate solution containing 0.1 g/L MWCNT and (c) as-received MWCNT.

The DTA data (Figure 5-30b) for the films prepared from the hyaluronate solutions containing MWCNT showed broader exothermic peak and additional peak at higher temperatures, compared to the DTA peaks for pure hyaluronate (Figure 5-30a). The TGA data (Figure 5-31) showed that burning out of films prepared from pure hyaluronate solutions was achieved at lower temperatures than that for composite. The difference can be attributed to higher burning out temperature of MWCNT compared to pure polymers. The results indicated the formation of composite films containing MWCNT.

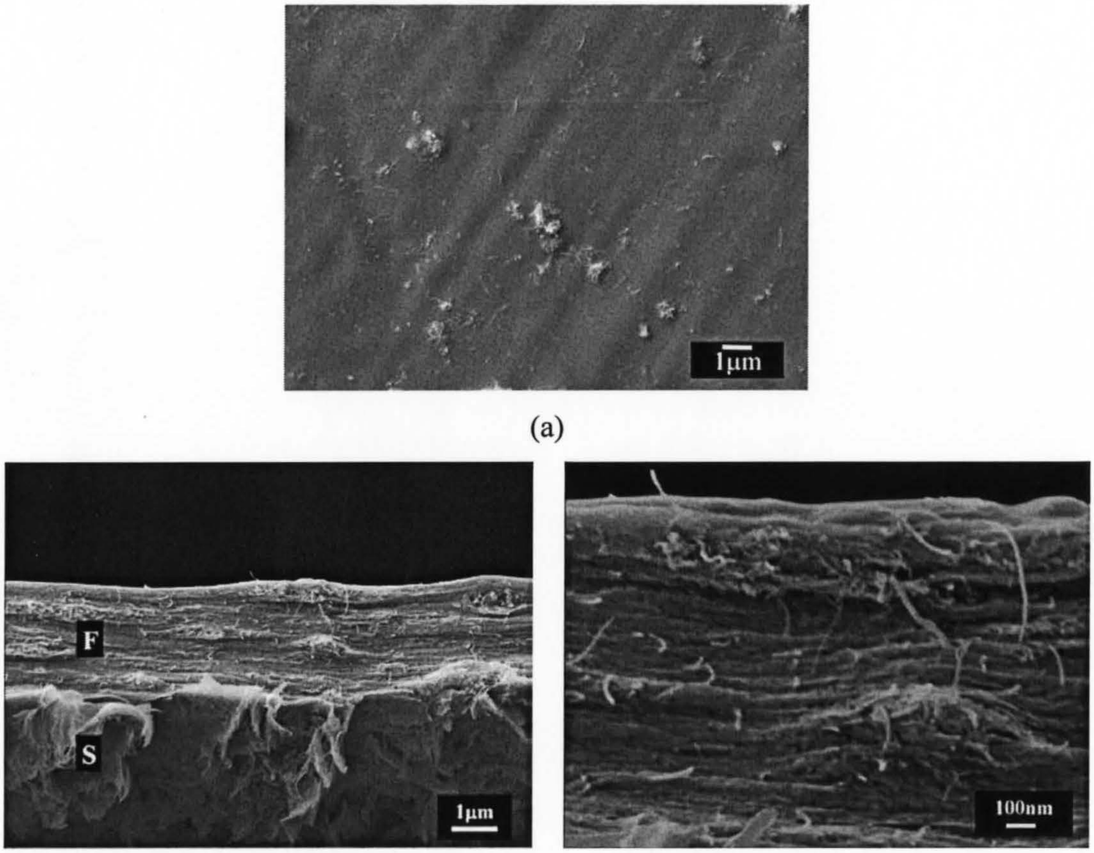

(a)

(b) (c)

Figure 5-32 SEM images of (a) surface and (b, c) cross section of the composite coatings prepared from 0.5 g/L sodium hyaluronate solutions containing 0.1 g/L MWCNT (F-film, S-substrate)

The DTA and TGA data are in good agreement with the results of SEM investigations. SEM image of the film surface clearly showed MWCNT in the hyaluronate matrix (Figure 5-32a). The SEM observations of the cross sections of the composite films (Figure 5-32b, c) showed that film thickness was varied in the range of 0.1-2.5 μm. The high magnification image (Figure 5-32c) of the cross section showed MWCNT in hyaluronic acid matrix.

5.3 EPD of alginate with HA, heparin, or hyaluronate

5.3.1 Codeposition of alginate and HA

The electrodeposition of alginate has been described in literature. The proposed mechanism of gel formation is based on the pH decrease at the anode owing to the electrochemical decomposition of water:

$$\mathbf{2H_2O \rightarrow O_2 + 4H^+ + 4e^-} \qquad \mathbf{(5.9)}$$

The dissociation of sodium alginate Na-Alg

$$\mathbf{Na\text{-}Alg \rightarrow Na^+ + Alg^-} \qquad \mathbf{(5.10)}$$

resulted in the formation of anionic alginate species. It was suggested that Alg– species formed alginic acid (H-Alg) gel in the low pH region around the electrode.

$$\mathbf{Alg^- + H^+ \rightarrow H\text{-}Alg} \qquad \mathbf{(5.11)}$$

The suspensions of HA particles were unstable and showed rapid sedimentation when ultrasonic agitation was interrupted. The addition of HA particles to the sodium alginate solutions enabled the formation of well-dispersed suspensions, which were stable against sedimentation for 1–2 days. It is suggested that the adsorption of anionic alginate species on the surface of the particles resulted in the electrosteric stabilization. The suspensions were used for electrodeposition.

SEM images (Figure 5-33) showed that composite coatings containing HA particles in alginate matrix were obtained. Figure 5-33 (a- d) indicates that higher HA concentration in the solutions resulted in a higher amount of HA in the deposits.

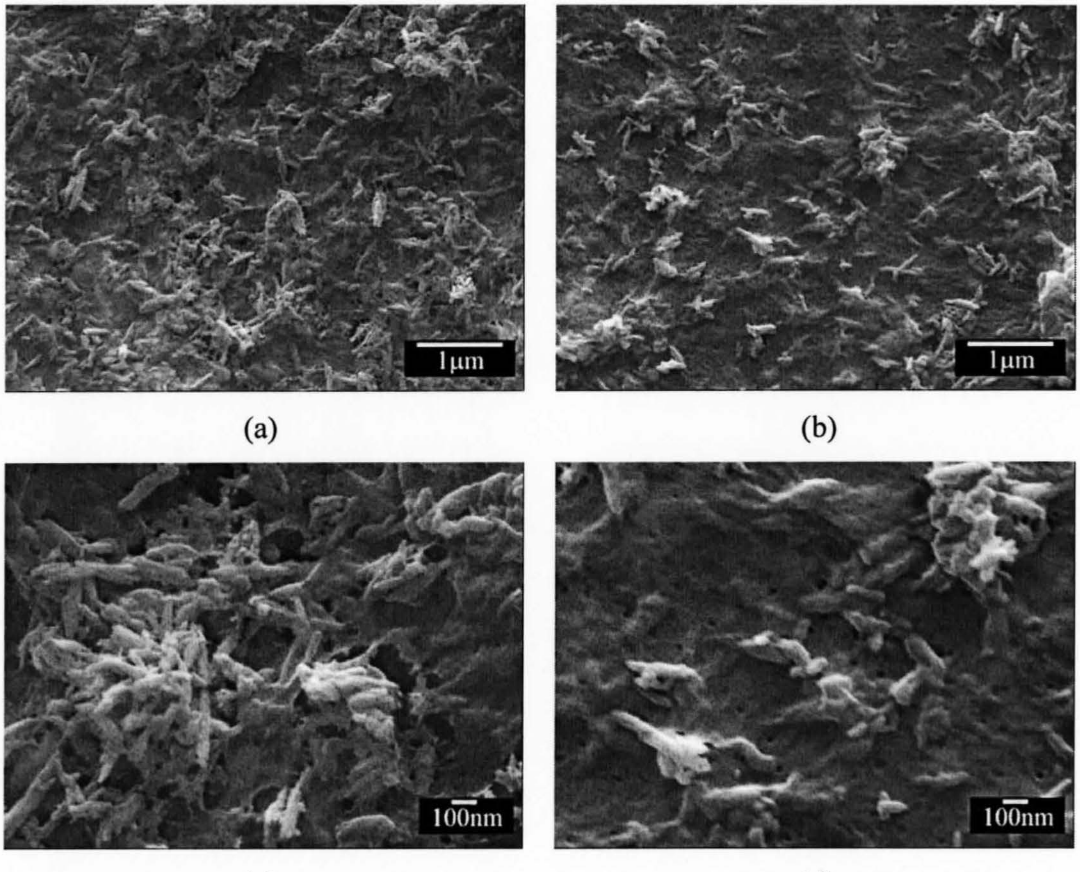

(a) (b)

(c) (d)

Figure 5-33 SEM images of the surface at different magnifications of the films prepared from the 1 g/L alginate solution, containing (a, c) 1 g/L HA or (b, d) 0.5 g/L HA.

5.3.2 Codeposition of alginate and heparin

5.3.2.1 Investigation of deposition yield

Figure 5-34 shows deposit mass versus heparin concentration in the 1.0 g/L sodium alginate solutions at a constant deposition voltage of 30 V and deposition time of 3 min. The increase in heparin concentration in the solutions resulted in an increasing deposit mass, indicating the formation of composite films with different heparin contents.

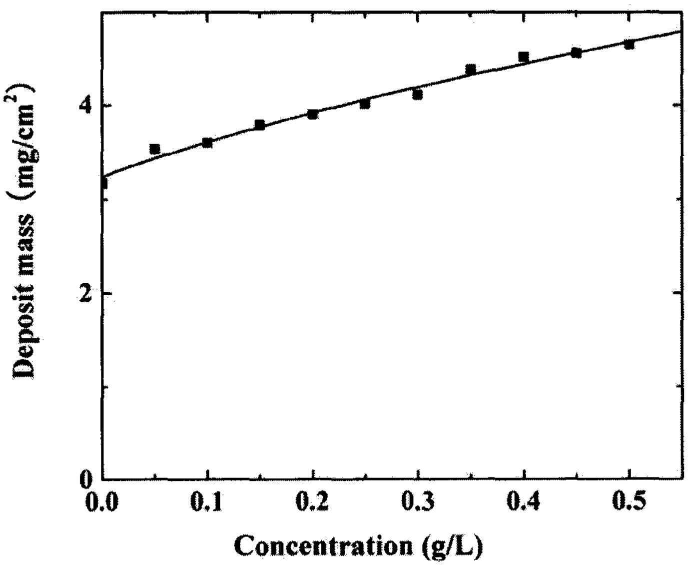

Figure 5-34 Deposit mass versus heparin concentration in 1.0 g/L sodium alginate solution at deposition voltage of 30 V and deposition time of 3 min

5.3.2.2 SEM studies of alginate-heparin composite deposits

Figure 5-35 shows the SEM images of the cross section of the composite films deposited on graphite substrate. SEM investigations showed that the thickness was varied in the range of 5-15 μm. The SEM image indicates that relatively uniform films can be obtained.

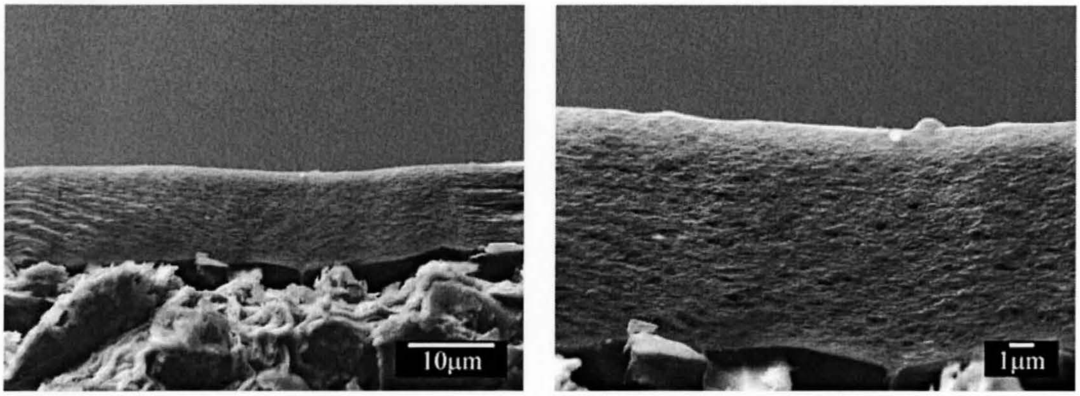

(a) (b)

Figure 5-35 SEM images at different magnifications of cross section of film prepared from the 1.0 g/L sodium alginate solution containing 0.5 g/L heparin

5.3.2.3 TGA&DTA studies of alginate-heparin composite deposits

Figure 5-36 and Figure 5-37 compare the TGA and DTA data for as-received heparin, pure alginate deposit, and alginate-heparin composite coatings.

The weight loss observed in the TGA data is attributed to dehydration and burning out of alginate and heparin. The weight loss occurs in several steps. The TGA data (Figure 5-36) showed differences in thermal behavior of the alginate-heparin deposit compared to pure alginate coating and as-received heparin. The decomposition temperature of the composite coating was lower than that for as-received heparin and higher than the decomposition temperature for alginic acid coating, although the difference was limited.

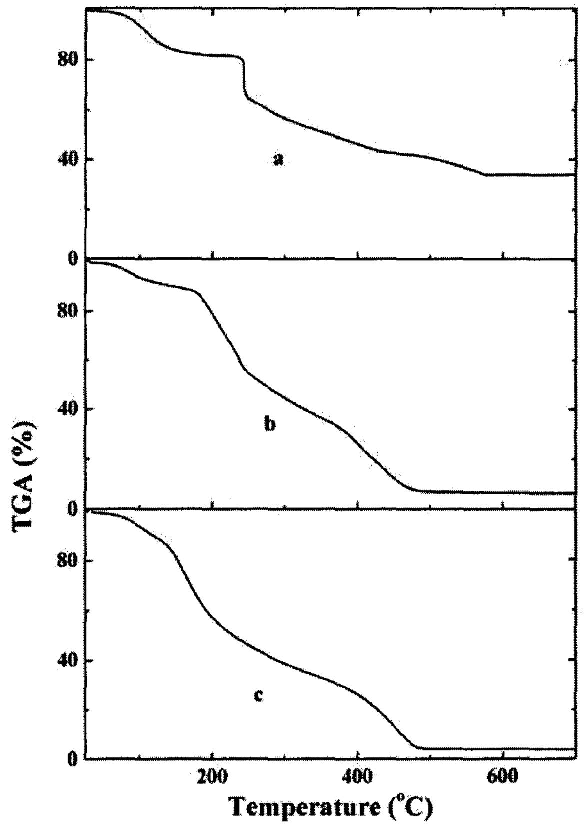

Figure 5-36 TGA data for (a) as-received heparin (b) a deposit prepared from the 1.0 g/L sodium alginate solution, and (c) a deposit prepared from the 1.0 g/L sodium alginate solution containing 0.5 g/L heparin

The DTA data (Figure 5-37) showed very broad endotherms around ~100 °C, related to dehydration of the materials and exotherms at higher temperatures related to the burning out of the organic materials. The DTA data are in a good agreement with the results of TGA investigation and indicate the difference in thermal behavior of alginate-heparin deposits, compared to pure alginate and heparin.

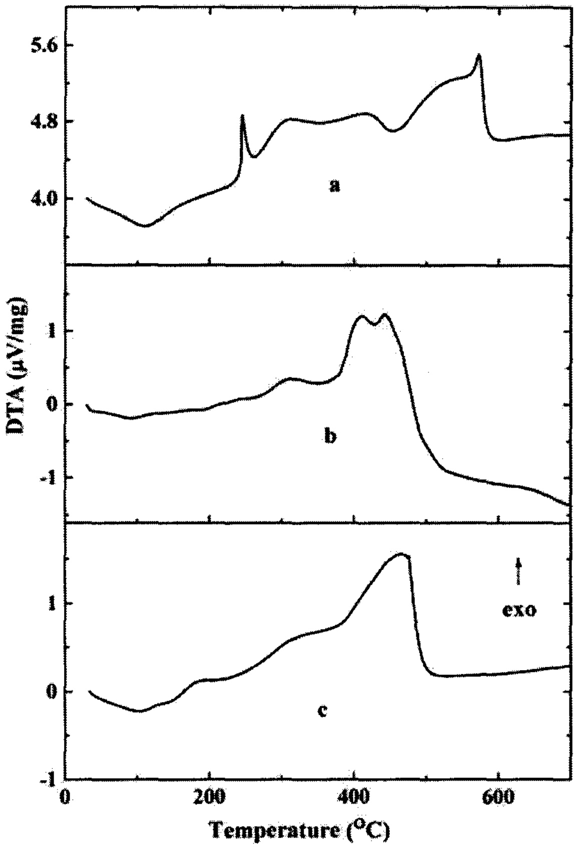

Figure 5-37 DTA data for (a) as-received heparin (b) a deposit prepared from the 1.0 g/L sodium alginate solution, and (c) a deposit prepared from the 1.0 g/L sodium alginate solution containing 0.5 g/L heparin

The TGA and DTA studies indicated the formation of composite coatings containing heparin in alginate matrix.

5.3.2.4 FTIR studies of alginate-heparin composite deposits

Figure 5-38 compared the FTIR spectrum of as-received heparin, pure alginate films and alginate-heparin composite deposits.

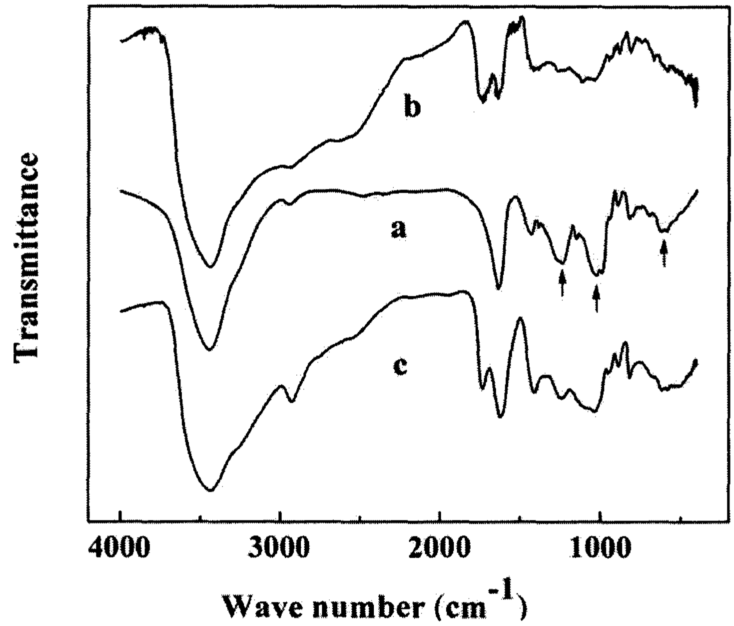

Figure 5-38 FTIR data for (a) as-received heparin (b) a deposit prepared from the 1.0 g/L sodium alginate solution, and (c) a deposit prepared from the 1.0 g/L sodium alginate solution containing 0.5 g/L heparin. The arrows show absorbance at 1232 and 1040 cm^{-1} due to $-SO_3^-$ asymmetric and symmetric stretching and the bands in the region 797–818 cm^{-1} related to sulphate half esters absorptions.

The characteristic peaks of heparin were pointed out by the arrows. The absorbance at 1232 cm^{-1} and 1040 cm^{-1} is due to $-SO_3^-$ asymmetric and symmetric stretching. The bands observed in the region 797–818 cm^{-1} are related to sulphate half ester absorption. The spectrum of alginate–heparin deposits is similar to the spectrum of pure alginate. However, the formation of alginate–heparin complexes resulted in additional peaks corresponding to the heparin absorbance at 1232 cm^{-1} and 1040 cm^{-1}. Such absorptions are characteristic for $-SO_3^-$ groups of heparin. The sulphate half ester absorptions were also observed in the FTIR spectrum of composite deposits at 797–818 cm^{-1} which can not be found in the spectrum of pure alginate. Therefore, these FTIR data indicated the formation of composite coatings.

5.3.2.5 Antithrombin adsorption test of alginate-heparin composite deposits

Figure 5-39 compares the results of antithrombin adsorption on the surface of films prepared from 1.0 g/L chitosan solution, 1.0 g/L chitosan solution containing 0.25 g/L heparin, 1.0 g/L chitosan solution containing 0.5 g/L heparin in mixed ethanol–water solutions.

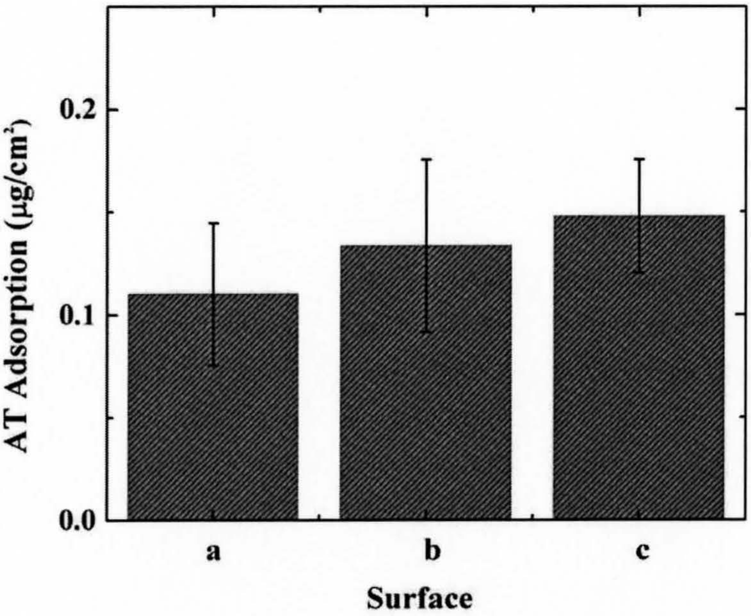

Figure 5-39 Antithrombin adsorption on the surface of films prepared from (a) 1.0 g/L alginate solution, (b) 1.0 g/L alginate solution containing 0.25 g/L heparin, (c) 1.0 g/L alginate solution containing 0.5 g/L heparin. Values are mean ±CD (n=2)

The surfaces of alginate–heparin composite films showed increase in the antithrombin adsorption compared to the surfaces of pure alginate films. The higher antithrombin adsorption on the surface of films prepared from alginate solution containing 0.5 g/L heparin compared to the films prepared from alginate solution containing 0.25 g/L heparin can be attributed to higher heparin content in the former films.

However, the differences among these results are not significant, which means that the amount of heparin in the composite films is small. Further work will need to be done to increase heparin content in the coatings.

5.3.3 Codeposition of alginate and hyaluronate

5.3.3.1 Investigation of deposition yield

Figure 5-40 shows deposition yield obtained from different solutions at a constant voltage of 30 V and deposition time of 3 min. The concentration of alginate was kept constant (0.5 g/L). The deposition yield increased with the increasing hyaluronate concentration.

As we discussed previously, pure hyaluronate can be deposited anodically in mixed ethanol-water solutions. So the significant increase in the deposition yields indicated the formation of composite coatings containing alginic acid and hyaluronic acid.

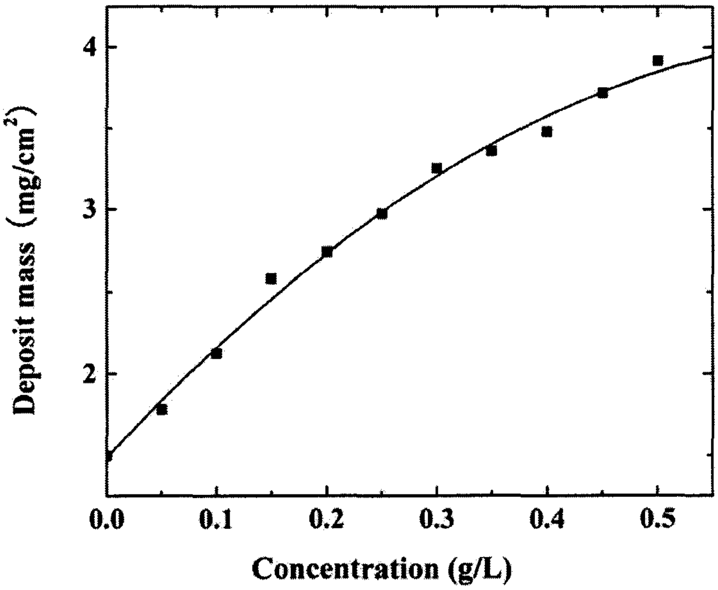

Figure 5-40 Deposit mass versus hyaluronate concentration in 0.5 g/L sodium alginate solution at deposition voltage of 30 V and deposition time of 3 min

5.3.3.2 SEM studies of alginate-hyaluronate composite deposits

Figure 5-41 shows the SEM images of the cross section of the composite films deposited on graphite substrate. SEM investigations showed that the thickness was varied in the range of 0.1-10 μm. The SEM image indicates that relatively uniform films can be obtained.

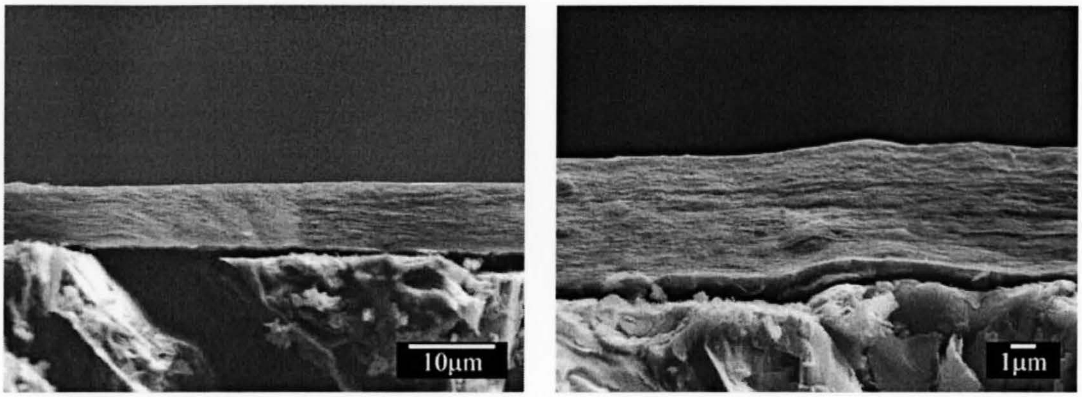

(a) (b)

Figure 5-41 SEM images at different magnifications of cross section of film prepared from the 0.5 g/L sodium alginate solution containing 0.25 g/L hyaluronate

5.3.3.3 TGA&DTA studies of alginate-hyaluronate composite deposits

The TGA data presented in Figure 5-36b and Figure 5-42d showed lower temperature (470 °C) of thermal decomposition of alginic acid compared to thermal decomposition temperature of hyaluronic acid film (550 °C).

Figure 5-42 and Figure 5-43 compare the TGA and DTA data for pure hyaluronate deposit and composite coatings with different ratio of alginate and hyaluronate. The weight loss observed in the TGA data is attributed to dehydration and burning out of polymers. The TGA data (Figure 5-42) showed differences in thermal behavior of the composite deposits compared to pure hyaluronate coating and pure alginate coatings. The decomposition temperatures of composite coatings were between decomposition temperatures of pure alginate deposit and hyaluronate deposit and higher ratio of hyaluronate/alginate resulted in higher decomposition temperature.

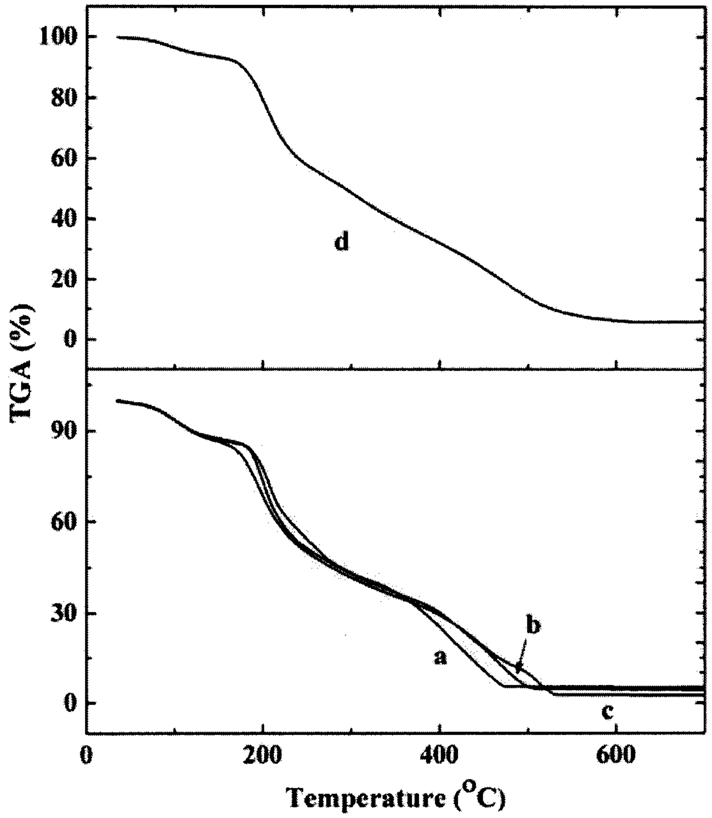

Figure 5-42 TGA data for deposit prepared from (a) 0.5 g/L sodium alginate solution containing 0.25 g/L hyaluronate, (b) 0.25 g/L sodium alginate solution containing 0.25 g/L hyaluronate, (c) 0.25 g/L sodium alginate solution containing 0.5 g/L hyaluronate, and (d) pure hyaluronate solutions

The DTA data (Figure 5-43) are in a good agreement with the results of TGA investigation and indicate the difference in thermal behavior of alginate-hyaluronate deposits, compared to pure alginate and hyaluronate. The DTA data showed very broad endotherms around ~100 °C, related to the liberation of adsorbed water and exotherms at higher temperatures related to the burning out of the organic materials.

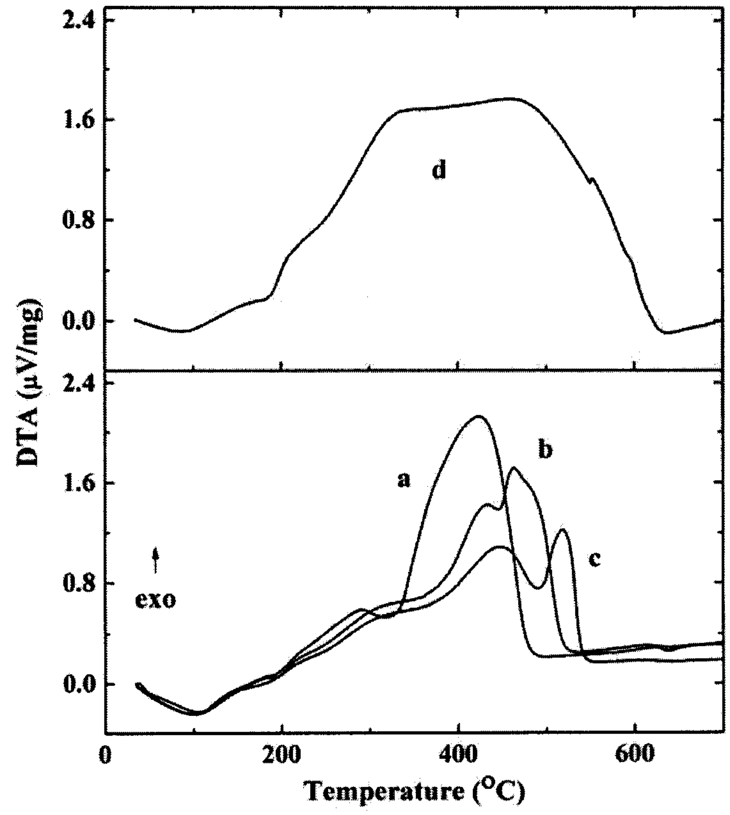

Figure 5-43 DTA data for deposit prepared from (a) 0.5 g/L sodium alginate solution containing 0.25 g/L hyaluronate, (b) 0.25 g/L sodium alginate solution containing 0.25 g/L hyaluronate, (c) 0.25 g/L sodium alginate solution containing 0.5 g/L hyaluronate, and (d) pure hyaluronate solutions.

The results of TGA and DTA studies indicated that composite coatings containing alginate and hyaluronate were obtained, which have different content of hyaluronate in the deposits.

5.3.3.4 FTIR studies of alginate-hyaluronate composite deposits

Figure 5-44 compared the FTIR spectrum of hyaluronic acid film and alginate-hyaluronate composite deposits with different ratios. The characteristic peaks of hyaluronic acid film at 1037, 1078 and 1155 cm^{-1} were attributed to the C–O– C, C–O and C–O–H stretching and peaks at 3440 cm^{-1} to OH$^-$ stretching. The characteristic peak of hyaluronic acid was pointed out by the arrow. The absorbance at 1560 cm^{-1} is due to the amide II band. The spectrum of alginate–hyaluronate deposits is similar to the spectrum of hyaluronic acid film. However, the increase in the alginate content in the deposit resulted in the compression of the absorbance peak at 1560 cm^{-1} which did not exist in the spectrum of pure alginate film. These results indicated the formation of composite coatings containing alginate and hyaluronate.

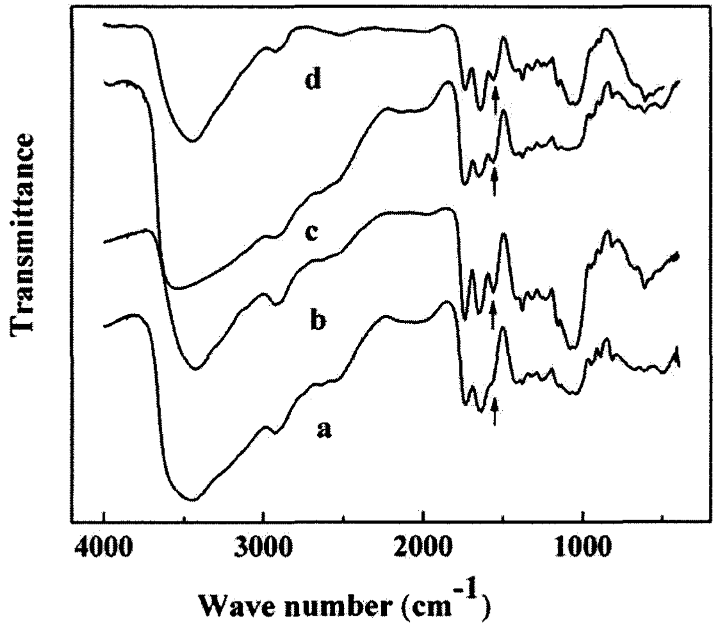

Figure 5-44 FTIR data for deposit prepared from (a) 0.5 g/L sodium alginate solution containing 0.25 g/L hyaluronate, (b) 0.25 g/L sodium alginate solution containing 0.25 g/L hyaluronate, (c) 0.25 g/L sodium alginate solution containing 0.5 g/L hyaluronate, and (d) pure hyaluronate solution. The arrows show absorbance at 1560 cm^{-1} due to the amide II band.

6 Conclusions

The main conclusions are summarized as follows:

- New electrophoretic deposition methods for the fabrication of advanced organic-inorganic composite coatings for metallic substrates have been developed.
- Cathodic EPD has been utilized for the fabrication of multilayer and functionally graded chitosan-HA coatings.
    - The HA particles showed preferred orientation of c-axis parallel to the layer surface.
    - The composition and thickness of the individual layers can be varied by the variation of deposition conditions.
    - Electrochemical studies showed that the obtained coatings provided corrosion protection of the metallic substrates, such as stainless steel and Nitinol.
- The feasibility of the chitosan-heparin composite deposition has been demonstrated.
    - The mechanism of chitosan deposition has been developed. The proposed mechanism of heparin deposition is based on the use of non-stoichiometric chitosan–heparin complexes.
    - The addition of heparin to chitosan solutions resulted in increasing deposition rate and enabled the formation of composite deposits of various thicknesses in the range of 0.5–5 μm.
    - The ability of the chitosan–heparin films to bind antithrombin, as measured by binding of ^{125}I-radiolabeled antithrombin, was much greater than that for

unmodified chitosan films. The films prepared in pure water solvent have much higher antithrombin adsorption than films prepared in mixed ethanol–water solutions. Composite chitosan–heparin layers were used for the surface modification of HA–chitosan coatings. Obtained results pave the way for the electrophoretic fabrication of novel coatings for biomedical implants with improved blood compatibility.

- The feasibility of deposition of hyaluronic acid and hyaluronic acid-HA-carbon nanotube composites has been demonstrated.
    - The deposit yield of pure hyaluronate can be varied by variation in the deposition time. The thickness of the hyaluronic acid film was in the range of 0.1–3 μm.
    - The mechanism of hyaluronic acid deposition has been developed. The deposition of hyaluronic acid in mixed ethanol-water solution can be attributed to the cross-linking of hyaluronic acid in ethanol-water solutions in acidic conditions.
    - Deposition yield measurements, TGA, DTA, FTIR, XRD and SEM studies showed that the co-deposition of hyaluronic acid and HA resulted in the formation of novel composite films by electrodeposition. The thickness of the composite films was in the range of 0.1–100 μm. Deposit composition can be varied by the variation of HA concentration in the sodium hyaluronate solutions. Composite films showed corrosion protection of stainless steel substrates in Ringer's physiological solutions.

  - Co-deposition of hyaluronic acid and multiwalled carbon nanotubes has been studied by TGA/DTA and SEM studies. The thickness of the composite film was varied in the range of 0.1-2.5 μm.

- The feasibility of deposition of novel composites based on alginic acid has been demonstrated. New electrochemical strategies were used for the fabrication of alginic acid-HA, alginic acid-heparin and alginic acid -hyaluronic acid nanocomposites. The mechanism of alginic acid deposition has been developed.
  - The composition of alginic acid-HA deposits can be varied by variation in bath composition for EPD.
  - The increase in heparin concentration in the solutions resulted in an increasing deposit mass and enabled the formation of alginate-heparin composite deposits of various thicknesses up to 15 μm. The ability of the alginate–heparin films to bind antithrombin was higher than that for pure alginate films.
  - The increase in hyaluronate concentration in the solutions resulted in an increasing deposit mass and enabled the formation of alginate-hyaluronate composite deposits of various thicknesses up to 10 μm.

New coatings and new electrochemical strategies for EPD can be utilized for the surface modification of biomedical implants.

7 References

1. Disegi, J.A. and L. Eschbach, *Stainless steel in bone surgery.* Injury, 2000. **31**: p. 2-6.
2. Wright, T.M., A.H. Burstein, and D.L. Bartel, *Retrieval analysis of total joint replacement components: a six-year experience*, in *Corrosion and degradation of implant materials*, A.C. Fraker and C.D. Griffin, Editors. 1985, ASTM STP 859.
3. Wroblewski, B.M., *Revision Surgery in Total Hip Arthroplasty.* 1990, London: Springer-Verlag.
4. Duerig, T., A. Pelton, and D. Stöckel, *An overview of nitinol medical applications.* Materials Science and Engineering A, 1999. **273-275**: p. 149-160.
5. Silva, T., et al., *NITINOL - A new material for biomedical applications.* Ciência e Tecnologia dos Materiais, 2005. **17**: p. 34-37.
6. Shabalovskaya, S., J. Anderegg, and J. Van Humbeeck, *Critical overview of Nitinol surfaces and their modifications for medical applications.* Acta Biomaterialia, 2008. **4**(3): p. 447-467.
7. Rondelli, G. and B. Vicentini, *Localized corrosion behaviour in simulated human body fluids of commercial Ni-Ti orthodontic wires.* Biomaterials, 1999. **20**(8): p. 785-792.
8. Hench, L.L., *Bioceramics.* Journal of American Ceramic Society, 1998. **81**(7): p. 1705-1728.
9. Ducheyne, P., et al., *Structural analysis of hydroxyapatite coatings on titanium.* Biomaterials, 1986. 7(2): p. 97-103.
10. P. Ducheyne, C.S.K., S. R. Pollack,, *The effect of phase differences on the time-dependent variation of the zeta potential of hydroxyapatite.* Journal of Biomedical Materials Research, 1992. **26**(2): p. 147-168.
11. Zhitomirsky, I. and L. Gal-Or, *Electrophoretic deposition of hydroxyapatite.* Journal of Materials Science: Materials in Medicine, 1997. **8**(4): p. 213-219.
12. Zhitomirsky, I., *Electrophoretic hydroxyapatite coatings and fibers.* Materials Letters, 2000. **42**(4): p. 262-271.
13. Hsieh, M.-F., L.-H. Perng, and T.-S. Chin, *Hydroxyapatite coating on Ti6Al4V alloy using a sol-gel derived precursor.* Materials Chemistry and Physics, 2002. **74**(3): p. 245-250.
14. LeGeros, R.Z. and J.P. LeGeros, *Dense hydroxyapatite*, in *An introduction to bioceramics*, L.L. Hench and J. Wilson, Editors. 1993, World Scientific: Singapore. p. 139-180.
15. Ducheyne, P., et al., *Calcium phosphate ceramic coatings on porous titanium: effect of structure and composition on electrophoretic deposition, vacuum sintering and in vitro dissolution.* Biomaterials, 1990. **11**(4): p. 244-254.
16. M. Wei, A.J.R., B. K. Milthorpe, C. C. Sorrell,, *Solution ripening of hydroxyapatite nanoparticles: Effects on electrophoretic deposition.* Journal of Biomedical Materials Research, 1999. **45**(1): p. 11-19.
17. Celaletdin Ergun, R.D., William Lanford,, *Hydroxylapatite and titanium: Interfacial reactions.* Journal of Biomedical Materials Research Part A, 2003. **65A**(3): p. 336-343.
18. Jagur-Grodzinski, J., *Biomedical application of functional polymers.* Reactive and Functional Polymers, 1999. **39**(2): p. 99-138.
19. Hubbell, J.A., *Synthetic biodegradable polymers for tissue engineering and drug delivery.* Current Opinion in Solid State and Materials Science, 1998. **3**(3): p. 246-251.
20. Saxena, A.K., et al., *Skeletal Muscle Tissue Engineering Using Isolated Myoblasts on Synthetic Biodegradable Polymers: Preliminary Studies.* Tissue Engineering, 1999. **5**(6): p. 525-531.
21. Nishinari, K. and R. Takahashi, *Interaction in polysaccharide solutions and gels.* Current Opinion in Colloid & Interface Science, 2003. **8**(4-5): p. 396-400.
22. Malafaya, P.B., G.A. Silva, and R.L. Reis, *Natural-origin polymers as carriers and scaffolds for biomolecules and cell delivery in tissue engineering applications.* Advanced Drug Delivery Reviews, 2007. **59**(4-5): p. 207-233.
23. Cascone, M.G., et al., *Bioartificial polymeric materials based on polysaccharides.* Journal of Biomaterials Science, Polymer Edition, 2001. **12**: p. 267-281.
24. Venugopal, J. and S. Ramakrishna, *Applications of polymer nanofibers in biomedicine and*

biotechnology. Applied Biochemistry and Biotechnology, 2005. **125**(3): p. 147-157.

25. Yano, H., et al., *Effect of N-acetyl-glucosamine on wound healing in rats.* Mie medical journal, 1985. **35**: p. 53-56.
26. Peter, M.G., *Applications and environmental aspects of chitin and chitosan.* Journal of Macromolecular Science - Pure and Applied Chemistry, 1995. **A32**(4): p. 629.
27. Austin, P.R., *Solvents for and purification of chitin,* in *US Patent.* 1977, University of Delaware (Newark, DE) US.
28. Austin, P.R., *Chitin solvents and solubility parameters,* in *Chitin and chitosan and related enzymes,* J.P. Zikakis, Editor. 1984, Academic Press Inc.: Orlando. p. 227-237.
29. T. Sannan, K.K., Y. Iwakura *Studies on chitin 1.* Makromolekulare Chemie Macromolecular Symposia, 1975. **176**: p. 1191-1195.
30. T. Sannan, K.K., Y. Iwakura *Studies on chitin 2.* Makromolekulare Chemie Macromolecular Symposia, 1976. **177**: p. 3589-3600.
31. Madihally, S.V. and H.W.T. Matthew, *Porous chitosan scaffolds for tissue engineering.* Biomaterials, 1999. **20**(12): p. 1133-1142.
32. Kyriacos, A.A., et al., *BASIC SCIENCE OF ARTICULAR CARTILAGE REPAIR.* Clinics in sports medicine, 2001. **20**(2): p. 223-247.
33. MICHAEL DORNISH, D.K., VIND SKAUGRUD,, *Standards and Guidelines for Biopolymers in Tissue-Engineered Medical Products.* Annals of the New York Academy of Sciences, 2001. **944**(BIOARTIFICIAL ORGANS III: TISSUE SOURCING, IMMUNOISOLATION, AND CLINICAL TRIALS): p. 388-397.
34. Kurita, K., *Controlled functionalization of the polysaccharide chitin.* Progress in Polymer Science, 2001. **26**(9): p. 1921-1971.
35. M. N. V. Ravi Kumar, R.A.A.M., C. Muzzarelli, H. Sashiwa, A. J. Domb,, *Chitosan Chemistry and Pharmaceutical Perspectives.* ChemInform, 2005. **36**(11).
36. Marguerite Rinaudo, *Chitin and Chitosan :Properties and Applications.* ChemInform, 2007. **38**(27).
37. F. G. Pearson, R.H.M., C. Y. Liang,, *Infrared spectra of crystalline polysaccharides. V. Chitin.* Journal of Polymer Science, 1960. **43**(141): p. 101-116.
38. Francis Suh, J.K. and H.W.T. Matthew, *Application of chitosan-based polysaccharide biomaterials in cartilage tissue engineering: a review.* Biomaterials, 2000. **21**(24): p. 2589-2598.
39. Pang, X. and I. Zhitomirsky, *Electrodeposition of composite hydroxyapatite-chitosan films.* Materials Chemistry and Physics, 2005. **94**(2-3): p. 245-251.
40. Pang, X. and I. Zhitomirsky, *Electrophoretic deposition of composite hydroxyapatite-chitosan coatings.* Materials Characterization, 2007. **58**(4): p. 339-348.
41. Pang, X.a.I.Z., *Electrodeposition of nanocomposite organic-inorganic coatings for biomedical applications.* International Journal of Nanoscience 2005. **4**(3): p. 409-418.
42. Wallis, T.E., *Unorganized Drugs.* 5th Ed ed. In Textbook of Pharmacognosy. 1985: CBS. 467-469.
43. A Haug, S.M., B Larsen, O Smidsrød *Correlation between chemical structure and physical properties of alginates.* Acta Chemica Scandinavica 1967. **21**: p. 768-778.
44. Haug, A., B. Larsen, and O. Smidsrφd, *Uronic acid sequence in alginate from different sources.* Carbohydrate Research, 1974. **32**(2): p. 217-225.
45. E.A. MacGregor, C.T.G., *Polymers in Nature In Polysaccharides.* 1980, New York: Wiley.
46. Timothy A. Becker, D.R.K., Tedd Brandon,, *Calcium alginate gel: A biocompatible and mechanically stable polymer for endovascular embolization.* Journal of Biomedical Materials Research, 2001. **54**(1): p. 76-86.
47. Grant, G.T., et al., *Biological interactions between polysaccharides and divalent cations: The egg-box model.* FEBS Letters, 1973. **32**(1): p. 195-198.
48. Stokke, B.T., et al., *Distribution of uronate residues in alginate chains in relation to alginate gelling properties.* Macromolecules, 1991. **24**(16): p. 4637-4645.
49. Draget, K.I., et al., *Swelling and partial solubilization of alginic acid gel beads in acidic buffer.* Carbohydrate Polymers, 1996. **29**(3): p. 209-215.
50. Lim, F. and A. Sun, *Microencapsulated islets as bioartificial endocrine pancreas.* Science, 1980.

210(4472): p. 908-910.

51. O'Shea, G.M., M.F.A. Goosen, and A.M. Sun, *Prolonged survival of transplanted islets of Langerhans encapsulated in a biocompatible membrane.* Biochimica et Biophysica Acta (BBA) - Molecular Cell Research, 1984. **804**(1): p. 133-136.
52. Scott, C.D., *Immobilized cells: a review of recent literature.* Enzyme and Microbial Technology, 1987. **9**(2): p. 66-72.
53. Levesque, L., P. Brubaker, and A. Sun, *Maintenance of long-term secretory function by microencapsulated islets of Langerhans.* Endocrinology, 1992. **130**(2): p. 644-650.
54. Langer, R., *New methods of drug delivery.* Science, 1990. **249**(4976): p. 1527-1533.
55. Pitt, C.G., *The controlled parenteral delivery of polypeptides and proteins.* International Journal of Pharmaceutics, 1990. **59**(3): p. 173-196.
56. Hertzberg, S., et al., *Alginate as immobilization matrix and stabilizing agent in a two-phase liquid system: Application in lipase-catalysed reactions.* Enzyme and Microbial Technology, 1992. **14**(1): p. 42-47.
57. Blandino, A., M. Macas, and D. Cantero, *Immobilization of glucose oxidase within calcium alginate gel capsules.* Process Biochemistry, 2001. **36**: p. 601-606.
58. Tanriseven, A. and S. Dogan, *Production of isomalto-oligosaccharides using dextransucrase immobilized in alginate fibres.* Process Biochemistry, 2002. **37**(10): p. 1111-1115.
59. Smith, T.J., *Calcium alginate hydrogel as a matrix for enteric delivery of nucleic acids.* Biopharm, 1994. **4**: p. 54-55.
60. Thomas, S., *Alginates: a guide to the properties and uses of the different. alginate dressings available today.* Journal of Wound Care, 1992. **1**: p. 29-32.
61. Cheong, M. and I. Zhitomirsky, *Electrodeposition of alginic acid and composite films.* Colloids and Surfaces A: Physicochemical and Engineering Aspects, 2008. **328**(1-3): p. 73-78.
62. Meyer, K. and J.W. Palmer, *THE POLYSACCHARIDE OF THE VITREOUS HUMOR.* J. Biol. Chem., 1934. **107**(3): p. 629-634.
63. Rinaudo, M.M.a.M., *Characterization and properties of hyaluronic acid (hyaluronan).* Polysaccharides: Structural Diversity and Functional Versatility, ed. S. Dimitriu. Vol. 22. 2005.
64. Bakoš, D., M. Soldán, and I. Hernández-Fuentes, *Hydroxyapatite-collagen-hyaluronic acid composite.* Biomaterials, 1999. **20**(2): p. 191-195.
65. Hahn, S.K. and A.S. Hoffman, *Preparation and characterization of biocompatible polyelectrolyte complex multilayer of hyaluronic acid and poly-l-lysine.* International Journal of Biological Macromolecules, 2005. **37**(5): p. 227-231.
66. Yamane, S., et al., *Feasibility of chitosan-based hyaluronic acid hybrid biomaterial for a novel scaffold in cartilage tissue engineering.* Biomaterials, 2005. **26**(6): p. 611-619.
67. Mensitieri, M., et al., *Viscoelastic evaluation of different knee osteoarthritis therapies.* Journal of Materials Science: Materials in Medicine, 1995. **6**(3): p. 130-137.
68. Chandy, T. and C.P. Sharma, *Chitosan--as a biomaterial.* Biomaterials, artificial cells, and artificial organs, 1990. **18**(1): p. 1-24.
69. Benedetti, L., et al., *Biocompatibility and biodegradation of different hyaluronan derivatives (Hyaff) implanted in rats.* Biomaterials, 1993. **14**(15): p. 1154-1160.
70. Nancy E. Larsen, C.T.P., Karen Reiner, Edward Leshchiner, Endre A. Balazs,, *Hylan gel biomaterial: Dermal and immunologic compatibility.* Journal of Biomedical Materials Research, 1993. **27**(9): p. 1129-1134.
71. Turley, E.A., *Proteoglycans and cell adhesion.* Cancer and Metastasis Reviews, 1984. **3**(4): p. 325-339.
72. Giusti, P., L. Lazzeri, and L. Lelli, Trends in Polymer Science, 1993. **1**: p. 261-262.
73. Pouyani, T. and G.D. Prestwich, *Functionalized Derivatives of Hyaluronic Acid Oligosaccharides: Drug Carriers and Novel Biomaterials.* Bioconjugate Chemistry, 1994. **5**(4): p. 339-347.
74. Gurny, R., et al., *Design and evaluation of controlled release systems for the eye.* Journal of Controlled Release, 1987. **6**(1): p. 367-373.
75. B. DELPECH, N.G, P. BERTRAND, M.-N. COUREL, C. CHAUZY, A. DELPECH,, *Hyaluronan: fundamental principles and applications in cancer.* Journal of Internal Medicine, 1997. **242**(1): p.

41-48.

76. Pianigiani, E., et al., *A new model for studying differentiation and growth of epidermal cultures on hyaluronan-based carrier.* Biomaterials, 1999. **20**(18): p. 1689-1694.
77. Turner, N.J., et al., *A novel hyaluronan-based biomaterial (Hyaff-11? as a scaffold for endothelial cells in tissue engineered vascular grafts.* Biomaterials, 2004. **25**(28): p. 5955-5964.
78. Renier, D., et al., *Pharmacokinetic behaviour of ACP gel, an autocrosslinked hyaluronan derivative, after intraperitoneal administration.* Biomaterials, 2005. **26**(26): p. 5368-5374.
79. Hiroyuki Kito, T.M., *Biocompatible coatings for luminal and outer surfaces of small-caliber artificial grafts.* Journal of Biomedical Materials Research, 1996. **30**(3): p. 321-330.
80. Woochan Hyung, H.K., Joseph Park, Eunkyung Lim, Sung Bae Park, Young-Joon Park, Ho Geun Yoon, Jin Suck Suh, Seungjoo Haam, Yong-Min Huh,, *Novel hyaluronic acid (HA) coated drug carriers (HCDCs) for human breast cancer treatment.* Biotechnology and Bioengineering, 2008. **99**(2): p. 442-454.
81. Laroui, H., et al., *Hyaluronate-Covered Nanoparticles for the Therapeutic Targeting of Cartilage.* Biomacromolecules, 2007. **8**(12): p. 3879-3885.
82. Toshimitsu Momose, P.C.A., Yu-Long Sun, Chunfeng Zhao, Mark E. Zobitz, Jeffrey R. Harrington, Kai-Nan An,, *Surface modification of extrasynovial tendon by chemically modified hyaluronic acid coating.* Journal of Biomedical Materials Research, 2002. **59**(2): p. 219-224.
83. Huang, L.-Y. and M.-C. Yang, *Hemocompatibility of Layer-by-Layer Hyaluronic Acid/Heparin Nanostructure Coating on Stainless Steel for Cardiovascular Stents and its Use for Drug Delivery.* Journal of Nanoscience and Nanotechnology, 2006. **6**: p. 3163-3170.
84. Linhardt, R.J., *Heparin: an important drug enters its seventh decade.* Chemistry and Industry, 1991. **2**: p. 45-50.
85. Ishan Capila, R.J.L., *Heparin-Protein Interactions.* Angewandte Chemie International Edition, 2002. **41**(3): p. 390-412.
86. Rosenberg, R.D. and P.S. Damus, *The Purification and Mechanism of Action of Human Antithrombin-Heparin Cofactor.* J. Biol. Chem., 1973. **248**(18): p. 6490-6505.
87. Olson, S., et al., *Role of the antithrombin-binding pentasaccharide in heparin acceleration of antithrombin-proteinase reactions. Resolution of the antithrombin conformational change contribution to heparin rate enhancement.* J. Biol. Chem., 1992. **267**(18): p. 12528-12538.
88. Kim, S.W. and H. Jacobs, *Design of Nonthrombogenic Polymer Surfaces for Blood-Contacting Medical Devices.* Blood Purification, 1996. **14**: p. 357-372.
89. Oliveira, G.B., L.B. Carvalho, and M.P.C. Silva, *Properties of carbodiimide treated heparin.* Biomaterials, 2003. **24**(26): p. 4777-4783.
90. Dong-Keon Kweon, S.-T.L., *Preparation and characteristics of a water-soluble chitosan-heparin complex.* Journal of Applied Polymer Science, 2003. **87**(11): p. 1784-1789.
91. Wen-Ching Lin, C.-H.T., Ming-Chien Yang,, *In-Vitro Hemocompatibility Evaluation of a Thermoplastic Polyurethane Membrane with Surface-Immobilized Water-Soluble Chitosan and Heparin.* Macromolecular Bioscience, 2005. **5**(10): p. 1013-1021.
92. Zhu, A.P., Z. Ming, and S. Jian, *Blood compatibility of chitosan/heparin complex surface modified ePTFE vascular graft.* Applied Surface Science, 2005. **241**(3-4): p. 485-492.
93. Zhu, A., et al., *Covalent immobilization of chitosan/heparin complex with a photosensitive hetero-bifunctional crosslinking reagent on PLA surface.* Biomaterials, 2002. **23**(23): p. 4657-4665.
94. Benjamin Thierry, Y.M., Jim Silver, Maryam Tabrizian,, *Biodegradable membrane-covered stent from chitosan-based polymers.* Journal of Biomedical Materials Research Part A, 2005. **75A**(3): p. 556-566.
95. Wang, X., et al., *Preparation and characterization of a collagen/chitosan/heparin matrix for an implantable bioartificial liver.* Journal of Biomaterials Science, Polymer Edition, 2005. **16**: p. 1063-1080.
96. Vasudev, S.C., T. Chandy, and C.P. Sharma, *Development of chitosan/polyethylene vinyl acetate co-matrix: controlled release of aspirin-heparin for preventing cardiovascular thrombosis.* Biomaterials, 1997. **18**(5): p. 375-381.

97. Liao, I.C., et al., *Controlled release from fibers of polyelectrolyte complexes.* Journal of Controlled Release, 2005. **104**(2): p. 347-358.
98. He, Q., et al., *In Vitro Cytotoxicity and Protein Drug Release Properties of Chitosan/Heparin Microspheres.* Tsinghua Science & Technology, 2007. **12**(4): p. 361-365.
99. Huang, M., et al., *Polyelectrolyte Complexes Stabilize and Controllably Release Vascular Endothelial Growth Factor.* Biomacromolecules, 2007. **8**(5): p. 1607-1614.
100. Williams, D., *A Concise Encyclopedia of Medical and Dental Materials.* 1991: Permagon Press.
101. Hench, L.L., *Medical materials for the next millennium.* MRS Bulletin, 1999. **24**(5): p. 13-19.
102. Sioshansi, P., *Surface modification of industrial components by ion implantation.* Materials Science and Engineering, 1987. **90**: p. 373-383.
103. Sodhi, R.N.S., *Application of surface analytical and modification techniques to biomaterial research.* Journal of Electron Spectroscopy and Related Phenomena, 1996. **81**(3): p. 269-284.
104. Cui, F.Z. and Z.S. Luo, *Biomaterials modification by ion-beam processing.* Surface and Coatings Technology, 1999. **112**(1-3): p. 278-285.
105. Chu, P.K., et al., *Plasma-surface modification of biomaterials.* Materials Science and Engineering: R: Reports, 2002. **36**(5-6): p. 143-206.
106. Hanawa, T., *In vivo metallic biomaterials and surface modification.* Materials Science and Engineering A, 1999. **267**(2): p. 260-266.
107. Takao Hanawa, Y.K., Satoru Yamamoto, Takao Kohgo, Akira Amemiya, Hidemi Ukai, Koichi Murakami, Kenzo Asaoka,, *Early bone formation around calcium-ion-implanted titanium inserted into rat tibia.* Journal of Biomedical Materials Research, 1997. **36**(1): p. 131-136.
108. Podbielska, H. and A. Ulatowska-Jarża, *Sol-gel technology for biomedical engineering.* Bulletin of the Polish Academy of Sciences - Technical Sciences, 2005. **53**(3): p. 261-271.
109. Cheng, F.T., P. Shi, and H.C. Man, *A preliminary study of TiO_2 deposition on NiTi by a hydrothermal method.* Surface and Coatings Technology, 2004. **187**(1): p. 26-32.
110. Decher, G., J.D. Hong, and J. Schmitt, *Buildup of ultrathin multilayer films by a self-assembly process: III. Consecutively alternating adsorption of anionic and cationic polyelectrolytes on charged surfaces.* Thin Solid Films, 1992. **210-211**(Part 2): p. 831-835.
111. Wang, Y., et al. *Biocompatible thin film coatings fabricated using the electrostatic self-assembly process.* in *Biomedical Instrumentation Based on Micro- and Nanotechnology.* 2001. San Jose, CA, USA: SPIE.
112. Van der Biest, O.O. and L.J. Vandeperre, *ELECTROPHORETIC DEPOSITION OF MATERIALS.* Annual Review of Materials Science, 1999. **29**(1): p. 327-352.
113. Boccaccini, A.R. and I. Zhitomirsky, *Application of electrophoretic and electrolytic deposition techniques in ceramics processing.* Current Opinion in Solid State and Materials Science, 2002. **6**(3): p. 251-260.
114. Payne, G.F., *Biopolymer-based materials: the nanoscale components and their hierarchical assembly.* Current Opinion in Chemical Biology, 2007. **11**(2): p. 214-219.
115. Zhitomirsky, I., *Cathodic electrodeposition of ceramic and organoceramic materials. Fundamental aspects.* Advances in Colloid and Interface Science, 2002. **97**(1-3): p. 277-315.
116. Derjaguin, B. and L. Landau, *Theory of the Stability of Strongly Charged Lyophobic Sols and of the Adhesion of Strongly Charged Particles.* Acta Physicochimica, 1941. **14**: p. 633-662.
117. Verwey, E.J.W. and J.T.G. Overbeek, *Theory of the Stability of Lyophobic Colloids.* 1948, Amsterdam: Elsevier.
118. Zhitomirsky, I., et al., *Electrodeposition of ceramic films from non-aqueous and mixed solutions.* Journal of Materials Science, 1995. **30**(20): p. 5307-5312.
119. Zhitomirsky, I., et al., *Electrochemical Al2O3-Cr2O3 alloy coatings on non-oxide ceramic substrates.* Journal of Materials Science, 1997. **32**: p. 5205-5213.
120. Zhitomirsky, I., *Cathodic electrosynthesis of titanium and ruthenium oxides.* Materials Letters, 1998. **33**: p. 305-310.
121. Zhitomirsky, I. and A. Petric, *Electrolytic and electrophoretic deposition of CeO2 films.* Materials Letters, 1999. **40**: p. 263-268.
122. Zhitomirsky, I. and L. Gal-Or, *Intermetallic and Ceramic Coatings*, ed. N.B. Dahotre and T.S.

Sudarshan. Vol. Chapter 3. 1999, New York: Marcel Dekker Inc.

123. Zhitomirsky, I., *Ceramic Films Using Cathodic Electrodeposition.* JOM-e Minerals, Metals and Materials Society, 2000. **52**: p. http://www.tms.org/pubs/journals/JOM/0001/Zhitomirsky/Zhitomirsky-0001.html.
124. Sun, F., et al., *Surface modifications of Nitinol for biomedical applications.* Colloids and Surfaces B: Biointerfaces, 2008. **67**(1): p. 132-139.
125. Sun, F., X. Pang, and I. Zhitomirsky, *Electrophoretic deposition of composite hydroxyapatite-chitosan-heparin coatings.* Journal of Materials Processing Technology, 2009. **209**(3): p. 1597-1606.
126. Damodaran, R. and B.M. Moudgil, *Electrophoretic deposition of calcium phosphates from non-aqueous media.* Colloids and Surfaces A: Physicochemical and Engineering Aspects, 1993. **80**(2-3): p. 191-195.
127. Paik, U., et al., *The effect of electrostatic repulsive forces on the stability of BaTiO3 particles suspended in non-aqueous media.* Colloids and Surfaces A: Physicochemical and Engineering Aspects, 1998. **135**(1-3): p. 77-88.
128. Ferrari, B. and R. Moreno, *Zirconia thick films deposited on nickel by aqueous electrophoretic deposition.* Journal of the Electrochemical Society 2000. **147**(8): p. 2987-2992.
129. Tabellion, J. and R. Clasen, *Electrophoretic deposition from aqueous suspensions for near-shape manufacturing of advanced ceramics and glasses—applications.* Journal of Materials Science, 2004. **39**(3): p. 803-811.
130. Hamaker, H.C., *Formation of a deposit by electrophoresis.* Transactions of the Faraday Society 1940. **35**: p. 279-287.
131. Hamaker, H.C. and E.J.W. Verwey, *The Role of the Forces between the Particles in Electrodeposition and Other Phenomena.* Transactions of the Faraday Society 1940. **36**: p. 180-185.
132. Kurella, A. and N.B. Dahotre, *Review paper: Surface Modification for Bioimplants: The Role of Laser Surface Engineering.* J Biomater Appl, 2005. **20**(1): p. 5-50.
133. Therese, G.H.A. and P.V. Kamath, *Electrochemical Synthesis of Metal Oxides and Hydroxides.* Chemistry of Materials, 2000. **12**(5): p. 1195-1204.
134. Rho, J.Y., L. Kuhn-Spearing, and P. Zioupos, *Mechanical properties and the hierarchical structure of bone.* Medical Engineering and Physics, 1998. **20**: p. 92-102.
135. Fratzl, P., et al., *Structure and mechanical quality of the collagen-mineral nano-composite in bone.* Journal of materials chemistry, 2004. **14**: p. 2115-2123.
136. Wise, E.R., et al., *The organic-mineral interface in bone is predominantly polysaccharide.* Chemistry of Materials, 2007. **19**(21): p. 5055-5057.
137. O. Prymak, D.B., S.A. Esenwein, M. Köller, M. Epple,, *NiTi shape memory alloys coated with calcium phosphate by plasma-spraying. Chemical and biological properties.* Materialwissenschaft und Werkstofftechnik, 2004. **35**(5): p. 346-351.